

Study of the heterogeneous catalytic oxidation of furfural and glycerol from lignocellulosic waste

Pablo Gil Selfa

Thesis to obtain the Master of Science Degree in
Chemical Engineering

Supervisors: Prof. Luísa Margarida Martins

Dr. Ana Paula da Costa Ribeiro

Examination Committee

Chairperson: Prof. Carlos Manuel Faria de Barros Henriques

Supervisor: Prof. Luísa Margarida Dias Ribeiro de Sousa Martins

Members of Committee: Dr. Marta Videira Amaral Santos Andrade

June 2021

I declare that this document is an original work of my own authorship and that it fulfils
all the requirements of the Code of Conduct and Good Practices of the
Universidade de Lisboa.

To my family, girlfriend, and friends, being part of your life is the best of my journey.

Acknowledgements

I wanted to thank everyone at IST that helped me during these months of hard work, thanks to Ivy, Marta and Gemma for that funny lunch and coffee moments, thanks to my supervisors Luísa and Ana for letting me work in this research and specially thank you Inês, my partner in laboratory for all our conversations, for all your help and advices and for all the smiles that we shared day by day, you truly became a good friend of mine that I will remember when I return to my home, Valencia.

Also, I can't forget all the friends I made and all the teachers that helped me in my home university, UPV and specially this year to César, my roommate and friend here in this hard and special year in Lisbon, we've been through a lot during this year, and we surpassed it always with a smile and effort.

Abstract

Biomass is the carbon-based resource with the potential to produce energy and the most notable for synthesizing valuable chemicals that are currently produced from fossil fuels. The transformation of lignocellulosic biomass, mainly waste from agrochemical industries, requires the search for environmentally friendly and sustainable catalytic routes that reduce environmental impact, considering the principles of green chemistry. This work proposes the microwave-assisted oxidation of substrates derived from biomass, such as glycerol and the furfural derivatives, 5-(hydroxymethyl)furfural (HMF) and 5-hydroxymethyl-2-furancarboxylic acid (HFCA), and, with the use of green oxidants such as *tert*-butyl hydroperoxide (TBHP), using a graphene-supported C-scorpionate gold(III) complex as catalyst. The gold C-scorpionate complex is synthesised avoiding the use of solvents thanks to mechanochemical procedure using a ball mill. Other C-scorpionate metal (Co, Ni or Cu) complexes are also synthesised by ball milling. Graphene is produced by a Portuguese company in collaboration. In this project, the effects of the main reaction parameters such as temperature and reaction time, the ratio of the reactants and mechanochemical parameters are investigated. Synthesis (*e.g.*, mechanochemistry and liquid phase), and characterization and quantification techniques (*e.g.*, FTIR, XPS, NMR, SEM/EDS and elementary analysis) are used. The experimental work and dissertation were developed in 6 months.

Keywords

Sustainable catalytic chemistry; microwave-assisted oxidation; mechanochemical synthesis; metal C-scorpionate catalysts; glycerol; furfural

Resumo

A biomassa é um recurso baseado em carbono com potencial para produzir energia, e o mais notável para sintetizar produtos químicos valiosos que atualmente são produzidos a partir de combustíveis fósseis. A transformação da biomassa lignocelulósica, principalmente resíduos oriundos de indústrias agroquímicas, exige a procura de vias catalíticas ambientalmente corretas e sustentáveis que reduzam o impacto ambiental, atendendo aos princípios da química verde. Neste trabalho propomos a oxidação de substratos derivados da biomassa, como o glicerol e os derivados do furfural 5-(hidroximetil)furfural (HMF) and ácido 5-hidroximetil-2-furancarboxílico (HFCA), e, utilizando oxidantes verdes como o hidroperóxido de *tert*-butilo (TBHP) e um catalisador C-escorpionato de ouro(III) suportado em grafeno. O complexo C-escorpionato de ouro é sintetizado evitando o uso de solvente graças ao método mecanoquímico de moinho de bolas. Outros complexos C-escorpionato metálicos como cobre, níquel e cobalto são também sintetizados por mecanoquímica. O grafeno utilizado neste trabalho é produzido por uma empresa portuguesa, em colaboração. Neste projeto vão ser investigados os efeitos dos principais parâmetros de reação tais como temperatura e tempo reacionais, quantidade de catalisador, concentração dos reagentes e parâmetros específicos do moinho de bolas. São utilizadas técnicas de síntese (mecanoquímica e síntese em estado líquido), caracterização e quantificação (e.g., FTIR, XPS, RMN, SEM/EDS e elemental análise). O trabalho experimental e dissertação foram realizados em 6 meses.

Palavras-chave

Química catalítica sustentável; oxidação assistida por micro-ondas; síntese mecanoquímica; Catalisadores C-escorpionato metálicos; glicerol; furfural.

Table of Contents

Acknowledgements	vii
Abstract... ..	ix
Resumo.....	x
Table of Contents.....	xii
List of Figures.....	xiv
List of Tables.....	xvii
List of Abbreviations	xviii
List of Symbols.....	xix
1 Introduction.....	1
1.1 Environmental crisis	1
1.2 Green chemistry	2
1.2.1 Mechanochemistry.....	7
1.2.2 Microwave assisted reactions.....	8
1.3 C-scorpionate complexes	9
1.3.1 Metal C-scorpionate complexes	10
1.3.2 Heterogenization, importance and advantages.....	12
1.4 Graphene.....	13
1.5 Biomass valorisation.....	16
1.5.1 Glycerol oxidation	18
1.5.2 5-(Hydroxymethyl)furfural and 5-hydroxymethyl-2-furancarboxylic acid oxidation	20
1.6 Characterization methods.....	23
1.6.1 FTIR	23
1.6.2 XPS.....	24
1.6.3 Elementary Analysis	24
1.6.4 ¹ H NMR.....	24
1.6.5 SEM/EDS.....	25
2 Experimental procedure.....	26
2.1 Synthesis of C-scorpionate complexes.....	26
2.1.1 Copper C-scorpionate complex [CuCl ₂ (Tpm)] (1)	26
2.1.2 Nickel C-scorpionate complex [NiCl(Tpm)]Cl (2).....	29

2.1.3	Cobalt C-scorpionate complex [CoCl ₂ (H ₂ O)(Tpm)] (3).....	32
2.1.4	Gold C-scorpionate complex [AuCl ₂ (Tpm)]Cl (4)	34
2.2	Immobilization of [AuCl ₂ (Tpm)]Cl on graphene.....	37
2.2.1	Wet impregnation (WI).....	37
2.2.2	Microwave (MW).....	38
2.2.3	Liquid Assisted Grinding (LAG)	40
2.3	Microwave-assisted oxidation reactions	41
2.3.1	Glycerol microwave-assisted oxidation	41
2.3.2	Furfural derivatives microwave-assisted oxidation.....	43
3	Results and discussion	48
3.1	Copper C-scorpionate complex [CuCl ₂ (Tpm)] (1)	50
3.1.1	Characterization.....	50
3.2	Nickel C-scorpionate complex [NiCl(Tpm)]Cl (2)	54
3.2.1	Characterization.....	54
3.3	Cobalt C-scorpionate complex [CoCl ₂ (H ₂ O)(Tpm)] (3)	58
3.3.1	Characterization.....	58
3.4	Gold C-scorpionate complex [AuCl ₂ (Tpm)]Cl (4)	62
3.4.1	Characterization.....	62
3.4.2	WI graphene supported gold(III) C-scorpionate complex [AuCl ₂ (Tpm)]Cl (4)	69
3.4.3	MW supported gold(III) C-scorpionate complex [AuCl ₂ (Tpm)]Cl (4).....	73
3.4.4	LAG supported C-scorpionate gold(III) complex [AuCl ₂ (Tpm)]Cl (4).....	75
3.5	Glycerol microwave-assisted oxidation.....	78
3.6	HMF microwave-assisted oxidation	83
3.7	HFCA microwave-assisted oxidation	86
4	Conclusions and future work.....	88
5	References	99

List of Figures

Figure 1: The 12 principles of Green Chemistry [9].	2
Figure 2: Illustration of mechanochemical reactions [17].	7
Figure 3: Inverted temperature gradients in microwave versus oil-bath heating [19].	8
Figure 4: a) C-scorpionate tris(pyrazol-1-yl)methane binding to a metal centre; b) illustration of how a scorpion resembles the C-scorpionate [25].	9
Figure 5: Structure of complex $[\text{CuCl}_2(\text{Tpm})]$ (1) [40].	10
Figure 6: Structure of complex $[\text{NiCl}(\text{Tpm})]\text{Cl}$ (2) [41].	10
Figure 7: Expected structure of complex $[\text{CoCl}_2(\text{H}_2\text{O})(\text{Tpm})]$ (3).	11
Figure 8: Structure of complex $[\text{AuCl}_2(\text{Tpm})]\text{Cl}$ (4) [44].	11
Figure 9: Graphite structure [51].	13
Figure 10: Graphene structure [52].	13
Figure 11: Aerobic oxidation of methanol with Au-supported catalysts [60].	15
Figure 12: Transesterification process for biodiesel production [63].	17
Figure 13: Schematic representation of reaction pathways to 5-hydroxymethylfurfural [65].	17
Figure 14: Glycerol (1,2,3- propanetriol) structure.	18
Figure 15: Products from glycerol oxidation [62, 66].	19
Figure 16: Typical production routes of bio-based polymers from lignocellulosic biomass [64].	20
Figure 17: 2,5-Furandicarboxylic acid structure.	21
Figure 18: Reaction pathway of HMF oxidation to produce FDCA [64].	21
Figure 19: Oxidative production of FDCA from HMF over Gold NPs supported catalysts [64].	22
Figure 20: Structural parameters and kinetic effects on supported metal catalysts [72].	23
Figure 21: Grinding jar (Retsch® Planetary Ball Mill PM100) with reagents and spheres (left) and mortar (right).	27
Figure 22: Different samples of copper(II) C-scorpionate complex $[\text{CuCl}_2(\text{Tpm})]$ (1) obtained by Ball Milling (PGCuBM1-6) and manual grinding (PGCuM7).	28
Figure 23: Washing with methanol by filtering (left) and vacuum oven drying (right).	28
Figure 24: C-scorpionate copper(II) complex $[\text{CuCl}_2(\text{Tpm})]$ (1) samples obtained by ball milling (an L after name was added).	29
Figure 25: Product after ball milling experience, attached to the spheres.	30
Figure 26: Different samples of C-scorpionate nickel(II) complex $[\text{NiCl}(\text{Tpm})]\text{Cl}$ (2) obtained by Ball Milling (PGNiBM1-6) and manual grinding (PGNiM7) (up) and (down) washed and dried samples (PGNiBMn').	31
Figure 27: Grinding jar (Retsch® Planetary Ball Mill PM100) before (left) and after (right) ball milling of $\text{CoCl}_2 \cdot 6\text{H}_2\text{O} + \text{Tpm}$.	33
Figure 28: Different samples of C-scorpionate cobalt(II) complex $[\text{CoCl}_2(\text{H}_2\text{O})(\text{Tpm})]$ (3) obtained by Ball Milling (PGCoBM1-6) and manual grinding (PGCoM7) and washed and dried samples (PGCoBM2').	33
Figure 29: Grinding jar before (left) and after ball milling (centre) and the 3 first samples of C-scorpionate gold(III) complexes obtained by ball milling.	34
Figure 30: Different samples of gold(III) C-scorpionate complex $[\text{AuCl}_2(\text{Tpm})]\text{Cl}$ (4) obtained by Ball Milling (PGAuBM1-6) and manual grinding (PGAuM7).	36
Figure 31: C-scorpionate gold(III) complex $[\text{AuCl}_2(\text{Tpm})]\text{Cl}$ (4) traditional synthetic method.	36
Figure 32: WI method: under continuous stirring (left) and after separation and dryness (right).	37
Figure 33: MW method: before (left) and after separation and dryness (right).	38
Figure 34: Grinding jar with reaction mixture before (left) and after dryness (right).	40

Figure 35: 10 mL vial for MW reaction (left) and collected final reaction product in flask for its refrigerated storage (right).	41
Figure 36: a) 5-(hydroxymethyl)furan-2-carboxylic acid structure and b) 5-hydroxymethylfurfural or 5-hydroxymethyl-2-furaldehyde structure	43
Figure 37: Light-protected flask that contains final reaction product from HMF microwave-assisted oxidation.	44
Figure 38: Different samples of HFCA microwave-assisted oxidation before being stored.	45
Figure 39: Bruker Advance 300 MHz (left) and different oxidation samples with deuterated acetone for its characterization (right).	46
Figure 40: Synthesis of Complexes 1 – 4 from hydrotris(pyrazol-1-yl)methane and the appropriate different metal chlorides.	49
Figure 41: MIR spectrum of PGCuBM4L	50
Figure 42: FAR spectrum of PGCuBM4L	51
Figure 43: PGCuBM6L MIR spectrum.	51
Figure 44: FAR spectrum of PGCuBM6L	52
Figure 45: PGNiBM4 MIR spectrum.	54
Figure 46: PGNiBM4 FAR spectrum.	55
Figure 47: PGNiBM6' MIR spectrum.	55
Figure 48: PGNiBM6' FAR spectrum.	56
Figure 49: PGCoBM4 MIR spectrum.	58
Figure 50: PGCoBM4 FAR spectrum.	59
Figure 51: PGCoBM6 MIR spectrum.	59
Figure 52: PGCoBM6 FAR spectrum.	60
Figure 53: BMAu3L MIR spectrum.	62
Figure 54: BMAu3L FAR spectrum.	63
Figure 55: [AuCl ₂ (Tpm)]Cl synthesised by traditional method MIR spectrum.	63
Figure 56: [AuCl ₂ (Tpm)]Cl synthesised by traditional method FAR spectrum.	64
Figure 57: SEM and EDS for the gold(III) complex. a) and b) represent ball milling and c) and d) traditional method reported in [44].	67
Figure 58: SEM and EDS of the carbon supports a) and b) are graphene and c) and d) are ultra-pure graphene.	70
Figure 59: SEM and EDS of the gold complex made by the wet impregnation method with carbon supports. a) and b) are graphene and c) and d) are ultra-pure graphene.	72
Figure 60: SEM and EDS of the gold complex made by the MW method with carbon supports. a) and b) are graphene and c) and d) are ultra-pure graphene.	74
Figure 61: SEM and EDS of the gold complex made by the LAG method with carbon supports. a) and b) are graphene and c) and d) are ultra-pure graphene.	76
Figure 62: The deformed spheres	77
Figure 63: Oxidation of glycerol to dihydroxyacetone.	78
Figure 64: DHA yield for the different homogeneous (red) and heterogeneous(blue) conditions for the glycerol oxidation.	81
Figure 65: The influence of temperature (80°C and 50°C) and support being ultra-pure graphene (left) and graphene(right) on DHA yield.	81
Figure 66: Influence of catalyst amount in DHA yields, under the same reaction conditions. ...	82
Figure 67: DHA yield for original vs. recovered catalyst.	83
Figure 68: 5-Hydroxymethylfurfural oxidation to furan-2,5-dicarbaldehyde.	83
Figure 69: Graphic showing different catalysts used in HMF oxidation and its DFF yields.	84
Figure 70: DFF yield for original vs. recovered catalyst.	85
Figure 71: 5-hydroxymethyl-2-furancarboxylic acid oxidation to 5-formylfuran-2-carboxylic acid.	86
Figure 72: Influence of temperature on HFCA oxidation.	87

List of Tables

Table 1: Representative specific areas for different type of materials [55].....	14
Table 2: Composition of lignocellulose; elemental composition of moisture and ash-free (maf) LC: 50 wt% C, 6 wt% H, 44 wt% O [61].	16
Table 3: Synthetic conditions used in the preparation of the C-scorpionate copper(II) complex [CuCl ₂ (Tpm)] (1) and corresponding yields.	27
Table 4: Different synthetic conditions used in the preparation of the C-scorpionate nickel(II) complex [NiCl(Tpm)]Cl (2) and corresponding yields.	30
Table 5: Different synthetic conditions used in the preparation of the C-scorpionate cobalt(II) complex [CoCl ₂ (H ₂ O)(Tpm)] (3) and corresponding yields.....	32
Table 6: First synthetic conditions used in the preparation of the C-scorpionate gold(III) complex [AuCl ₂ (Tpm)]Cl (4) and corresponding yields.	34
Table 7: Synthetic conditions used in the preparation of the C-scorpionate gold(III) [AuCl ₂ (Tpm)]Cl (4) and corresponding yields.	35
Table 8: Synthetic conditions used in the WI immobilization of C-scorpionate gold(III) [AuCl ₂ (Tpm)]Cl (4) on two different graphenes.....	38
Table 9: Synthetic conditions used in the MW immobilization of C-scorpionate gold(III) [AuCl ₂ (Tpm)]Cl (4) on two different graphenes.....	39
Table 10: Synthetic conditions used in the LAG immobilization of C-scorpionate gold(III) [AuCl ₂ (Tpm)]Cl (4) on two different graphenes.....	40
Table 11: Glycerol microwave-assisted oxidation samples.	42
Table 12: HMF microwave-assisted oxidation samples.....	44
Table 13: Different HFCA microwave-assisted oxidation samples.....	46
Table 14: Best mechanochemical conditions for the synthesis of complexes 1-4.....	48
Table 15: Comparison between theoretical values and those obtained in elementary analysis.	53
Table 16: Comparison between theoretical values and those obtained in elementary analysis.	57
Table 17: Comparison between theoretical values and those obtained in elementary analysis.	61
Table 18: Comparison between theoretical values and those obtained in elementary analysis.	65
Table 19: XPS global quantification of gold(III) C-scorpionate complex [AuCl ₂ (Tpm)]Cl (4).....	68
Table 20: Glycerol oxidation using homogeneous conditions.....	79
Table 21: Glycerol oxidation using heterogeneous conditions.	80
Table 22: HMF MW-assisted oxidation conditions and results.	84
Table 23: HFCA MW-assisted oxidation conditions and results.....	86

List of Abbreviations

CNTs	Carbon Nanotubes
DFF	2,5-Diformylfuran /2,5-Furandicarboxaldehyde
DHA	Dihydroxyacetone
EG	Ethylene glycol
ESCA	Electron Spectroscopy for Chemical Analysis
FA	Formic acid
FDCA	2,5-Furandicarboxylic acid
FFCA	5-Formyl-2-furancarboxylic acid
FTIR	Fourier-transform infrared
GHG	Green House Gas
GLYA	Glycerid acid
GLYCA	Glycoic acid
HFCA	5-Hydroxymethyl-2-furancarboxylic acid
HMF	5-(Hydroxymethyl)furfural
LC	Lignocellulose
LCB	Lignocellulosic Biomass
maf	Moisture and ash free
MCM-41	Mobil Composition of Matter No. 41
MOF	Metal Organic Framework
MW	Microwave
NMR	Nuclear Magnetic Resonance
NP	Nanoparticle
NSP	Non-starch polysaccharides
OXA	Oxalic acid
PEF	Polyethylene 2,5-furandicarboxylate
PET	Polyethylene terephthalate
PMO	Periodic Mesoporous Organosilicas
rGO	Reduced Graphene Oxide
RPM	Rotations per minute
TA	Tartronic acid
TBHP	<i>tert</i> -Butyl hydroperoxide
TOF	Turnover frequency
TON	Turnover number
TPA	Terephthalic acid
Tpm	Hydrotris(pyrazol-1-yl)methane
XPS	X-ray Photoelectron Spectroscopy
ZSM	Zeolite Socony Mobil

List of Symbols

δ Chemical shift

ν Vibration

1 Introduction

This first chapter starts with a brief introduction of the current environmental crisis and different chemical routes for confronting it. Different mechanisms that are related to green chemistry are presented with their currently state-of-the-art, as well as information about the raw materials that are used in this project. C-scorpionates, graphene and biomass derived materials like glycerol and furfural derivatives will be introduced. Follows different characterization techniques that are mentioned to understand why they were chosen to this work.

1.1 Environmental crisis

Global warming is presented nowadays as one of the humanity's major concerns with the depletion of fossil fuel resources, the continuous generation of greenhouse gas (GHG) emissions and the dramatic increase of the world population (near 8 billion people) [1]. Big part of these GHG emissions is related to the huge amount of waste generated. Only in Europe in 2018, the total waste generated by all economic activities and households amounted to 2 317 million tons. [2]. As waste potentially represents an enormous loss of resources in the form of both materials and energy, different options for reducing, recycling, and reusing the waste are indispensable weapons against this waste problematic. Not only the waste but the use of fossil fuels is also an important problem related to this huge amount of GHG emissions. Following the idea of finding alternatives to the energy that is produced is also a trending topic of the last and future years. The use of greener fuels is identified as one of the most promising solutions, leading to a competitive, energy efficient, and low carbon future. A new sustainable alternative to traditional petrochemical feedstock processes can be attained by using organic wastes as feedstock for producing fuel, that is critically important, particularly to the transport sector but also in chemical industry where a major part of commodity chemicals come from fossil fuel resources [3].

Biomass appears as one of the most promising resources to produce biofuel and fine chemicals. The main advantage of using biomass is its renewable nature: 75% of biomass consists of carbohydrates and 20% consists of lignin, and the remaining fraction consists in fats, oils, proteins, terpenes, and waxes. [4]

Following the idea to promote and improving biofuels production and using biomass to produce valuable products, this dissertation cases of study are the oxidation of glycerol and the furfural derivatives 5-(hydroxymethyl)furfural (HMF) and 5-hydroxymethyl-2-furancarboxylic acid (HFCA) using greener techniques that also allows to use less or no solvents. Glycerol, that is an important by-product of biodiesel manufacture, is produced in significant amounts by transesterification of triglycerides with methanol and can be used as feedstock to produce high-added-value products [5]. On the other hand, the furfural derivatives, produced by glucose or fructose dehydration, can be a key reagent to produce many important products as polymers, pharmaceuticals, solvents, and fuels [6]. Herein, we have performed the microwave (MW) assisted oxidation of glycerol and of the furfural derivatives 5-

(hydroxymethyl)furfural and 5-hydroxymethyl-2-furancarboxylic acid (HFCA) with *tert*-butyl hydroperoxide (TBHP). All reactions were catalysed by a C-scorpionate gold(III) complex in homogeneous conditions and supported on graphene, to compare the performance in both conditions.

1.2 Green chemistry

Green chemistry is a term that indicates the creation of chemical products and procedures that reduce the utilization and production of harmful materials. The goals of green chemistry for safeguarding the environment are often achieved via many main directions. Some of them are biocatalysis, use of alternative renewable raw materials (biomass), alternative reaction solution (such as ionic liquids, supercritical fluids, water), alternative reaction conditions (mechanochemistry, microwave activation) further on new photocatalytic reactions [7]. Moreover, keep natural resources on earth without using harmful materials is the main objective of green chemistry.

The concept emerged in the 1990s by Paul Anastas and John Warner [8] when they created twelve principles (Figure 1) [9, 10, 11] to guide both industry and researchers to reduce the environmental impact and the negative effects of chemicals on public health.

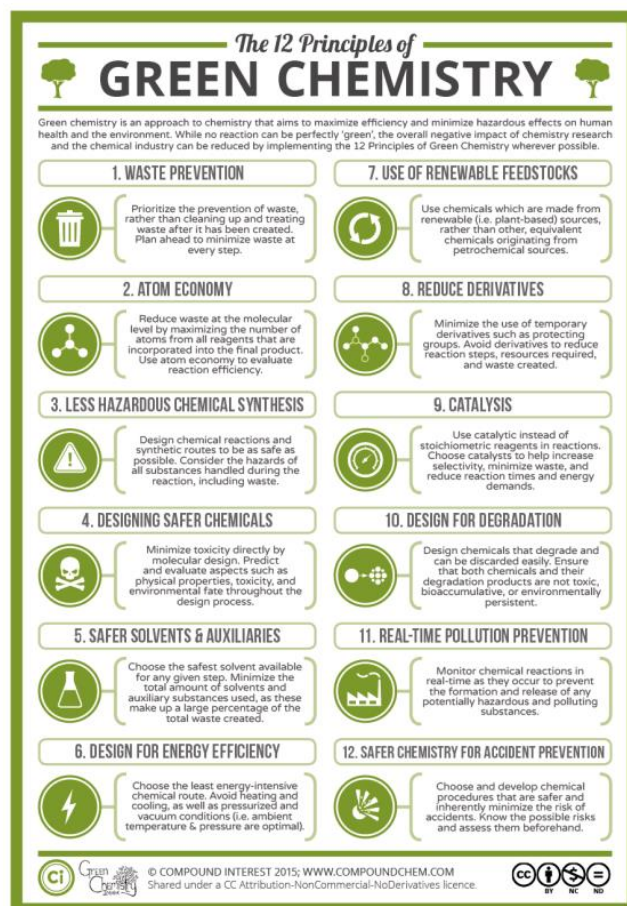


Figure 1: The 12 principles of Green Chemistry [9].

1. Waste prevention

Chemical processes should be optimized to produce the minimum amount of waste possible. A metric, known as the environmental factor (or E factor for short), was developed to take into account the amount of waste a process created, and is calculated by simply dividing the mass of waste the production process produces by the mass of product obtained, with a lower E factor being better.

$$E \text{ factor} = \frac{\text{kg waste produced}}{\text{kg product obtained}} \quad \text{Eq. 1}$$

As it can be seen, an E factor of 0 would be the ideal result as it would be a production free of waste production, while the greater the E-factor, the greater the production of waste in the obtaining the desired product.

Inside the chemical industry drug production processes had notoriously high E factors, but the application of some of the other green chemistry principles can help to reduce this [12]. Other methods of assessing amounts of waste, such as comparing the mass of the raw materials to that of the product, are also used.

2. Atom economy

Is the measure of the number of atoms from the starting material that are present in the useful products at the end of the process. By-products from reactions that are not useful can lead to a lower atom economy which means also more waste. Atom economy is defined as the percentage mass of the atoms of the reagents that is present in the main products:

$$\text{Atom economy}(\%) = \frac{\text{amount of atoms in final product}}{\text{amount of atoms in all reagents}} \cdot 100 \quad \text{Eq. 2}$$

In many ways, atom economy is a better measure of reaction efficiency than the yield of the reaction; the yield compares the amount of useful product obtained compared to the amount you would theoretically expect from calculations. Therefore, processes that maximise atom economy are preferred.

3. Less hazardous chemical synthesis

During the syntheses, the use of dangerous products, as well as the formation of them, is something that should be avoided. However, not always being possible, many reactions use toxic or dangerous chemicals.

Ideally, it is wanted that the chemicals we create for whatever purpose do not represent a health hazard to humans. Also, it's wanted to make the synthesis of chemicals as safe as possible, so the aim is to avoid using hazardous chemicals as starting points if safer alternatives are available. Additionally, having hazardous waste from chemical processes is something we want to avoid, as this can cause problems with disposal. Occasionally, chemists do produce molecules that have toxic or other hazardous effects, and the next principle will have something to say about designing safer molecules.

4. Designing safer chemicals

This principle requires that the chemist has knowledge not only of chemistry, but also of environmental toxicology (as is that the compound affects the environment) and human (the physiological effect of it due to exposure).

5. Safer solvents and auxiliaries

Most chemical reactions happen in the presence of solvent and/or other additives that promote the reaction. The solvent is responsible for between 50-80% of the reaction volume and for mass and energy transfer. The choice of solvent is in fact an important choice for the safety of the process: they are responsible for most of the energy consumption (reaction, distillation, vacuum drying, pumps). Therefore, the solvent must be such that it allows heat and mass exchanges easily (reducing the energy consumption), have low or no risk of flammability, volatility, or explosion, be possible to reuse and safe to release into the environment having little impact on the stability of the same.

6. Design for energy efficiency

Energy-intensive processes must be avoided in green chemistry. Where it is possible, it is better to minimise the energy used to produce a chemical product, by carrying out reactions at mild conditions. Considerations of the reaction design also must be made as removal of solvents, or processes to remove impurities can increase the energy required, and by association increase the process's environmental impacts.

7. Use of renewable feedstocks

The extensive use of natural resources as raw material, without having considered the speed at which they can be replaced, it is simply unsustainable in the long term, both economic and environmental. High fossil fuel consumption not only endanger their availability for future generations, but also entails high environmental impacts for present and future generations [11].

Biomass resources, such as agro-industry waste, as well as solar energy, are a good alternative due to their wide availability. The technical challenge in the use of such renewable raw materials is the development of new non-toxic processes that convert biomass into useful chemical products, in such a way that they generate fewer environmental impacts, especially with a more positive balance in the generation of GHG, compared to those generated using fossil fuels. Also, most solvents used in the chemical industry come from fossil resources and they should be replaced to renewable solvents. Many of these solvents, called renewable solvents or bio-solvents like solvents based in lactic acid [13], have low toxicity, low volatility, are not corrosive and are not carcinogenic. Furthermore, many of them are obtained from plant waste, which makes them economically competitive. In this way, principles 5 and 7 of the Green Chemistry are also applied.

8. Reduce derivatives

It often happens that the chemical reactions necessary to obtain a final product are part of a process that involves several steps. During them, it is often necessary to modify or protect parts or groups of the molecule, which would not resist or would be affected by the aggressiveness of a chemical medium or a particular reagent. In such cases, different substances are used, such as the so-called blocking groups, to protect a sensitive part of the molecule; or substances that are used so that the product acquires a certain property or is formulated in a certain way (for example, a salt), or the reagents used for substitution reactions, are some examples of commonly used derivatives. These substances only participate in a stage of the synthesis process and are not part of the final product, therefore they become by-products or waste. So, this principle urges to minimize the use of this type of chemical agents.

9. Catalysis

Stoichiometric reagents are generally used in excess, only once, and their selectivity is not always good nor are they always part of the final product, obtaining by-products that increase the generation of waste.

Catalysts can improve that problem as they can enable reactions with higher atom economies. Catalysts themselves are not consumed by chemical processes, and they can be recycled many times over, contributing to generate less waste. They can allow for the utilisation of reactions which would not proceed under normal conditions, but which also produce less waste.

10. Design for degradation

According to the principles of green chemistry, the ideal compound would be one that, when it had fulfilled its purpose, disintegrates into non-harmful products with no environmental impact or public health.

Organic products become pollutants because they accumulate in the atmosphere forming ozone in the lower layers of the atmosphere or decomposing it at the top of the same as the famous CFCs. These can be replaced by compounds that decompose in water, through UV radiation or through biological means.

11. Real time pollution prevention

Careful control and monitoring of chemical processes, in real time, is essential for safe and efficient operation with minimal waste. This goal has been made much more accessible by modern automated controls. However, a precise knowledge of the concentration of substances and by-products in the system, measured continuously, is required.

Therefore, the successful practice of Green Chemistry requires monitoring or evaluation techniques in real time, coupled with process control, to detect even trace levels or very small amounts of unwanted toxic substances, to be able to adjust the reaction parameters.

12. Safer chemistry for accident prevention

It is better to avoid the use or generation of substances that are likely to react violently, develop excessive pressure, cause burns, or, in any way, cause unforeseen accidents when they are used in industry.

To achieve this principle, it is possible to choose solids over liquids, or substances with low vapor pressure instead of volatile liquids or gases, which are associated with most chemical accidents.

It is also very important in the task of preventing accidents, training, and knowledge by all personnel of an industry of the inherent risks of each substance, how to act in the event of an accident, how to use elements to control a fire, know the causes and factors associated with said accident and all relevant information in this regard. Setting up security protocols, restricted entry to certain work areas, emergency evacuation planning, emergency exits, etc., are some of the measures that are implemented to minimize the risk of accidents.

All the procedures made in this thesis aimed at to be aligned with the principles of the green chemistry: prioritizing the prevention of waste rather than cleaning up and treating waste after it has been created (1); reducing the waste at the molecular level by maximizing the number of atoms from all reagents that will be incorporated into the final product (2) (excess reagents were not used); designing chemical reactions and synthetic routes to be as safe as possible, minimizing the toxicity and choosing safest solvents available (or no solvents in our case in mechanochemistry or MW-assisted reactions) (3-5). Thanks to the use of microwave-assisted reaction, less energy-intensive chemical route was used (6). Commercial glycerol and furfural derivatives were used as model raw materials, but they can come from lignocellulosic feedstock and can be reused (7,10); no temporary derivatives were used (8) and the study of the catalysed oxidations was the main goal of this study (9). Finally, again thanks to microwave-assisted reaction monitoring the chemical reaction is possible and it is possible to have a safe control of the reaction performance (11,12).

1.2.1 Mechanochemistry

As a representative new technique of green chemistry, mechanochemistry was known by IUPAC like one of the top 10 world-changing chemistry innovations [14]. This enabling technology is characterised by mechanical grinding of reactants and induces chemical reactivity by mechanical force (e.g., by compression, shear, or friction, Figure 2). In general, mechanochemical procedures provide advantages like preventing the utilization of excessive solvent, enabling short reaction time, high efficiency, unique reactivity, and unlocks an alternative route toward numerous compounds not achievable by alternative synthetic techniques [15].

There are several benefits of mechanochemical methods over solution-based wet process. Mechanochemical processing not only circumvents the need of reagents solubility and large consumption of solvent, but additionally avoids complicated post-treatment steps such as solvent removal and product purification [16].

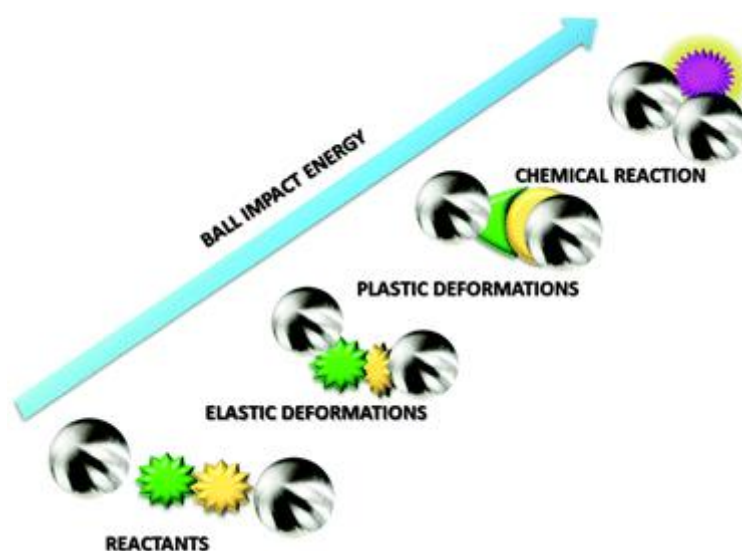


Figure 2: Illustration of mechanochemical reactions [17].

Despite the remarkable capability in biomass valorisation of mechanochemistry, the intake of energy is still too high to scale-up. Instead, combining mechanical milling with other technology to reduce energy consumption could, in addition, improve the performance and may be the way forward [16]. That is why ball milling-assisted synthesis and liquid assisted grinding synthesis (LAG) can be widely used in other applications such as energy storage, adsorbents, and synthesis of catalysts. This last application is the one that was part of the study of this project.

1.2.2 Microwave-assisted reactions

Microwave technologies have been showed up to be efficient to get better reaction yields and product selectivity comparing to conventional methods during the last years [18]. There are many advantages of microwave-assisted reactions [19]:

- Microwave processing frequently gives reduced reaction times, higher yields, and cleaner reaction profiles.
- The monitoring for temperature and pressure in allows an excellent control of reaction parameters, which generally leads to more reproducible reaction conditions.
- The overall process is more energy efficient than classical oil-bath heating, as direct “in-core” heating of the medium happens (Figure 3).

Among the advantages of microwave assisted reactions, fast heating rates, uniform temperature and easy reaction control can be highlighted.

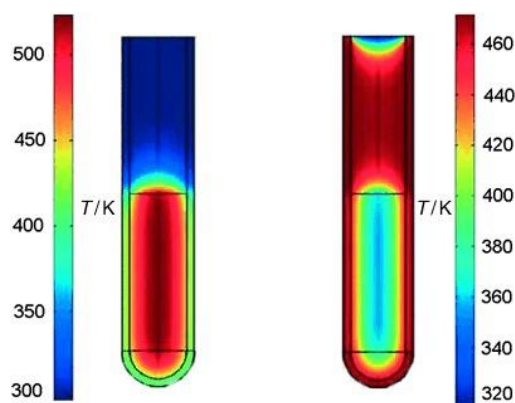


Figure 3: Inverted temperature gradients in microwave versus oil-bath heating [19] : Difference in the temperature profiles (finite element modelling) after 1 min of microwave irradiation (left) and treatment in an oil-bath (right). Microwave irradiation raises the temperature of the whole volume simultaneously (bulk heating) whereas in the oil-heated tube, the reaction mixture in contact with the vessel wall is heated first.

1.3 C-scorpionate complexes

C-scorpionate complexes (Figure 4) are known as one of the few mononuclear types of metal compounds that can catalyse the oxidation of hydrocarbons like xylene [20], secondary alcohols [21], ketones [22] and alkenes [23]. They can be used as homogeneous or heterogeneous catalysts and in the last years their application has experienced interesting advances [24] due to C-scorpionate ligands and their stability toward hydrolysis [23]. The scorpionate designation represents the parallel between the tris(pyrazol-1-yl)methane metal (M) binding and the scorpion attack. Like the pincers of a scorpion, tris(pyrazol-1-yl)methanes bind to metal centres through the nitrogen heteroatoms of two pyrazolyl rings, and the third pyrazolyl group may (or may not) rotate forward to “sting” the metal (Figure 4).



Figure 4: a) C-scorpionate tris(pyrazol-1-yl)methane binding to a metal centre; b) illustration of how a scorpion resembles the C-scorpionate [25].

C-scorpionates, RCp_3 (pz = pyrazolyl, R = H or substituent at the methine carbon atom), were first reported by Hückel *et al.* in 1937 [26] and many years later in 1966, anions, tris(pyrazol-1-yl)borate (RBp_3^-) and di(pyrazol-1-yl)borate ($R_2Cp_3^-$) were synthesized for the first time by Trofimenko [27]. These compounds are called scorpionates, due to their structure and binding mode to a metallic centre in a coordination compound (Figure 4). In 1967, Jesson [28] was the one who reported Co(II) and Ni(II) chelate systems of both ligands.

However, there were very low yields on the synthesis of C-scorpionates until Elguero *et al.*, improved the synthetic strategy known at that moment for the production of hydrotris(pyrazol-1-yl)methane and functionalized derivatives [29]. The introduction of microwave-assisted synthesis for the production of tris(pyrazol-1-yl)methanes played an important role on the development of this promising class of ligands [30], for which, in the last decades have attracted considerable interest with their application in bio-inorganic, organic and catalytic chemistry [20, 23, 24]. With carbon scorpionates, several complexes are reported, including zinc [31], vanadium [32], iron [33], rhenium [34], copper [35], molybdenum [36], silver [37], ruthenium [38], among others, including gold.

1.3.1 Metal C-scorpionate complexes

Four different metal C-scorpionate complexes are synthesised in this work, trying to avoid the use of solvents on their synthesis. The simplest member of the C-scorpionate class, the hydrotris(pyrazol-1-yl)methane, HC(pz)₃ (Tpm, pz = pyrazolyl ring), was chosen.

The first complex to be synthesised in this work was the copper one, [CuCl₂(Tpm)] (1) (Figure 5). It was recently reported as a promising green catalyst in the oxidation of styrene to benzaldehyde [39] with hydrogen peroxide (H₂O₂) in an ultra-fast way, achieving 70% of yield after 5 min of reaction at 80 °C (TOF, 1.4·10⁴ h⁻¹). The oxidation method developed by Duarte et al. presents the highest catalytic activity (TOF) of all reported catalysts (e.g., metal complexes with Schiff bases, porphyrins, salen, polyoxo- or N-ligands) for the oxidation of styrene with hydrogen peroxide and provides an easy method for catalyst separation at the end of the reaction by cooling down the reaction media followed by centrifugation. However, during the workup [CuCl₂(Tpm)] (1) undergoes decomposition impairing its reuse.

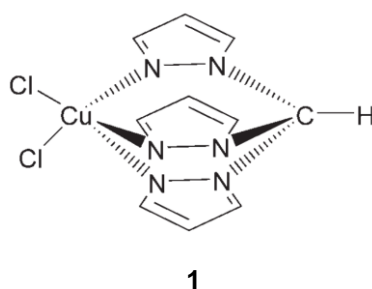


Figure 5: Structure of complex [CuCl₂(Tpm)] (1) [40].

Nickel C-scorpionate complexes, as the [NiCl(Tpm)]Cl depicted on Figure 6, were reported [41] as promising low-cost metal catalysts to replace the palladium ones towards the development of sustainable Heck C-C coupling synthesis. Among the several requirements for a suitable catalyst, its recyclability with possibility to be used in consecutive cycles is often crucial for an economically feasible process. Another important issue in sustainable catalytic processes concerns the use of solvents. Thus, in this work, both issues were addressed, as said before, by trying to synthesise it by mechanochemistry.

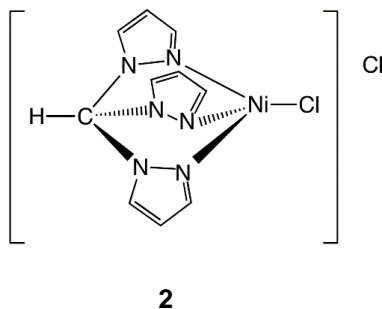


Figure 6: Structure of complex [NiCl(Tpm)]Cl (2) [41].

Some cobalt complexes bearing scorpionate ligands were reported [42] along with their effects on DNA and catalytic ability but, to the best of our knowledge, no cobalt half-sandwich C-scorpionate $\text{HC}(\text{pz})_3$ (Tpm, pz = pyrazolyl ring) has been reported in the literature. Thus, in this work is the first time that the synthesis of complex $[\text{CoCl}_2(\text{H}_2\text{O})(\text{Tpm})]$ (**3**) (Figure 7) is tried. Mechanochemical methods were chosen for this synthesis.

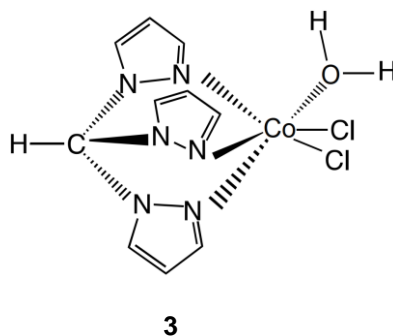


Figure 7: Expected structure of complex $[\text{CoCl}_2(\text{H}_2\text{O})(\text{Tpm})]$ (**3**).

The first gold complexes with scorpionates appeared in 1982 by Canty *et al.*, [43]. In 2001 boron scorpionates were complexed with gold and it was only in 2013 by Martins *et al.* [44] that C-scorpionates are again complexed with gold. An example is depicted in Figure 8:

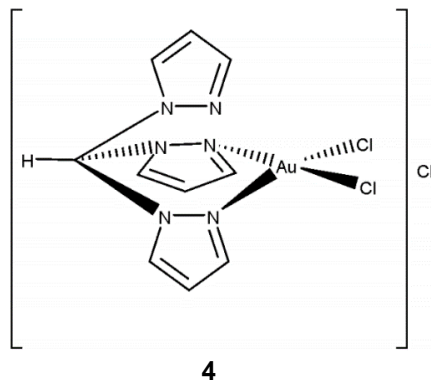


Figure 8: Structure of complex $[\text{AuCl}_2(\text{Tpm})]\text{Cl}$ (**4**) [44].

Organometallic gold complexes have experienced great success as catalysts for several reactions such as hydrogenation, low temperature CO oxidation and selective oxidations like oxidation of alcohols, aldehydes, and epoxidations, among others [45].

1.3.2 Heterogenization, importance and advantages

The design of environmental and economically better catalytic processes for selective oxidations additionally addresses catalysts stability and their reuse, aiming to overcome issues presented by the current homogeneous systems. The chance of mixing the benefits of homogeneous and heterogeneous catalysts by the immobilization of metal complexes on solid supports is thus of great importance [23].

Some advantages of heterogeneous catalysis over homogeneous, taking into account the importance of the easier recycling of the catalyst for the heterogeneous one, are as follows [46]:

1. The scope for introducing multifunctional catalysts is greater with heterogeneous than with homogeneous catalysts.
2. The nature of the active sites in heterogeneous catalysis is immobilized, avoiding certain deactivation processes.
3. Certain chemical transformations can be performed efficiently only with heterogeneous catalysts.
4. Heterogeneous catalysts are generally stable and easy to prepare.

A general strategy to convert a homogeneous process into a heterogeneous one is to support the soluble C-scorpionate metal catalyst onto a solid matrix [47]. To this purpose, many sorts of materials can be used, being the zeolitic and carbon materials obtained by different approaches most recently proposed in the literature [48]. It has been reported [48] that recovering the catalyst from the reaction mixture (cyclohexane oxidation with hydrogen peroxide) by an easy filtration and reusing it without loss of activity for five consecutive cycles (it was at the sixth cycle when the activity dropped to 94%) while maintaining the high selectivity of the reaction is possible.

In the next subsection, graphene as a solid matrix suitable for gold support will be highlighted, as is the purpose in the current study.

1.4 Graphene

Although the existence of graphene was better-known since the first years of the twentieth century, throughout the development of X-ray diffraction as a crystallographic technique by Henry and L. Bragg [49], interest in this material has appeared with much bigger force thanks to the grant of the Nobel prize in Physics to A. Geim and K. Novoselov [50] who managed to isolate an individual layer of graphene and study its electrical conductivity in 2010. During the starting years of the development of crystallography, following the discovery of X-rays by Röntgen in the last years of the nineteenth century, graphite (Figure 9) was one of the materials whose structural study attracted so much attraction for its simplicity.

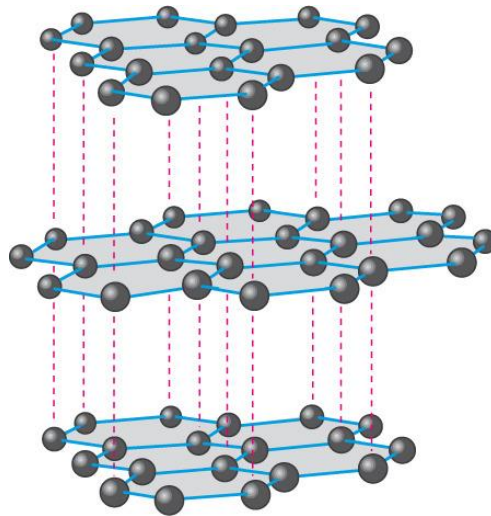


Figure 9: Graphite structure [51].

By means of X-ray crystallography it had been possible to determine that graphite is constituted by the stacking of carbon sheets that receive the name of graphene. Graphene is a layer made of carbon atoms in a hexagonal arrangement (Figure 10) [47].

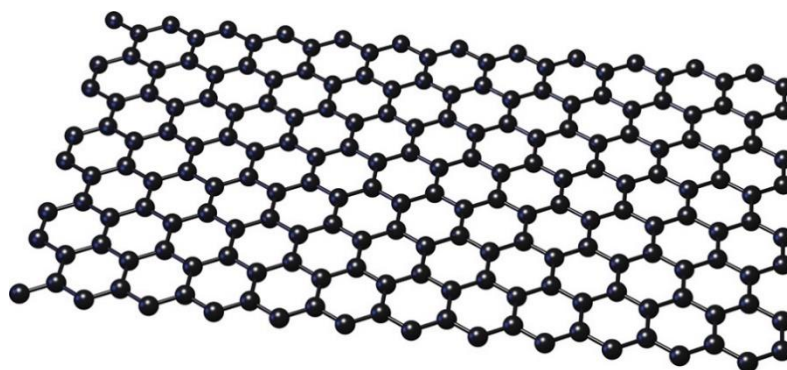


Figure 10: Graphene structure [52].

From the physical point of view, graphene represents the limit of the ideal concept of surface where the thickness has been taken to the minimum possible limit. It is known that many physical and chemical properties of materials derive from their surface properties, in particular surface area and electron density. Thus, it has been established that the theoretical specific surface area of graphene should be $2630 \text{ m}^2 \text{ g}^{-1}$ and in this material all the atoms would be superficial and accessible to interact with adsorbates [53, 54].

This surface area value is one of the highest among those described for any type of material and compares favourably with the surface area described for materials that have been considered as exhibiting elevated specific surface areas. Table 1 summarizes some of the specific areas that have been described for various types of materials.

Table 1: Representative specific areas for different type of materials [55].

Material	BET area (m^2g^{-1})
ZSM-5 Zeolite	251
Zeolite Y	675
TiO ₂ NP	47
CeO ₂ NP	93
MCM-41	1031
PMO	1170
Activated Carbon (Norit)	1200
MOF MIL-101	4000

The importance of the surface area derives from the fact that it indicates the part of a material that can interact with molecules by adsorbing them (adsorption capacity) or promoting changes or reactions of these molecules (heterogeneous catalysis). Thus, a common property of solid adsorbent materials or catalysts is the high surface area that they present and that, together with the electron density on these surfaces and the presence of functional groups may be responsible for adsorption or catalysis phenomena [55].

Most of the works where the use of graphene in catalysis is described, these materials are used as supports for nanoparticles (NPs), the direct use of graphene as a carbocatalyst represent a much lower percentage of cases [56]. There is a great tradition in heterogeneous catalysis where activated carbons are used as metal supports [57].

Thus, graphene has been found to be a suitable support for metallic NPs, including NPs of Pt, Pd, Au (Figure 11), Ru, Ni, Cu, as well as their oxides. The characteristics of graphene, particularly, high surface area, π -extended orbital available for interaction and the ease of dispersion in liquid phases, determine that there are great number of studies in the literature [58, 59] showing that the catalytic activity of metal NPs and metal oxides supported on graphene is higher than that achieved when NPs of this same metal, with similar size and the same charge, are supported on another type of materials including activated carbons, nanotubes of single or multiple wall carbon, high area metal oxides, etc.

		<i>Catalyst</i>	<i>Conversion (%)</i>	<i>Selectivity (%)</i>	<i>TOF (h⁻¹)</i>
CH ₃ OH	Catalyst →	Au ₁ -Pd ₂ /rGO	90	100	0.377
		Au ₁ -Pd ₂ /Al ₂ O ₃	75	41	0.011
		Au ₁ -Pd ₂ /TiO ₂	34	20	0.002
		Au ₁ -Pd ₂ /CNTs	17	100	0.072

Figure 11: Aerobic oxidation of methanol with Au-supported catalysts [60].

A recent PhD thesis reported the use of gold in graphene that has been doped with nitrogen by pyrolysis of nanometric films on quartz, under an inert atmosphere at 900 °C of HAuCl₄ absorbed on chitosan [55].

In our case, mild conditions and normal graphene will be used to make the support happen, moreover, the same gold precursor will be used to produce the gold complex of Figure 8.

1.5 Biomass valorisation

As above presented, the current fossil fuel share of 80% and maintaining business at actual level, the growing world population will use all the proved and achievable economically recoverable coal, oil and gas reserves in no more than a century [61]. Although, it is possible to delay this to happen by improving the current energy efficiency, exploring of new fossil reserves, but preferably above all, a rapid development and market introduction of renewable energies.

We are already experiencing the long and complex transition period to renewables where biomass plays a unique and pivotal role as the only renewable carbon source to produce carbon products, fine chemicals, and hydrocarbon fuels [61].

Lignocellulosic biomass (LCB) like straw or wood is the main component of the rigid construction material of the cell walls of all terrestrial plants being almost 90% the most abundant type of land biomass. The major constituents of lignocellulose are the ones as presented in the following Table 2:

Table 2: Composition of lignocellulose; elemental composition of moisture and ash-free (maf) LC: 50 wt% C, 6 wt% H, 44 wt% O [61].

Component	Value (wt%)
Cellulose	40-50
Hemicellulose	20-30
Lignin	15-25
Water	<15
Ash	0.5
Heteroatoms	NSP low

Being Lignocellulosic biomass (LCB) the most abundant type of land biomass, the major chemical conversion routes on biorefineries are based on LCB. LCB is quite abundant in the natural world with a wide geographical distribution and can thus be explored to produce green bio-based chemicals. LCB is usually available in the forms of crop residues, forest leftovers, wastepaper etc. The use of LCB as a feedstock for the biorefinery will reorient the global chemical industry and boost rural economy.

Glycerol appears as an important by-product of biodiesel production from LCB, and it is produced in significant amounts by transesterification of triglycerides with methanol (Figure 12) [62].

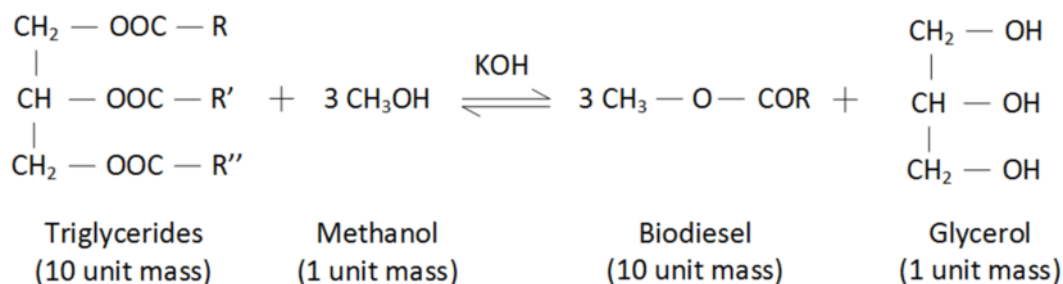


Figure 12: Transesterification process for biodiesel production [63].

On the other hand, 5-(hydroxymethyl)furfural (HMF) is also presented as an important monomer that can be obtained from LCB (Figure 13) to produce an interesting precursor of polyethylene 2,5-furandicarboxylate (PEF) such as furan dicarboxylic acid (FDCA) [64].

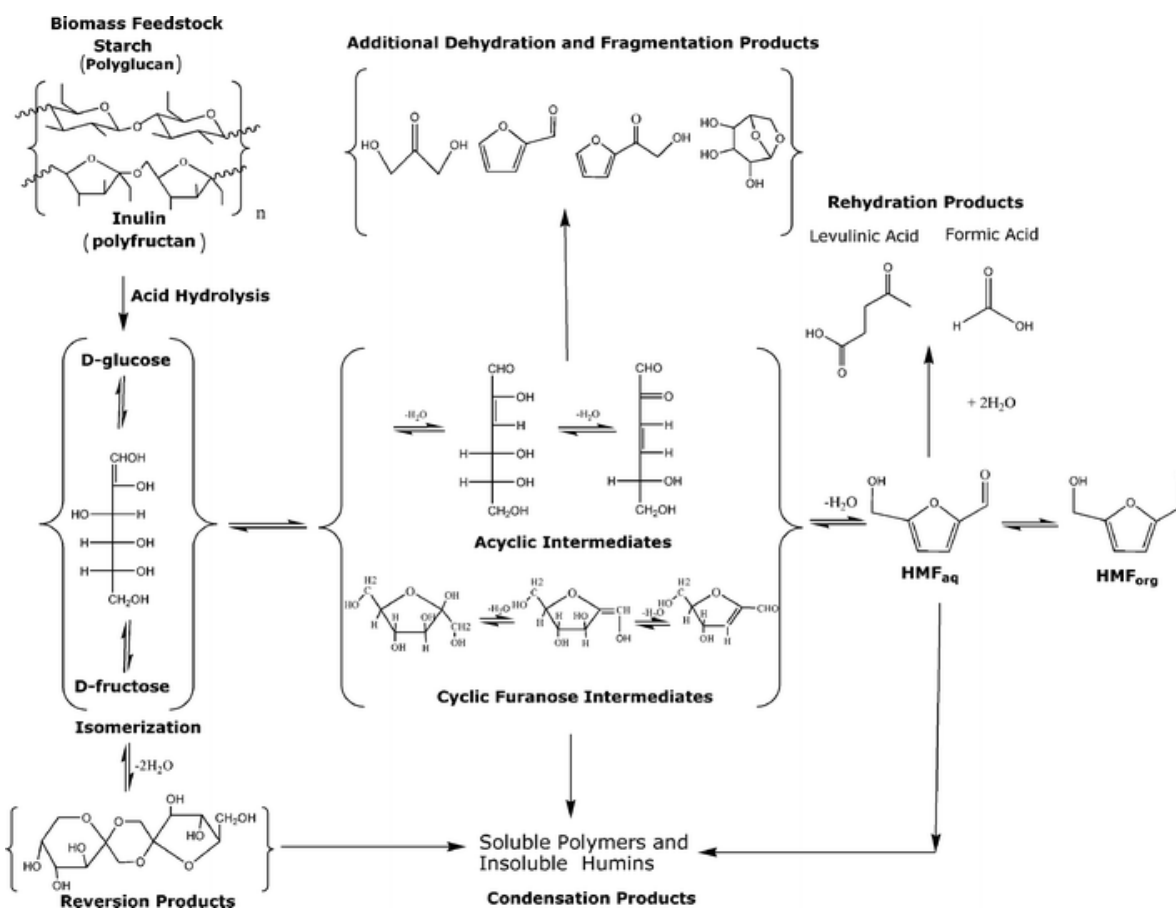


Figure 13: Schematic representation of reaction pathways to 5-hydroxymethylfurfural [65].

1.5.1 Glycerol oxidation

As introduced in the previous sections, using biomass to produce biofuels and fight against climate change have led us to improve this type of conversion technologies.

In the case of biodiesel, there are several ways to produce it from renewable biomass feedstocks, by methods such as transesterification, blending of raw oils, microemulsion, dilution, pyrolysis, or thermal cracking. The predominant biodiesel production process involves a step of transesterification having glycerol (1,2,3-propanetriol, Figure 14) as a by-product [66].

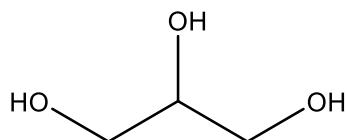


Figure 14: Glycerol (1,2,3- propanetriol) structure.

Effective utilization of glycerol and its efficient conversion into various value-added products will have a positive effect on biodiesel production economics, increasing the production and utilization of this alternative fuel resource [5].

The composition of crude glycerol depends on the method used for biodiesel production also as on the nature of feedstock [67]. As such, there is a large sort of potential alternatives to add value to glycerol: manufacture of commodities, production of polymers, production of biofuels and biogas and use of purified glycerol. Thus, the multifunctionality of glycerol makes it an appropriate bio-renewable platform chemical.

The production of bio-based products from glycerol has become a priority in the chemical market, especially in the plastic, solvents, lubricants and surfactants industries and it's forecasted to increase its demand in the following years [62]. It also offers a great alternative in reducing fossil feedstocks dependence, decreasing the CO₂ emissions in this sector, boosting cleaner, more efficient, modern, and better oriented industries finding satisfied the increasing demand on eco-friendly, safer, and healthier products.

As mentioned previously, among all reaction pathways of glycerol, its oxidation will be addressed by our research. Different valuable products can be obtained from glycerol oxidation as can be observed in the Figure 15:

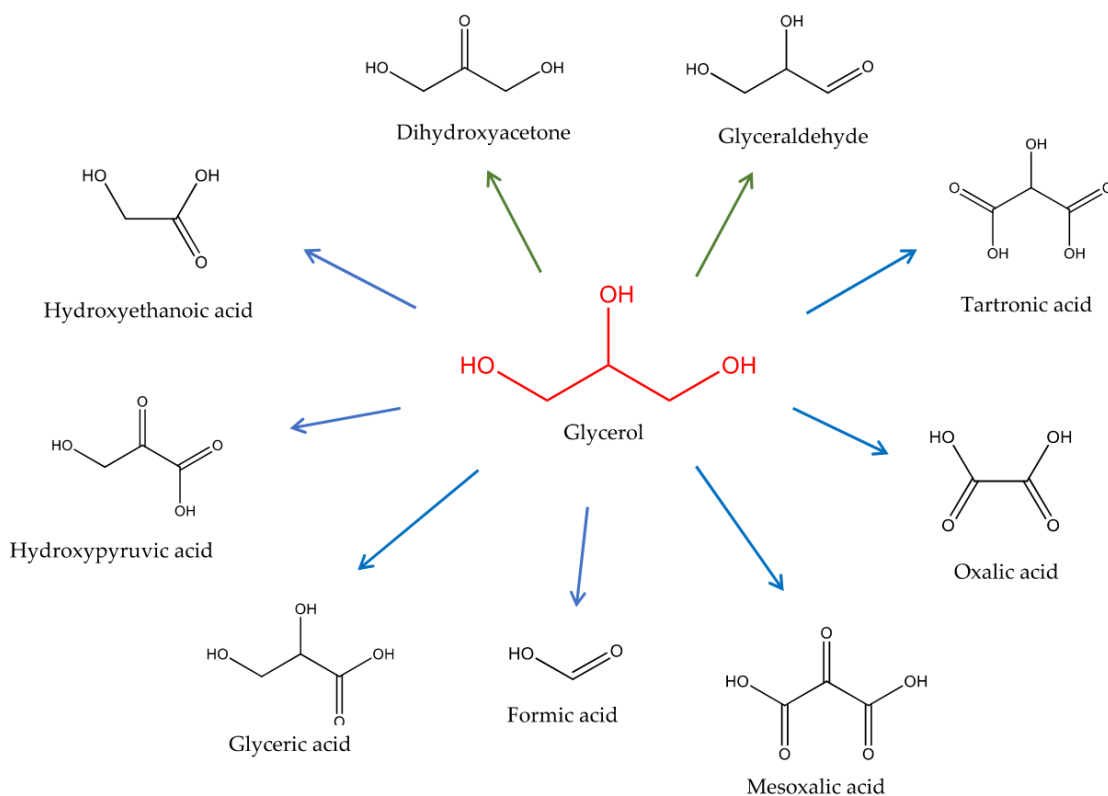


Figure 15: Products from glycerol oxidation [62, 66].

Many cases of glycerol oxidation using metal catalysts have been reported [5]. The selective oxidation of glycerol follows a complex reaction pathway yielding different C₃ products (glyceric acid (GLYA), dihydroxyacetone (DHA), and tartronic acid (TA)), C₂ products (glycolic acid (GLYCA) and oxalic acid (OXA)), and even C₁ products (formic acid (FA)) as it can be observed in Figure 15.

Most of those products are obtained by using high-priced and non-environmentally friendly stoichiometric oxidants, including potassium permanganate and chromic acid, or by rather low productivity fermentation processes [68]. It has been demonstrated that supported metallic nanoparticles, including Pd or Pt, in the presence of relative cheaper oxidizing agents (oxygen, air, hydrogen peroxide) constitute an environmentally friendly and low-price alternative to these traditional methodologies [69].

It is also reported [5] that gold catalysts have shown better performance with respect to Pd- and Pt-based catalysts in term of selectivity to glycerate. Moreover, using Pd or Pt catalysts during liquid phase glycerol oxidation, have led on poisoning from by-products and high sensitivity to deactivation due to overoxidation [68, 69].

In this research, our contribution to glycerol oxidation is the use of a C-scorpionate gold(III) complex supported on graphene which is expected to be a green method also with the help of microwave assisted oxidation. All literature talks about gold nanoparticle catalysts, but no C-scorpionate gold catalysts supported on graphene have been found in the literature.

1.5.2 5-(Hydroxymethyl)furfural and 5-hydroxymethyl-2-furancarboxylic acid oxidation

Polymeric materials such as polyethylene terephthalate, polyamides, and polyurethanes have played vital roles in the modern economy. Several industries have started considering using bio-based chemicals to produce bioplastics. Technically, bioplastics can be produced by different routes starting from LCB as described in the following Figure 16:

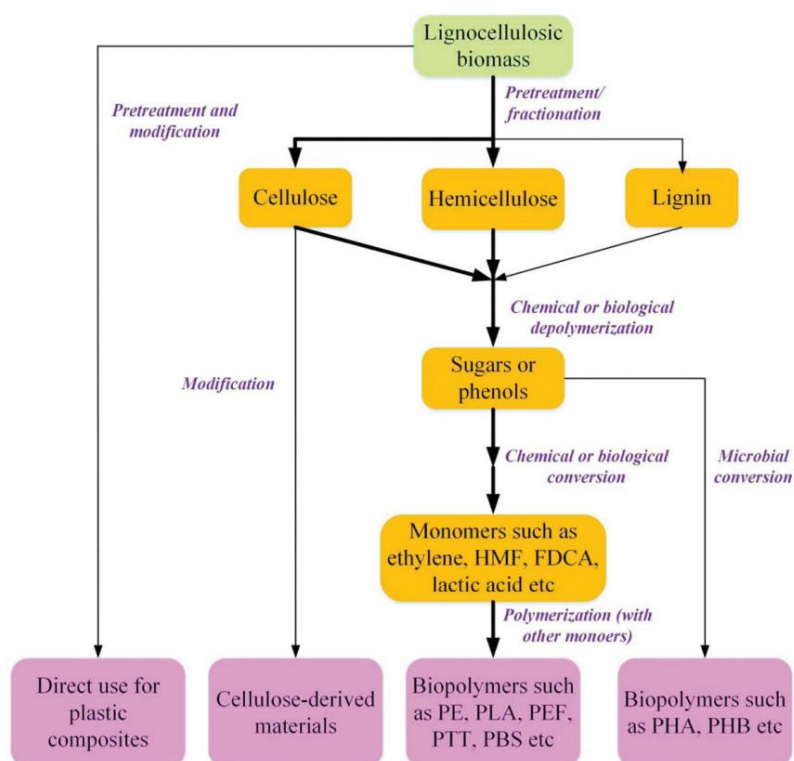


Figure 16: Typical production routes of bio-based polymers from lignocellulosic biomass [64].

In a recent attempt, bioplastics have been successfully produced from bio-based ethylene glycol (EG) and 2,5-furandicarboxylic acid (FDCA, Figure 17). FDCA synthesis is considered as a precursor to produce these green polymers, especially polyethylene 2,5-furandicarboxylate (PEF). FDCA derived PEF is a real alternative to the fossil based terephthalic acid (TPA) derived polyethylene terephthalate (PET). PEF will not only serve as a novel replacement but will also improve salient features like excellent gas barrier performance, recyclability and extended mechanical properties.

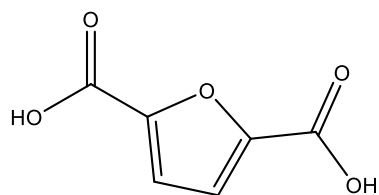


Figure 17: 2,5-Furandicarboxylic acid structure.

There are generally four methods to produce FDCA:

- (1) biological and chemical conversion of HMF;
- (2) catalytic transformation of numerous furan derivatives;
- (3) oxidation of 2,5 di-substituted furans;
- (4) dehydration of hexose derivatives.

As mentioned, one of the objectives of this work is focused on the conversion of HMF to produce FDCA, catalyzed by a C-scorpionate gold(III) complex supported on graphene.

Depending on the system applied, the conversion of HMF to FDCA can proceed through the preferred aldehyde group oxidation to 5-hydroxymethyl-2-furan carboxylic acid (HFCA) (Figure 18, route A), or the alcoholic group oxidation to 2,5-furan carboxaldehyde (Figure 18, route B). These process intermediates are then oxidized to 5-Formyl-2-furancarboxylic acid (FFCA), which is in turn transformed into FDCA as the final product.

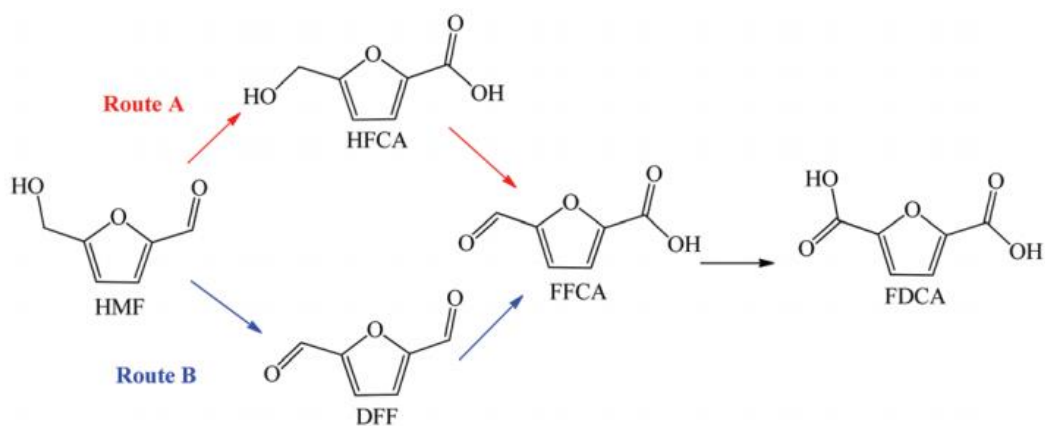


Figure 18: Reaction pathway of HMF oxidation to produce FDCA [64].

Gold NPs supported catalysts display encouraging performance for HMF oxidation (Figure 19), and their catalytic efficiency is strongly influenced by supporting materials, being like other noble metal (Pt and Pd) catalysts.

Catalyst	Base	Oxygen pressure	Time (h)	T (°C)	FDCA yield (%)	HMF conc. (%)
Au/C	2 equiv. NaOH	6.9 Bar O ₂	6	23	7	100
Au/CeO ₂	2 equiv. NaOH	10 Bar air	5	130	96	100
Au/TiO ₂	4 equiv. NaOH	10 Bar air	8	130	84	100
Au/Ce _{0.9} Bi _{0.1} O _{2-δ}	5 equiv. NaOH	1 Bar O ₂	2	65	>99	100
Au/HY	5 equiv. NaOH	0.3 Bar O ₂	6	60	>99	>99
Au/CeO ₂	5 equiv. NaOH	0.3 Bar O ₂	6	60	73	>99
Au/TiO ₂	5 equiv. NaOH	0.3 Bar O ₂	6	60	85	>99
Au/Mg(OH) ₂	5 equiv. NaOH	0.3 Bar O ₂	6	60	76	>99
Au/H-MOR	5 equiv. NaOH	0.3 Bar O ₂	6	60	15	96
Au/Na-ZSM5-25	5 equiv. NaOH	0.3 Bar O ₂	6	60	1	92
Au/TiO ₂	20 equiv. NaOH	20 Bar O ₂	18	30	71	100
Au/TiO ₂	pH = 13	10 Bar O ₂	4	50	80	100
Au-Cu/TiO ₂	4 equiv. NaOH	10 Bar O ₂	4	95	99	100
Au ₈ -Pd ₂ /C	2 equiv. NaOH	30 Bar O ₂	2	60	>99	>99
Au/HT	Base-free	1 Bar O ₂	7	95	>99	>99
Au-Pd/CNT	Base-free	5 Bar O ₂	12	100	94	100
Au-Pd/CNT	Base-free	10 Bar air	12	100	96	100
Au/TiO ₂	4 equiv. NaOH	10 Bar O ₂	4	70	19	100
Au/m-CeO ₂	4 equiv. NaOH	10 Bar O ₂	4	70	92	100
Au/CeO ₂	0.2 equiv. Na ₂ CO ₃	5 Bar O ₂	15	140	91	>99

Figure 19: Oxidative production of FDCA from HMF over Gold NPs supported catalysts [64].

The utilization of homogeneous catalysts is less attractive as compared to heterogeneous catalysts, due to the separation and recycling problems [70]. It also suffers lower FDCA yield and the production of undesirable by-products. In contrast, heterogeneous catalysts, shows several advantages with its easy separation and recycling. Thus, heterogeneous catalysts have attracted more interest for practical application and potential commercialization while investigating the literature.

Same as with glycerol oxidation, in furfural derivatives oxidation, no cases of C-scorpionate catalysts supported on graphene have been reported yet as this is the contribution to HMF oxidation that this research aims to do.

1.6 Characterization methods

The catalytic properties of a surface are determined by its composition and structure on the atomic scale. Hence, it is not sufficient to know that a surface consists of a metal and a promoter, but it is essential to know the exact structure of the iron surface, including any defects and steps, as well as the exact location of the promoter atoms. The goal of catalyst characterization should be to examine the surface atom by atom, and under reaction conditions, from a fundamental point of view [71]. The many aspects that we need to study to properly understand supported catalysts on a fundamental level are shown schematically in Figure 20:

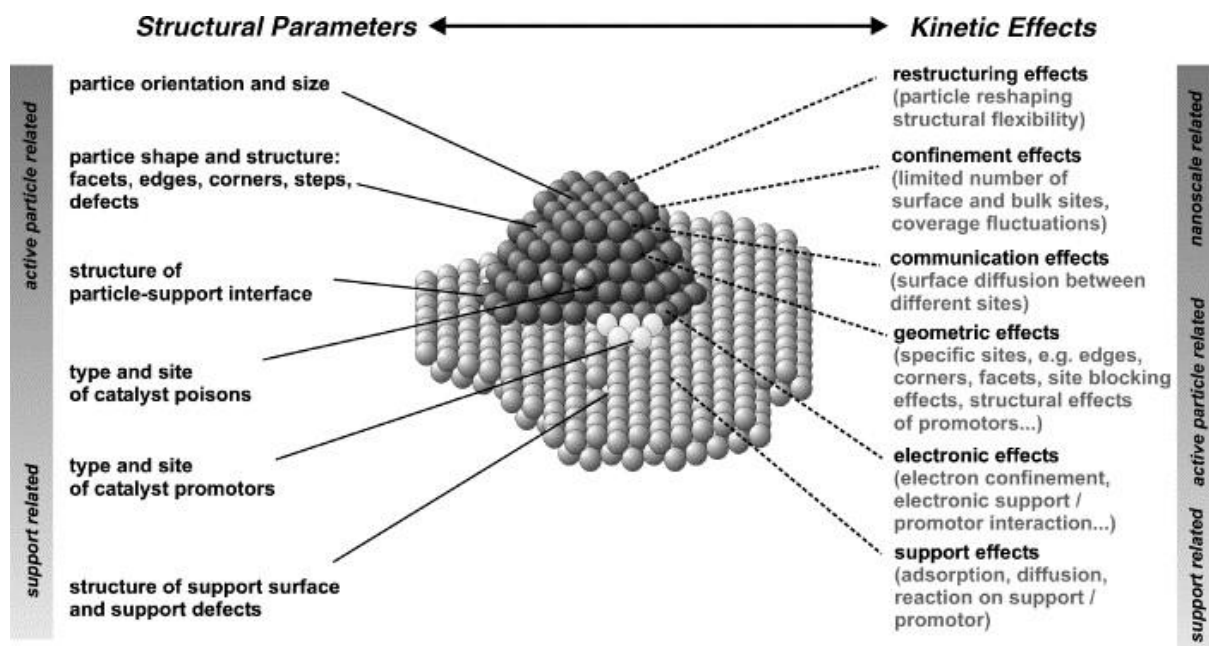


Figure 20: Structural parameters and kinetic effects on supported metal catalysts [72].

1.6.1 FTIR

Some of the catalysts were characterized by FTIR. FTIR stands for Fourier-transform infrared, the preferred method of infrared spectroscopy. When infrared (IR) radiation is passed through a sample, some radiation is absorbed by the sample and some passes through (is transmitted). The resulting signal at the detector is a spectrum representing a molecular 'fingerprint' of the sample. The usefulness of infrared spectroscopy arises because different chemical structures (molecules) produce different spectral fingerprints. Spectra from MIR (4000 to 400 cm^{-1}) needs to prepare KBr pellets (that are invisible in that region) and FAR (400 to 180 cm^{-1}) that needs CsI pellets in this region. Other type of infrared characterization method used was FTIR-ATR. Attenuated total reflectance (ATR) is a special accessory unit which can be used with Fourier transform infrared (FTIR) spectrometers. It enables you to measure directly onto a solid-state sample surface by pressing the sample towards an ATR crystal (e.g., diamond), including liquid and gas samples, thus avoiding the need to prepare pellets.

1.6.2 XPS

X-ray Photoelectron Spectroscopy (XPS) also known as Electron Spectroscopy for Chemical Analysis (ESCA) is the most widely used surface analysis technique because it can be applied to a broad range of materials and provides valuable quantitative and chemical state information from the surface of the material being studied. XPS is typically accomplished by exciting a samples surface with mono-energetic Al $K\alpha$ x-rays causing photoelectrons to be emitted from the sample surface. An electron energy analyzer is used to measure the energy of the emitted photoelectrons. From the binding energy and intensity of a photoelectron peak, the elemental identity, chemical state, and quantity of a detected element can be determined [73].

1.6.3 Elementary Analysis

This characterization method is a process where a sample of some material is analyzed for its elemental and sometimes isotopic composition. It can be qualitative(determining what elements are present or the presence of a particular element) and quantitative (determining how much of a particular or each element is present) [74]. Elemental analysis can be performed on a solid, liquid, or gas. However, depending on the technique employed the sample may have to be pre-reacted, e.g., by combustion or acid digestion. The amounts required for elemental analysis range from a few grams (g) to a few milligram (mg) or less.

The elementary analysis of C, H and N was carried out to know the purity of the different C-scorpionate metal complexes produced.

1.6.4 ^1H NMR

Proton nuclear magnetic resonance (^1H NMR) is the application of nuclear magnetic resonance in NMR spectroscopy with respect to hydrogen-1 nuclei within the molecules of a substance, to determine the structure of its molecules [75].

Deuterated solvents are preferred, like deuterated water, D_2O , deuterated acetone, $(\text{CD}_3)_2\text{CO}$, deuterated methanol, CD_3OD , deuterated dimethyl sulfoxide, $(\text{CD}_3)_2\text{SO}$, and deuterated chloroform, CDCl_3 . However, a solvent without hydrogen, such as carbon tetrachloride, CCl_4 or carbon disulphide, CS_2 , may also be used.

Proton NMR spectra of most organic compounds are characterized by chemical shifts in the range +14 to -4 ppm and by spin-spin coupling between protons. The integration curve for each proton reflects the abundance of the individual protons.

^1H NMR is a powerful tool for molecular structure characterization and is used in this work to characterize the different products obtained by the oxidation reactions performed.

1.6.5 SEM/EDS

Scanning electron microscopy (SEM) and energy dispersive X-ray spectroscopy (EDS) allow for targeted analysis of sample surfaces. These techniques are widely used for material surface analysis, investigation of product failures, reverse engineering, contaminant identification, solder joint analysis and more [76]. SEM and EDS were performed to observe the morphology of the surface of the C-scorpionate gold(III) complex $[\text{AuCl}_2(\text{Tpm})]\text{Cl}$ (**4**) immobilized on graphene by different techniques. Also to compare the surface of each sample $[\text{AuCl}_2(\text{Tpm})]\text{Cl}$ (**4**) supported in graphene and ultra-pure graphene.

2 Experimental procedures

This chapter shows the different experimental synthetic methods used during this work to:

- i) afford the different C-scorpionate metal complexes of nickel(II), cobalt(II), copper(II) and gold(III);
- ii) support the C-scorpionate gold(III) complex on graphene; and
- iii) oxidize glycerol and furfural derivatives (5-hydroxymethyl-2-furaldehyde and 5-hydroxymethyl-2-furancarboxylic-acid).

2.1 Synthesis of C-scorpionate complexes

Several C-scorpionate complexes of nickel(II), cobalt(II), copper(II) and gold(III) were synthesized by a green method. We have chosen the mechanochemical synthesis using a Ball Mill (solid state conditions), instead of the traditional method reported in literature [39, 44, 77], to prepare the complexes **1** – **4**. All complexes were obtained by the reaction of hydrotris(pyrazol-1-yl)methane (Tpm) and the appropriate metal chloride.

We have performed different reaction conditions such as mixing time, number of spheres and stirring speed for non-precious metals such as copper(II), nickel(II), and cobalt(II) before producing the gold(III) C-scorpionate complex that is the one that have been used for the microwave-assisted oxidations.

2.1.1 Copper C-scorpionate complex [CuCl₂(Tpm)] (**1**)

The copper C-scorpionate complex [CuCl₂(Tpm)] (**1**) was prepared using the following reagents: copper(II) chloride dihydrate, 99+%, (ACROS Organics™) obtained from commercial sources was used as received and hydrotris(pyrazol-1-yl)methane (Tpm) was synthesized in our laboratory according to methodologies described in the literature [77].

The amount of reagents was: 42.55 mg of Tpm + 33.62 mg of CuCl₂·2H₂O to work under equimolar conditions (0.2 mmol). Both reagents were added together into the grinding jar (Figure 21, left) of the Retsch® Planetary Ball Mill PM100 [78] with different configuration of spheres (see Table 3). The grinding jar (Figure 21, left) must be secured inside the ball mill before the it starts its work.

The reaction conditions tested are presented in Table 3. In the last experiment, the reagents were grinded with a mortar (Figure 21, right). The meaning of the name of the different entries are PG: Pablo Gil (name of the user), Cu: copper samples, BM: Ball Milling, M: Mortar and the number indicates the order of the experiments performed. Same happens with next complexes **2-4**. The different samples are showed in Figure 22.



Figure 21:Grinding jar (Retsch® Planetary Ball Mill PM100) with reagents and spheres (left) and mortar (right).

Table 3: Synthetic conditions used in the preparation of the C-scorpionate copper(II) complex $[\text{CuCl}_2(\text{Tpm})]$ (1) and corresponding yields.

Entry	Time (min)	Number of spheres in the jar	rpm
PGCuBM1	5	3	250
PGCuBM2	10	3	250
PGCuBM3	15	3	100
PGCuBM4	15	3	500
PGCuBM5	15	1	250
PGCuBM6	15	5	250
PGCuM7	15	-	-

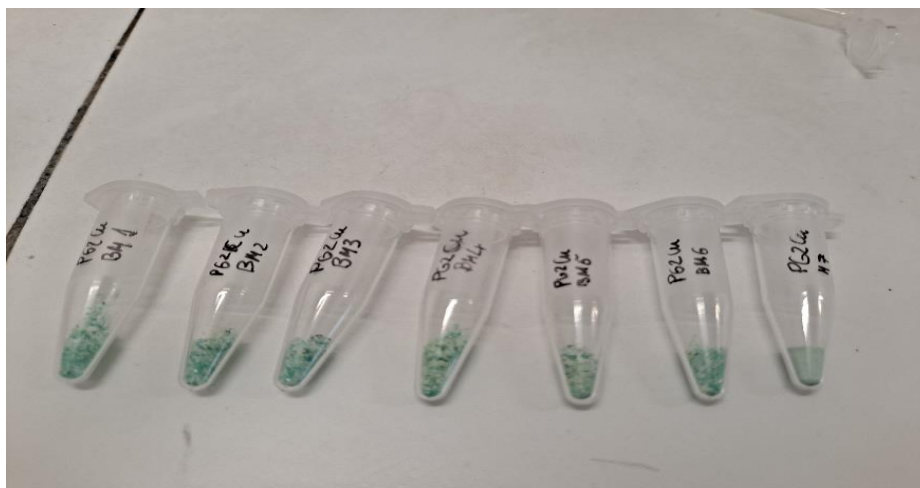


Figure 22: Different samples of copper(II) C-scorpionate complex $[\text{CuCl}_2(\text{Tpm})]$ (1) obtained by Ball Milling (PGCuBM1-6) and manual grinding (PGCuM7).

After the reaction, methanol was added to remove the reaction mixture from the jar and the solid was dried in vacuum oven at the temperature of 50 °C during 12 h as it can be observed in Figure 23 and Figure 24.

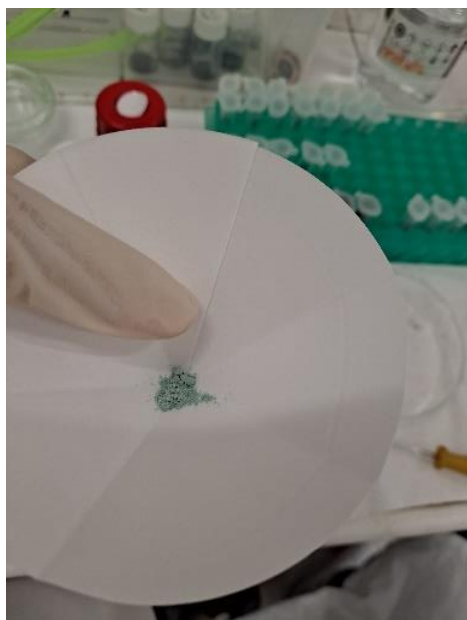


Figure 23: Washing with methanol by filtering (left) and vacuum oven drying (right).

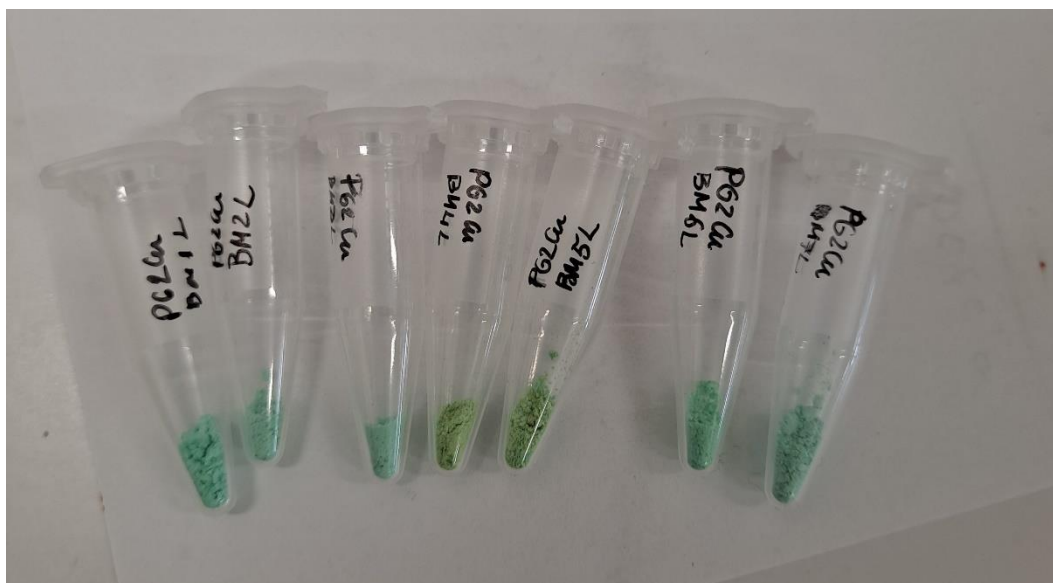


Figure 24: C-scorpionate copper(II) complex $[\text{CuCl}_2(\text{Tpm})]$ (1) samples obtained by ball milling (an L after name was added).

2.1.2 Nickel C-scorpionate complex $[\text{NiCl}(\text{Tpm})]\text{Cl}$ (2)

The C-scorpionate nickel(II) complex $[\text{NiCl}(\text{Tpm})]\text{Cl}$ (2) was prepared using the following reagents: nickel(II) chloride hexahydrate, 98% (Sigma Aldrich), obtained from commercial sources and used as received, and hydrotris(pyrazol-1-yl)methane (Tpm) that was synthesized in our laboratory according to methodologies described in the literature [77].

Same as with copper complexes, the conditions were equimolar (0.2 mmol) being the different amounts of reagents: 42.55 mg of Tpm + 47.538 mg of $\text{NiCl}_2 \cdot 6\text{H}_2\text{O}$.

Different conditions were tested in the ball mill (presented in Table 4), and the last one of the samples was grinded with mortar, same as described before with copper complexes. In this case, the experience by ball milling was different as many samples had the problem of part of the product going into the spheres (see following Figure 25 for more detail). All samples are showed in Figure 26.

To try to solve the problem, the balls and the reactor were washed with diethyl ether and after this, heated in vacuum oven at 50 °C for 30 minutes. After being dried it is possible to extract the product from the balls and obtain the remaining product. All these cases are named with a 'after the normal code of the sample: PGNiBM1 & PGNiBM1' for example, being the second the one that has been washed and the first one the product directly extracted after the ball milling:

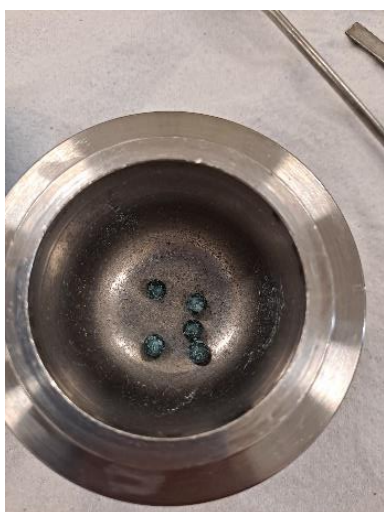


Figure 25: Product after ball milling experience, attached to the spheres.

Table 4: Different synthetic conditions used in the preparation of the C-scorpionate nickel(II) complex $[\text{NiCl}(\text{Tpm})]\text{Cl}$ (**2**) and corresponding yields.

Entry	Time (min)	Number of spheres in the jar	rpm	diethyl ether? (yes/no)
PGNiBM1	5	3	250	no
PGNiBM1'	5	3	250	yes
PGNiBM2	10	3	250	no
PGNiBM2'	10	3	250	yes
PGNiBM3	15	3	100	no
PGNiBM3'	15	3	100	yes
PGNiBM4	15	3	500	no
PGNiBM5	15	1	250	no
PGNiBM5'	15	1	250	yes
PGNiBM6	15	5	250	no
PGNiBM6'	15	5	250	yes
PGNiM7	15	-	-	no

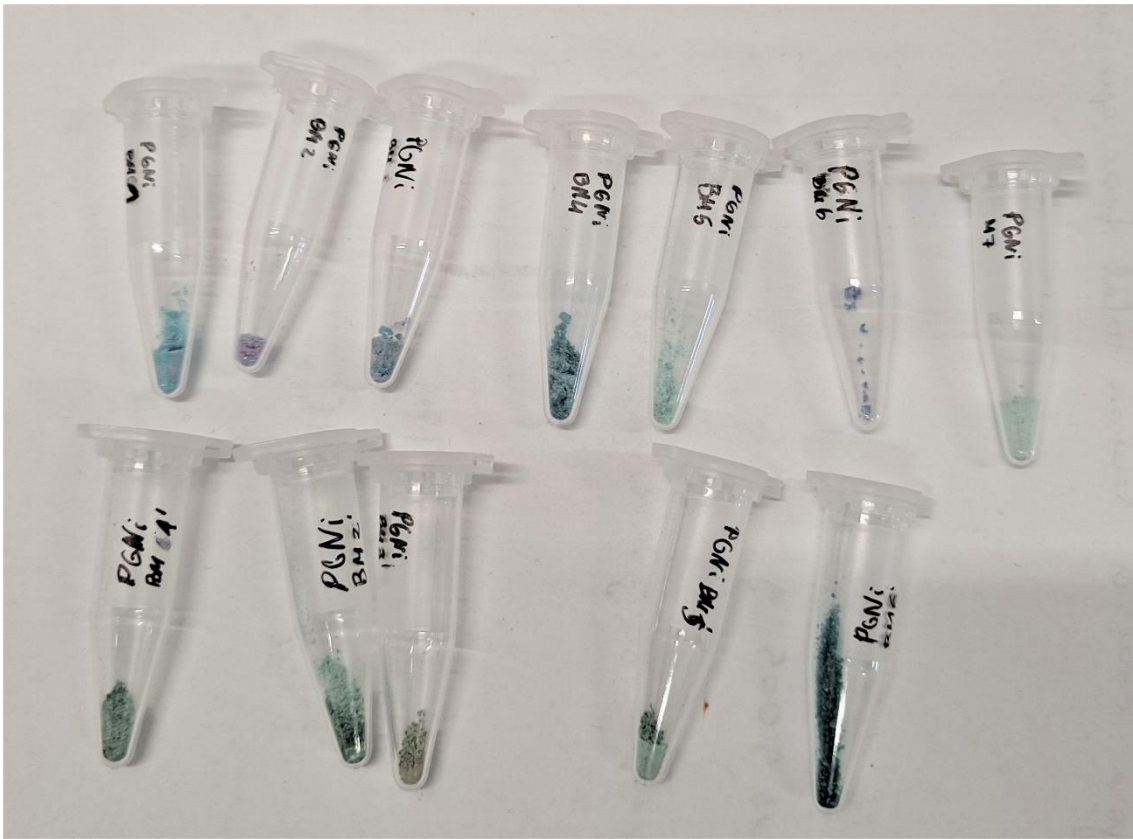


Figure 26: Different samples of C-scorpionate nickel(II) complex $[\text{NiCl}(\text{Tpm})]\text{Cl}$ (**2**) obtained by Ball Milling (**PGNiBM1-6**) and manual grinding (**PGNiM7**) (up) and (down) washed and dried samples (**PGNiBMn'**).

2.1.3 Cobalt C-scorpionate complex [CoCl₂(H₂O)(Tpm)] (3)

As mentioned in 1.3.1 (Metal C-scorpionate complexes), some cobalt complexes bearing scorpionate ligands were reported [42] but, to the best of our knowledge, no cobalt half-sandwich C-scorpionate HC(pz)₃ (Tpm, pz = pyrazolyl ring) has been reported in the literature. Thus, in this work is the first time that the synthesis of complex [CoCl₂(H₂O)(Tpm)] (3) was tried.

The C-scorpionate cobalt(II) complex [CoCl₂(H₂O)(Tpm)] (2) was prepared using the following reagents: cobalt(II) chloride hexahydrate (Sigma Aldrich), obtained from commercial sources and was used as received and hydrotris(pyrazol-1-yl)methane (Tpm) that was synthesized in our laboratory according to methodologies described in the literature [77].

Same as with copper and nickel complexes, the conditions were equimolar (0.2 mmol) being the different amounts of reagents: 42.55 mg of Tpm + 47.586 mg of CoCl₂·6H₂O, Figure 27 and Figure 28 represent how complex 3 was synthesized by ball milling and its different samples.

Being hexahydrate as the previous nickel chloride reagent, the same problem mentioned at section Nickel C-scorpionate complex [NiCl(Tpm)]Cl (2) 2.1.2 happened in several samples, by trying to remove the product attached to the spheres washing and drying with diethyl ether (indicated in Table 5).

Table 5: Different synthetic conditions used in the preparation of the C-scorpionate cobalt(II) complex [CoCl₂(H₂O)(Tpm)] (3) and corresponding yields.

Entry	Time (min)	Number of spheres in the jar	rpm	diethyl ether? (yes/no)
PGCoBM1	5	3	250	no
PGCoBM2	10	3	250	no
PGCoBM2'	10	3	250	yes
PGCoBM3	15	3	100	no
PGCoBM4	16	3	500	no
PGCoBM5	17	1	250	no
PGCoBM6	18	5	250	no
PGCoM7	19	-	-	no

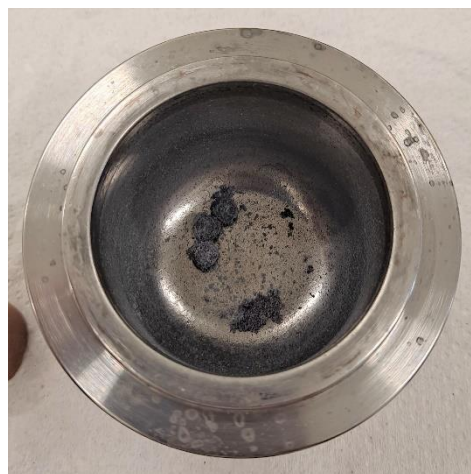


Figure 27: Grinding jar (Retsch® Planetary Ball Mill PM100) before (left) and after (right) ball milling of $\text{CoCl}_2 \cdot 6\text{H}_2\text{O} + \text{Tpm}$.

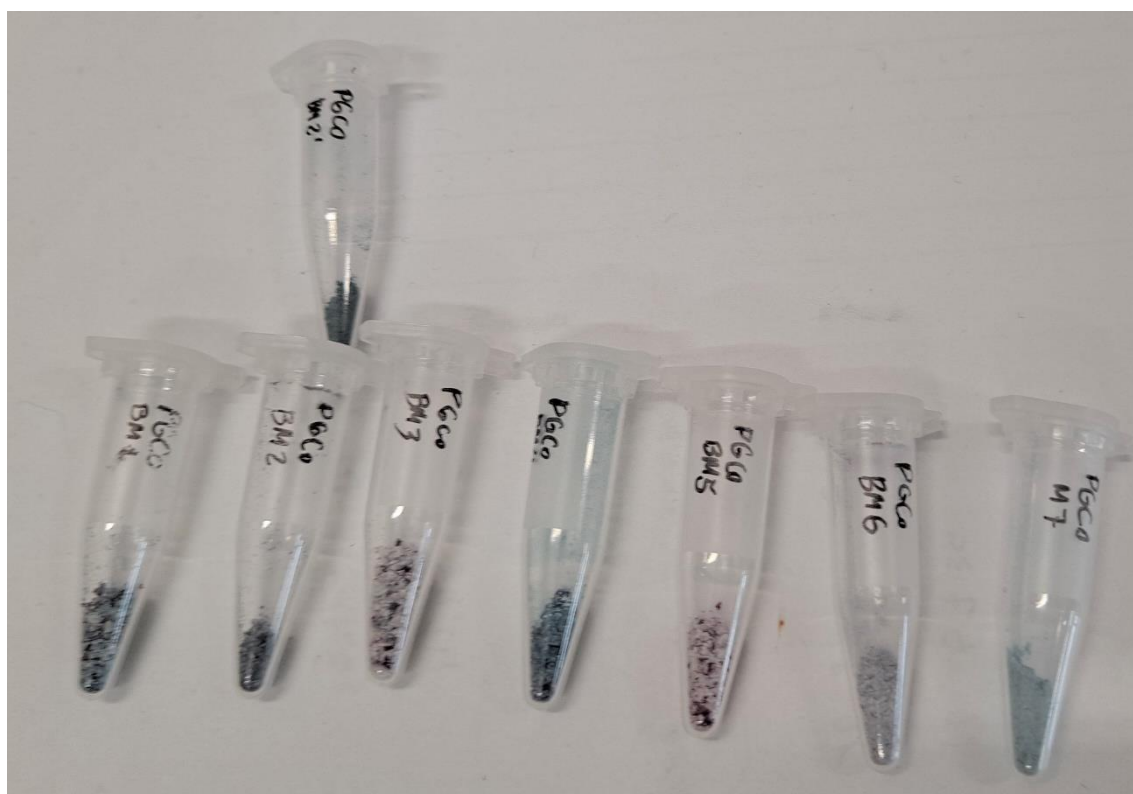


Figure 28 Different samples of C-scorpionate cobalt(II) complex $[\text{CoCl}_2(\text{H}_2\text{O})(\text{Tpm})]$ (**3**) obtained by Ball Milling (**PGCoBM1-6**) and manual grinding (**PGCoM7**) and washed and dried samples (**PGCoBM2'**).

2.1.4 Gold C-scorpionate complex $[\text{AuCl}_2(\text{Tpm})]\text{Cl}$ (4)

Following the same parameters as made with copper, nickel, and cobalt, 7 different samples of C-scorpionate gold(III) complexes will be made by ball milling (Table 6). Before synthesising these 7 different samples, 3 big samples were made (Figure 29). The reason was to have enough catalyst for the microwave-assisted oxidation that went after. Also, traditional synthesis of $[\text{AuCl}_2(\text{Tpm})]\text{Cl}$ (4) [44] was used to compare its catalytic performance with the ones made by ball milling.

Gold C-scorpionate complexes were prepared using the following reagents: Gold(III) chloride hydrate $\text{HAuCl}_4 \cdot \text{H}_2\text{O}$ 99.995% trace metal basis (Sigma Aldrich), obtained from commercial sources and was used as received and hydrotris(pyrazol-1-yl)methane (Tpm) that was synthesized in our laboratory according to methodologies described in the literature [77]. The biggest one, BMAu3, was also cleaned with methanol on the following day changing its name to BMAu3L.

Table 6: First synthetic conditions used in the preparation of the C-scorpionate gold(III) complex $[\text{AuCl}_2(\text{Tpm})]\text{Cl}$ (4) and corresponding yields.

Code	Mass $\text{HAuCl}_4 \cdot \text{H}_2\text{O}$ (mg)	Mass Tpm (mg)	n (mmol) (1:1)	Time (min)	Number of spheres in the jar	rpm
BMAu1	79.50	49.78	0.23	15.00	3	500
BMAu2	78.00	48.84	0.23	15.00	3	500
BMAu3L	173.70	108.76	0.51	15.00	3	500



Figure 29: Grinding jar before (left) and after ball milling (centre) and the 3 first samples of C-scorpionate gold(III) complexes obtained by ball milling.

After this first experience with ball milling and gold, the following 7 different samples with same configurations as before (copper, nickel, and cobalt complexes) were made (Figure 30). It is important to highlight that in this case of synthesising gold complexes, gold precursor was more difficult to manipulate, that is the reason why not all samples had the same amount of gold or Tpm, but in every case the synthesis is made under equimolar(1:1) conditions as indicated in Table 7:

Table 7: Synthetic conditions used in the preparation of the C-scorpionate gold(III) $[\text{AuCl}_2(\text{Tpm})]\text{Cl}$ (**4**) and corresponding yields.

Entry	Time (min)	Number of spheres in the jar	rpm	Mass $\text{HAuCl}_4 \cdot \text{H}_2\text{O}$ (mg)	Mass Tpm (mg)	n (mmol)(1:1)
PGAuBM1	5	3	250	73.10	45.77	0.22
PGAuBM2	10	3	250	76.00	47.59	0.22
PGAuBM3	15	3	100	73.50	46.02	0.22
PGAuBM4	15	3	500	84.70	53.04	0.25
PGAuBM5	15	1	250	89.80	56.23	0.26
PGAuBM6	15	5	250	67.80	42.45	0.20
PGAuM7	15	0	-	74.00	46.34	0.22

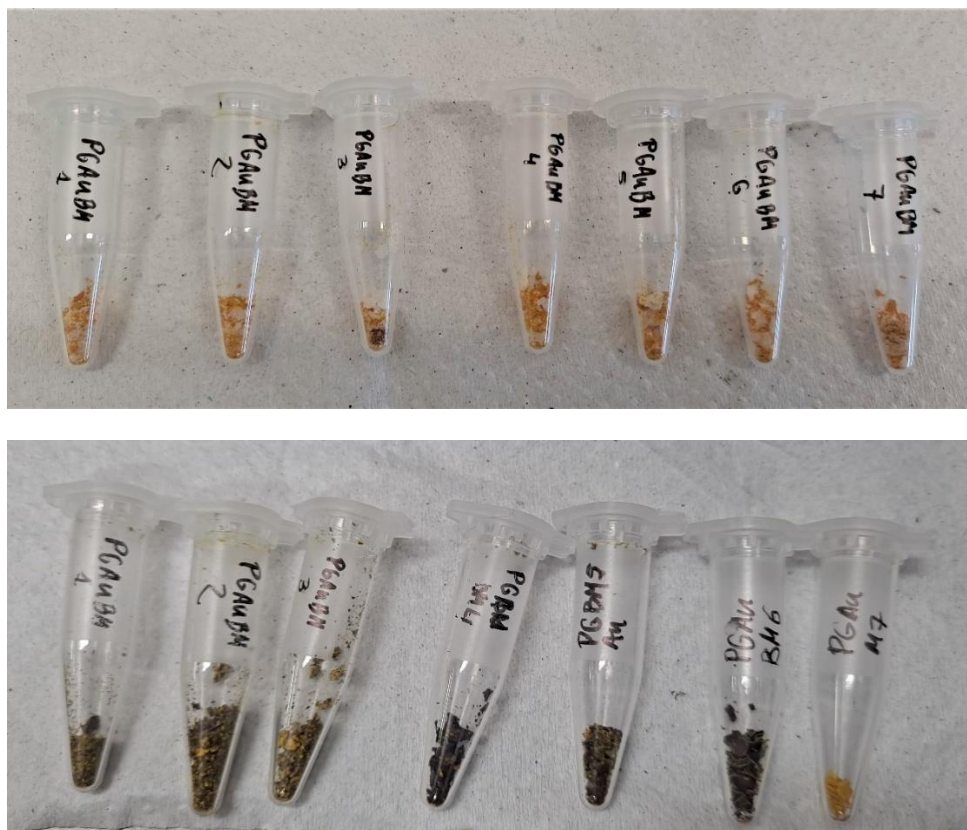


Figure 30: Different samples of gold(III) C-scorpionate complex $[\text{AuCl}_2(\text{Tpm})]\text{Cl}$ (**4**) obtained by Ball Milling (PGAuBM1-6) and manual grinding (PGAuM7).

The gold(III) C-scorpionate complex $[\text{AuCl}_2(\text{Tpm})]\text{Cl}$ (**4**) was also synthesised (Figure 31) by the method reported on literature [44]: 42.55 mg of Tpm is added to 5 mL of distilled water, under continuous stirring at room temperature. On the other hand, the gold precursor $\text{HAuCl}_4 \cdot \text{H}_2\text{O}$ was also dissolved in distilled water (5 mL) and added dropwise in a stoichiometric proportion of 1:1 (67.96 mg, 0.2 mmol) to the ligand solution and under continuous stirring for 24 h. After, the final solution is filtered by gravity and the suspension collected was washed with more distilled water and dried overnight at 50 °C.



Figure 31: C-scorpionate gold(III) complex $[\text{AuCl}_2(\text{Tpm})]\text{Cl}$ (**4**) traditional synthetic method.

2.2 Immobilization of $[\text{AuCl}_2(\text{Tpm})]\text{Cl}$ on graphene

Different ways on supporting the gold complexes into graphene were tested: Wet impregnation (WI), microwave (MW) and by Liquid Assisted Grinding (LAG). The purpose of trying different techniques was compare the results as LAG will use 1-2 mL of solvent, MW, 10-15 mL and traditional WI 20 mL. If results are similar LAG method could avoid the excessive use of solvents. On the other hand, two different types of graphene were used to compare, again its performance on support and catalysis.

The two different types of graphene will be referred as graphene and ultra-pure graphene, due to although both being the same compound (formed only by C), ultra-pure graphene has its different layer structure very well defined, as it will be showed in Chapter 3.

2.2.1 Wet impregnation (WI)

Two different samples (Table 8) were prepared by WI, one of them was prepared with graphene, and the other one with “ultra-pure” graphene provided by a company in collaboration with this project.

The first sample was prepared with 2%wt. of C-scorpionate gold(III) complex obtained by mechanochemical synthesis and graphene, and second sample was made with 10%wt. of catalyst synthesised by the traditional method and “ultra-pure” graphene.

Graphene and catalyst are both put together with 20 mL of solvent (distilled water, Figure 32) under continuous stirring for 24 h, then the observed liquid and solid phases are separated after another 24 h and dried in vacuum oven at 50 °C overnight.



Figure 32: WI method: under continuous stirring (left) and after separation and dryness (right).

Table 8: Synthetic conditions used in the WI immobilization of C-scorpionate gold(III) $[\text{AuCl}_2(\text{Tpm})]\text{Cl}$ (4) on two different graphenes.

Code	Au sample	m_{Au} (mg)	Graphene	m_{graph} (mg)	%Au	Obs.
PGAuGWI	BMAu3L	4	normal	196	2	Stirring 24h
PGAuGWI_up	$[\text{AuCl}_2\text{Tpm}]\text{Cl}$	10	ultra-pure	90	10	Stirring 24h

2.2.2 Microwave (MW)

Microwave support was made with Monowave 300 Anton Paar® [79] microwave reactor using for the first sample, like with WI, 2%wt of gold catalyst made by ball milling, and graphene with 15 mL of distilled water. For the second sample, 10%wt. of traditional method gold catalyst was used together with ultra-pure graphene and 15 mL of distilled water (Table 9). Microwave assisted reaction conditions were: 30 min, 40 °C, 650 rpm with magnetic stirrer, 25 W and 30 mL borosilicate vial (Figure 33). After microwave assisted reaction, solid and liquid phases were separated after 24 h and then dried in vacuum oven at 50 °C overnight for later, get the solid phase.

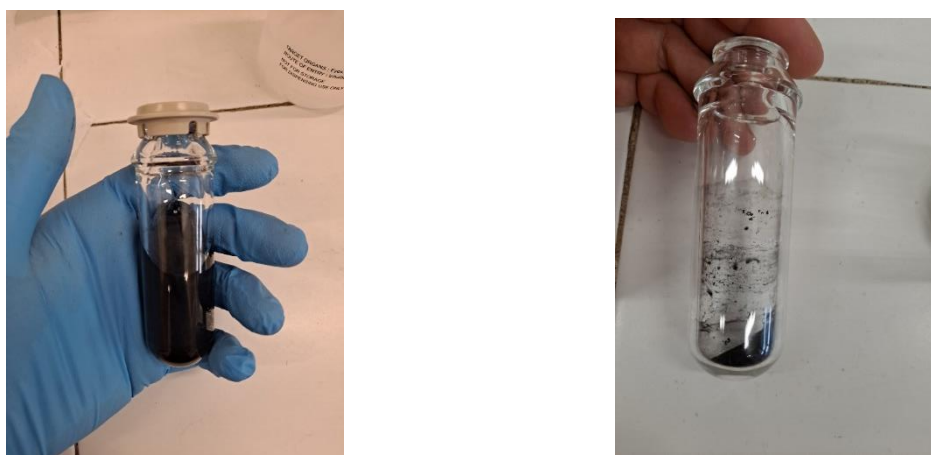


Figure 33: MW method: before (left) and after separation and dryness (right).

Table 9: Synthetic conditions used in the MW immobilization of C-scorpionate gold(III) $[\text{AuCl}_2(\text{Tpm})]\text{Cl}$ (4) on two different graphenes.

Code	Au sample	m_{Au} (mg)	Graphene	m_{graph} (mg)	%Au	Obs.
PGAuGMW	BMAu3L	4.00	normal	196	2	40 °C 650 rpm 25 W 15 mL H ₂ O
PGAuGMW_up	$[\text{AuCl}_2\text{Tpm}]\text{Cl}$	11.11	ultra-pure	100	10	40 °C 650 rpm 25 W 15 mL H ₂ O

2.2.3 Liquid Assisted Grinding (LAG)

Liquid-assisted grinding (LAG), also known as solvent-drop grinding, is an extension of traditional solvent-free mechanochemical techniques by which a small amount of liquid is used as an additive to enhance or control reactivity [15].

To perform LAG, the Emax High Energy Ball Mill of Retsch® [80] was used. Two different samples (Table 10) were made being the first one 2%wt. of gold catalyst synthesised by mechanochemistry, graphene, and a small amount of 2 mL of distilled water. The second one, as in the previous techniques, 10%wt. of gold complex produced by traditional method, ultra-pure graphene, and 2 mL of distilled water. The parameters and conditions for the Emax machine for perform the LAG were: 3 spheres, 15 mins and 800 rpm. After LAG, the grinding jar (Figure 34) was dried overnight by vacuum oven at 50 °C, and the solid phase was recollected.

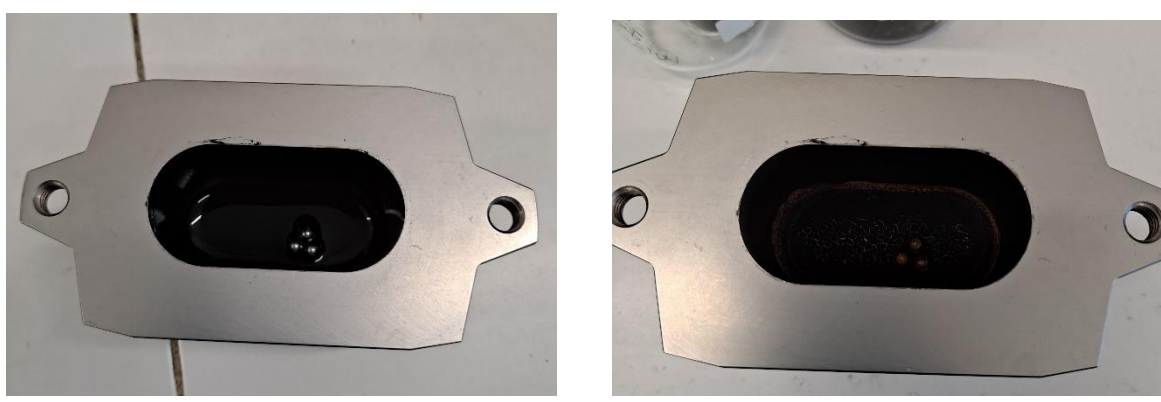


Figure 34: Grinding jar (Emax High Energy Ball Mill) with reaction mixture before (left) and after dryness (right).

Table 10: Synthetic conditions used in the LAG immobilization of C-scorpionate gold(III) $[\text{AuCl}_2(\text{Tpm})\text{Cl}]$ (**4**) on two different graphenes.

Code	Au sample	m_{Au} (mg)	Graphene	m_{graph} (mg)	%Au	Obs.
PGAuGLAG	BMAu3L	4	normal	196	2	3 spheres 15 min 800 rpm 2 mL H ₂ O
PGAuLAG_up	$[\text{AuCl}_2\text{Tpm}]\text{Cl}$	10	ultra-pure	90	10	3 spheres 15 min 800 rpm 2 mL H ₂ O

2.3 Microwave-assisted oxidation reactions

All oxidation reactions were performed using the Monowave 300 Anton Paar® and changing the type and amount of catalyst under homogeneous and heterogeneous conditions, different temperatures of reaction were also tested. Further details will be showed up in the following subsections dedicated to each reagent.

2.3.1 Glycerol microwave-assisted oxidation

For glycerol microwave-assisted oxidation (Table 11) general conditions were:

- 10 mL borosilicate vial
- none, 5 mg or 10 mg of catalyst
- 460.47 mg, 5 mmol of glycerol used as received
- 901.2 mg, 10 mmol TBHP 70% used as received
- stirring bar
- 50 °C or 80 °C
- 650 rpm
- 25 W
- 2 h reaction

First, the needed amount of catalyst is introduced in the vial, following the glycerol (Sigma Aldrich) [81] used as received, and the stirring bar. When the equipment is properly programmed for starting the reaction, TBHP (Sigma Aldrich) [82] used as received, is introduced slowly, as is the oxidating agent. The vial is closed with the cap and introduced inside the microwave equipment. After microwave reaction stops, the final solution is collected inside a little glass flask and kept refrigerated in fridge (3-5 °C) as it can be observed in Figure 35.



Figure 35: 10 mL vial for MW reaction (left) and collected final reaction product in flask for its refrigerated storage (right).

Table 11: Glycerol microwave-assisted oxidation samples.

Code	T (°C)	Catalyst	m _{catalyst} (mg)	Condition
PGAu1	50	BMAu2	5	Homogeneous
PGAu2	50	BMAu2	10	Homogeneous
PGAu3	80	BMAu2	5	Homogeneous
PGAu4	50	HAuCl ₂ ·xH ₂ O	5	Homogeneous
PGAu5	50	[AuCl ₂ (Tpm)]Cl	5	Homogeneous
PGAu6	50	[AuCl ₂ (Tpm)]Cl	10	Homogeneous
PGAu7	80	[AuCl ₂ (Tpm)]Cl	5	Homogeneous
PGAu8	50	HAuCl ₄ ·xH ₂ O	5	Homogeneous
PGAu9	50	HAuCl ₄ ·xH ₂ O	10	Homogeneous
PGAu10	80	HAuCl ₄ ·xH ₂ O	5	Homogeneous
PGAu11	50	PGAuGLAG	10	Heterogeneous
PGAu12	50	PGAuGMW	10	Heterogeneous
PGAu13	50	PGAuGWI	10	Heterogeneous
PGAu14	50	-	10	Homogeneous
PGAu15	50	graphene	10	Heterogeneous
PGAu16	50	ultra-pure graph.	10	Heterogeneous
PGAu17	80	PGAuGLAG	10	Heterogeneous
PGAu18	80	PGAuGMW	10	Heterogeneous
PGAu19	80	PGAuGWI	10	Heterogeneous
PGAu20	50	PGAuGLAG_up	10	Heterogeneous
PGAu21	50	PGAuGMW_up	10	Heterogeneous
PGAu22	50	PGAuGWI_up	10	Heterogeneous
PGAu23	80	PGAuGLAG_up	10	Heterogeneous
PGAu24	80	PGAuGMW_up	10	Heterogeneous
PGAu25	80	PGAuGWI_up	10	Heterogeneous
PGAu26	50	PGAuGLAG	5	Heterogeneous
PGAu27	50	PGAuGLAG_up	5	Heterogeneous
PGAu28	50	ultrapure graph.	5	Heterogeneous
PGAu29	50	PGAuGWI_up	5	Heterogeneous
PGAu30	80	PGAuGWI_up	5	Heterogeneous

Reaction conditions: 650 rpm, 2 h, and 25 W.

2.3.2 Furfural derivatives microwave-assisted oxidation

Two different furfural derivatives (Figure 36) were tested for their oxidation:



Figure 36: a) 5-(hydroxymethyl)furan-2-carboxylic acid structure and b) 5-hydroxymethylfurfural or 5-hydroxymethyl-2-furaldehyde structure.

Both appear in Figure 18 in the reaction pathway of HMF oxidation to produce FDCA and different conditions of oxidation were tested for its study.

2.3.2.1 5-Hydroxymethylfurfural (HMF)

For HMF microwave-assisted oxidation (Table 12) general conditions were:

- 10 mL borosilicate vial
- None or 5 mg of catalyst
- 630.55 mg, 5 mmol of HMF used as received
- 901.2 mg, 10 mmol TBHP 70% used as received
- stirring bar
- 50 °C or 80 °C
- 650 rpm
- 25 W
- 2h reaction

First, the needed amount of catalyst is introduced in the vial, following the HMF obtained from TCI Chemicals [83], used as received and the stirring bar. When the equipment is properly programmed for starting the reaction, TBHP is introduced slowly, as is the oxidating agent. The vial is closed with the cap and introduced inside the microwave equipment. After microwave reaction stops, the final solution is collected inside a little glass flask under nitrogen atmosphere and kept refrigerated and protected from light in fridge (3-5 °C) as it can be observed in Figure 37:



Figure 37: Light-protected flask that contains final reaction product from HMF microwave-assisted oxidation.

Table 12: HMF microwave-assisted oxidation samples.

Code	T(°C)	Catalyst	m_{catalyst} (mg)	Conditions
PGff1	50	-	-	Homogeneous
PGff2	50	graphene	5	Heterogenous
PGff3	50	ultrapure graph.	5	Heterogenous
PGff4	50	PGAuGLAG	5	Heterogenous
PGff5	50	PGAuGMW	5	Heterogenous
PGff6	50	PGAuGWI	5	Heterogenous
PGff7	50	PGAuGLAG_up	5	Heterogenous

Reaction conditions: 650 rpm, 2 h, and 25 W.

2.3.2.2 5-Hydroxymethyl-2-furancarboxylic acid (HFCA)

For HFCA microwave-assisted oxidation (Table 13) general conditions were:

- 10 mL borosilicate vial
- None or 10 mg of catalyst
- 71.055 mg, 0.5 mmol of HFCA used as received
- 90.12 mg, 1 mmol TBHP 70% used as received
- 1 mL acetonitrile
- stirring bar
- 50 °C or 80 °C
- 650 rpm
- 25 W
- 2h reaction

Same as with HMF, the needed amount of catalyst is introduced in the vial, following the HFCA obtained from TCI Chemicals [84], used as received, 1 mL of acetonitrile and the stirring bar. When the equipment is properly programmed for starting the reaction, TBHP is introduced slowly. The vial is closed with the cap and introduced inside the microwave equipment. After microwave reaction stops, the final solution is collected inside a little glass flask under nitrogen atmosphere and kept refrigerated and protected from light in fridge (3-5 °C) same as with HMF (Figure 38). It's important to highlight that HFCA product from TCI Chemicals came in solid state, and that's the reason why in this reaction is added 1 mL of acetonitrile, if not, the stirring bar could not have worked properly. The amount of reagents were switched from 5 mmol and 10 mmol to 0,5 mmol and 1 mmol (HFCA and TBHP respectively) to be able to have more reagent as HMF ended after 7 reactions.



Figure 38: Different samples of HFCA microwave-assisted oxidation before being stored.

Table 13: Different HFCA microwave-assisted oxidation samples.

Code	T(°C)	Catalyst	m _{catalyst} (mg)	Conditions
PGff8	50	-	-	Homogenous
PGff9	50	PGAuGLAG_up	10	Heterogenous
PGff10	50	PGAuGMW_up	10	Heterogenous
PGff11	50	PGAuGWI_up	10	Heterogenous
PGff12	50	ultrapure graphene	10	Heterogenous
PGff13	50	BMAu2	10	Heterogenous
PGff14	50	[AuCl ₂ (Tpm)]Cl	10	Homogenous
PGff15	50	HAuCl ₄ ·xH ₂ O	10	Homogenous
PGff16	80	PGAuGLAG_up	10	Homogenous

Reaction conditions: 650 rpm, 2 h, and 25 W.

¹H NMR characterization was performed for glycerol and furfural derivatives on Bruker Advance 300 MHz at room temperature and using deuterated acetone as solvent as showed in Figure 39. This characterization method was used to identify the compounds obtained in each oxidation test.

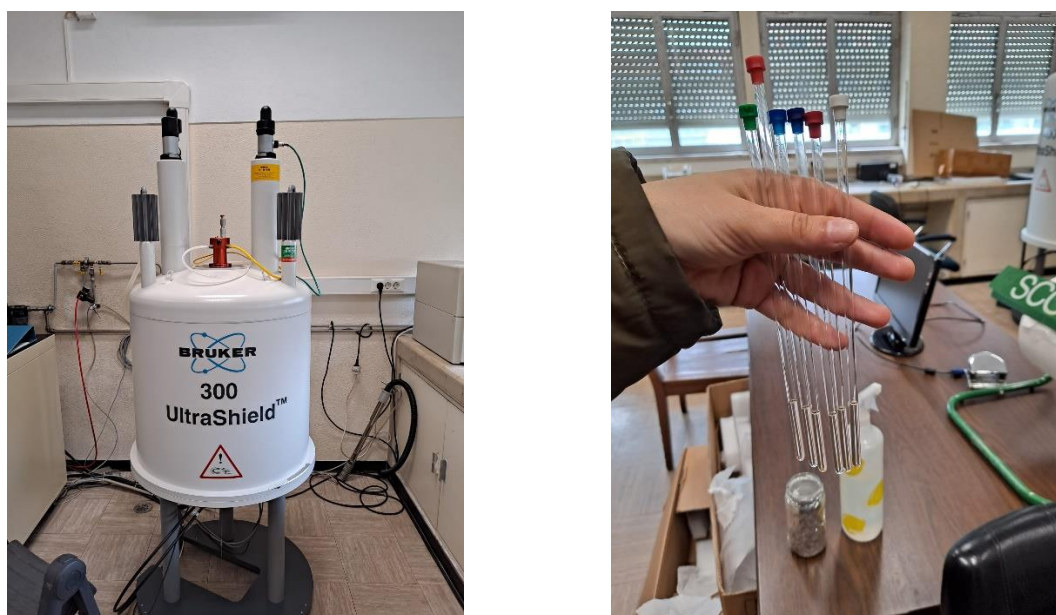


Figure 39: Bruker Advance 300 MHz (left) and different oxidation samples with deuterated acetone for its characterization (right).

3 Results and discussion

In this third chapter, all results obtained from the different experimental procedures (catalysts preparation and immobilization, and catalytic oxidation reactions) are presented and discussed.

After the synthetic procedure described in the last chapter, the characterization of the formed complexes is presented in this chapter.

First, different infrared spectra FTIR-ATR, MIR and FAR regions from the different metal C-scorpionate synthesised are presented and discussed.

To characterize the different immobilization methods of complex **4** on graphene, FTIR spectra are showed along with SEM/EDS.

Following the same order as in the previous chapter, thanks to ¹H NMR spectra the performance results are presented from the different microwave-assisted oxidations of glycerol, HMF and HFCA.

The complexes **1-4** depicted in the Figure 40 were successfully synthesised as described in Chapter 2. The characterization results that follow indicate such synthetic achievement. The best mechanochemical conditions for the synthesis of complexes **1-4** are presented in Table 14.

Table 14: Best mechanochemical conditions for the synthesis of complexes **1-4**.

Complex	Sample code	Yield (%)	Conditions
1	PGCuBM6	82.60	15 min 5 spheres 250 rpm
2	PGNiBM4	55.90	15 min 3 spheres 500 rpm
3	PGCoBM4	69.50	15 min 3 spheres 500 rpm
4	PGAuBM4	59.90	15 min 3 spheres 500 rpm

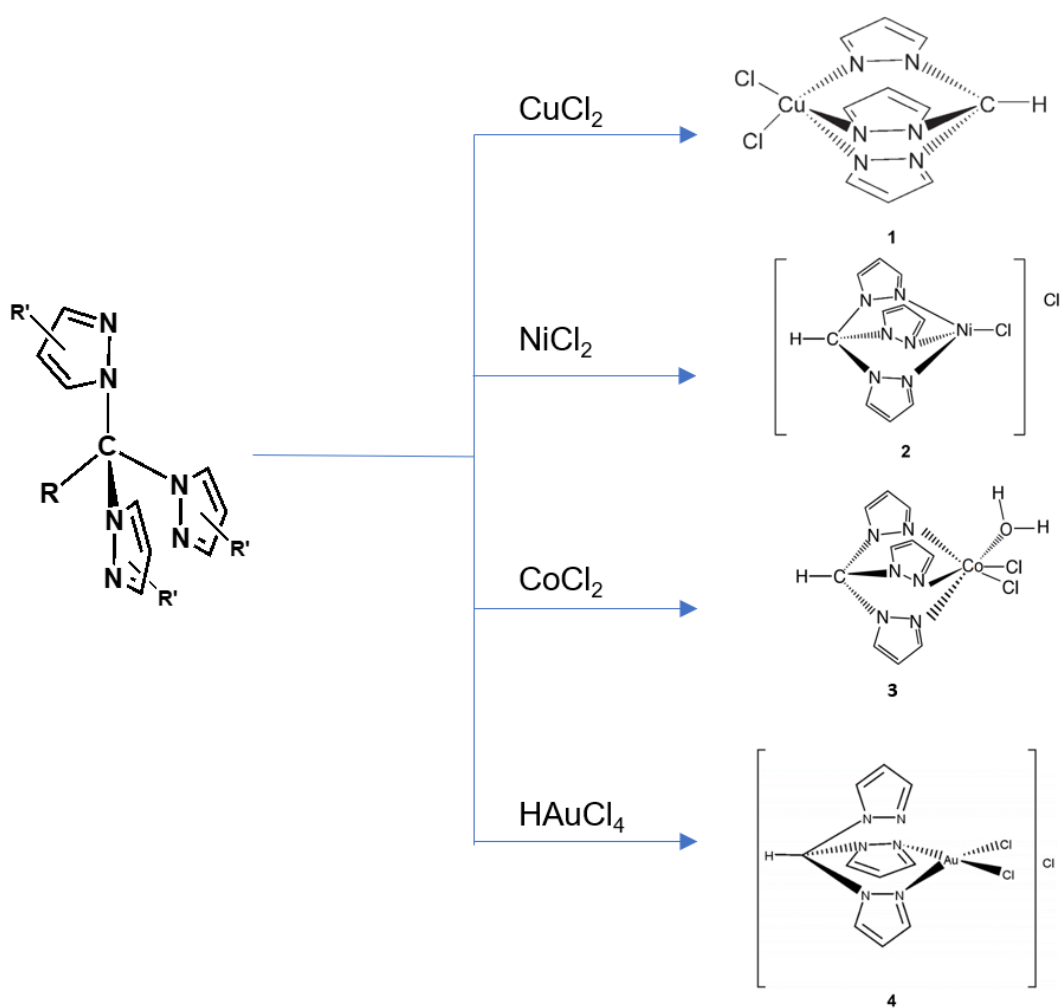


Figure 40: Synthesis of Complexes 1 – 4 from hydrotris(pyrazol-1-yl)methane and the appropriate different metal chlorides.

3.1 Copper C-scorpionate complex [CuCl₂(Tpm)] (1)

3.1.1 Characterization

MIR (4000–400 cm⁻¹) and FAR-IR (400–100 cm⁻¹) were recorded on a Vertex 70 (Bruker) instrument in KBr pellets for IR and CsI for the FAR analysis.

Two samples above all were selected for proper MIR and FAR regions (Figure 41, Figure 42, Figure 43, and Figure 44): PGCuBM4L and PGCuBM6L because their representative time, number of spheres and rpm.

PGCuBM4L was 15 min inside PM100 Planetary Ball Mill, with 4 spheres and 500 rpm:

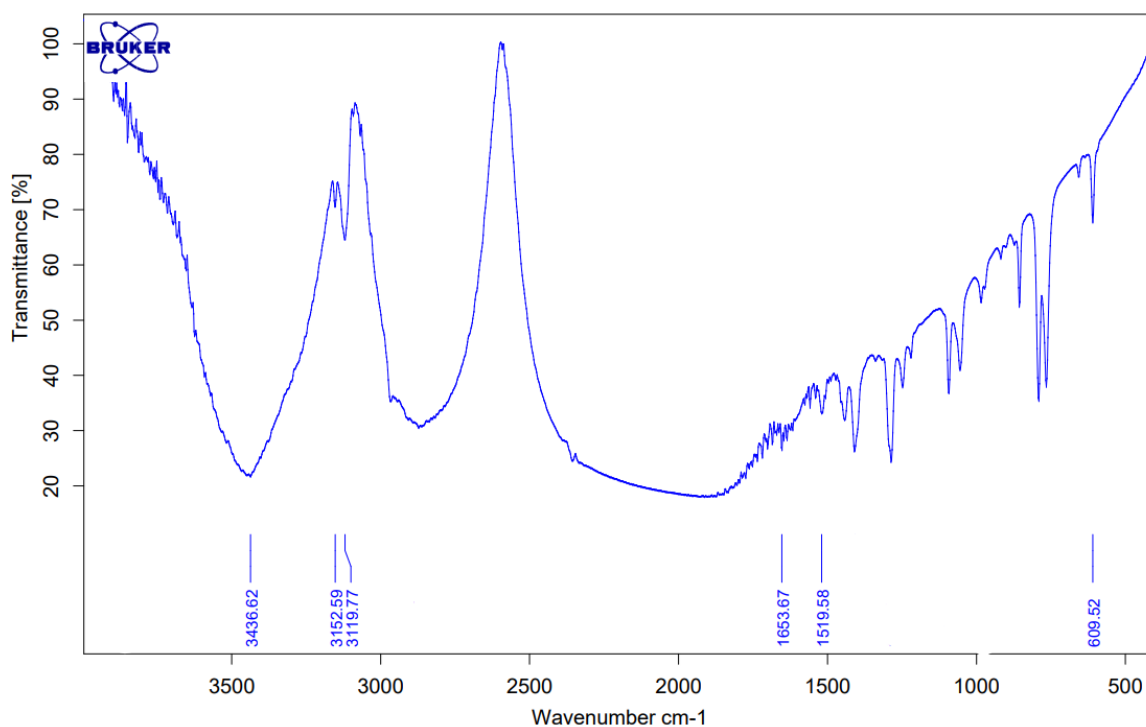


Figure 41: MIR spectrum of PGCuBM4L

IR (cm⁻¹): 3436.62 br [ν(O-H)], 3152.59 sh, 3119.77 m [ν(C-H)], 1653.67 br [ν(O-H)], 1519.58 m, 609.52 s [ν(Cu-Cl)].

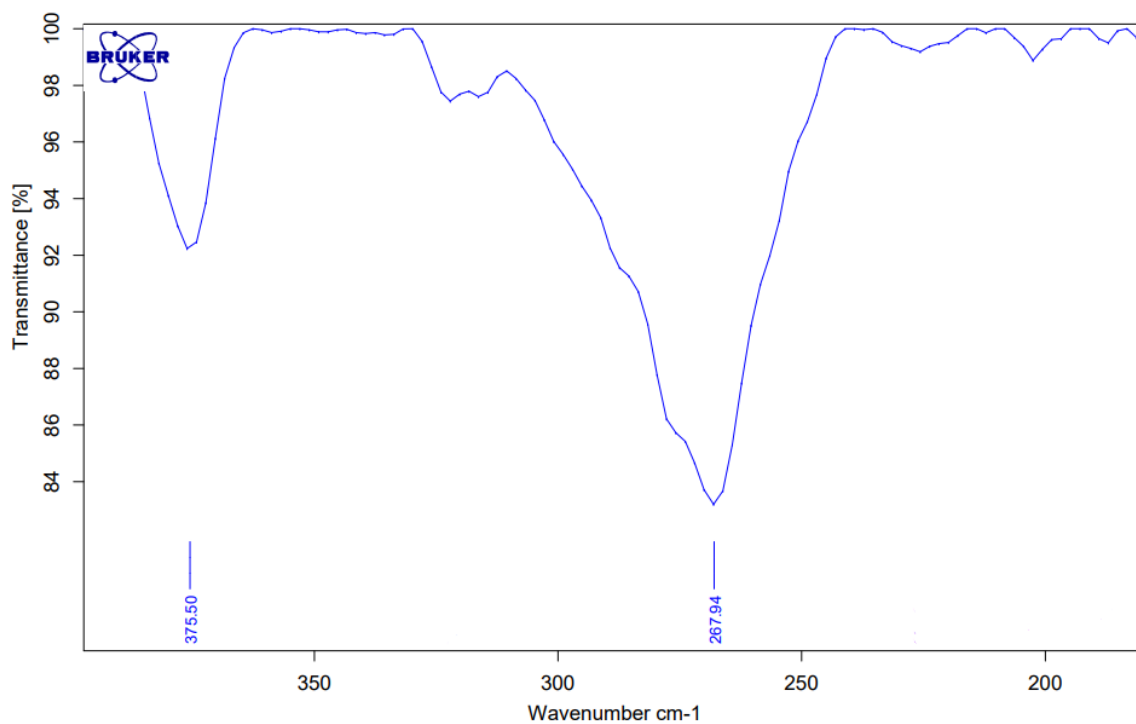


Figure 42: FAR spectrum of PGCuBM4L

FAR (CsI pellet) (cm^{-1}): 375.50 s, 267.94 s [$\nu(\text{Cu-Cl})$].

In the case of PGCuBM6L, it was also 15 minutes inside the ball Mill, but with 5 spheres and 250 rpm.

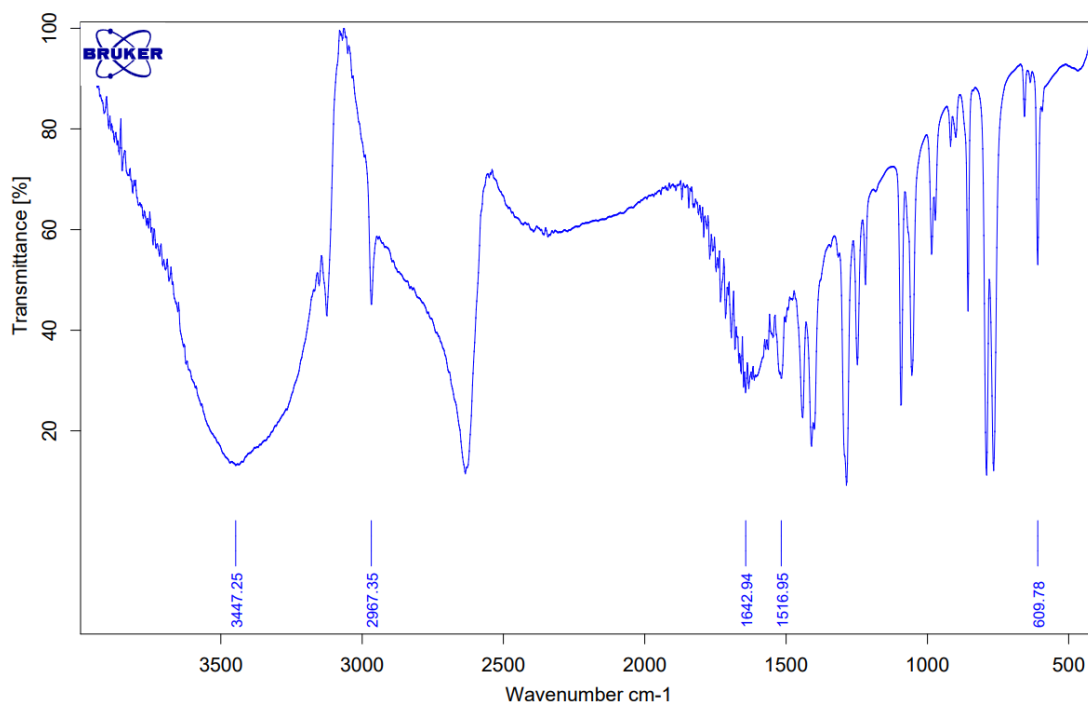


Figure 43: PGCuBM6L MIR spectrum.

IR (cm^{-1}): 3447.25 br [$\nu(\text{O-H})$], 3125.30 sh, 2967.35 m [$\nu(\text{C-H})$], 1642.94 br [$\nu(\text{O-H})$], 1519.95 m, 609.78 s [$\nu(\text{Cu-Cl})$].

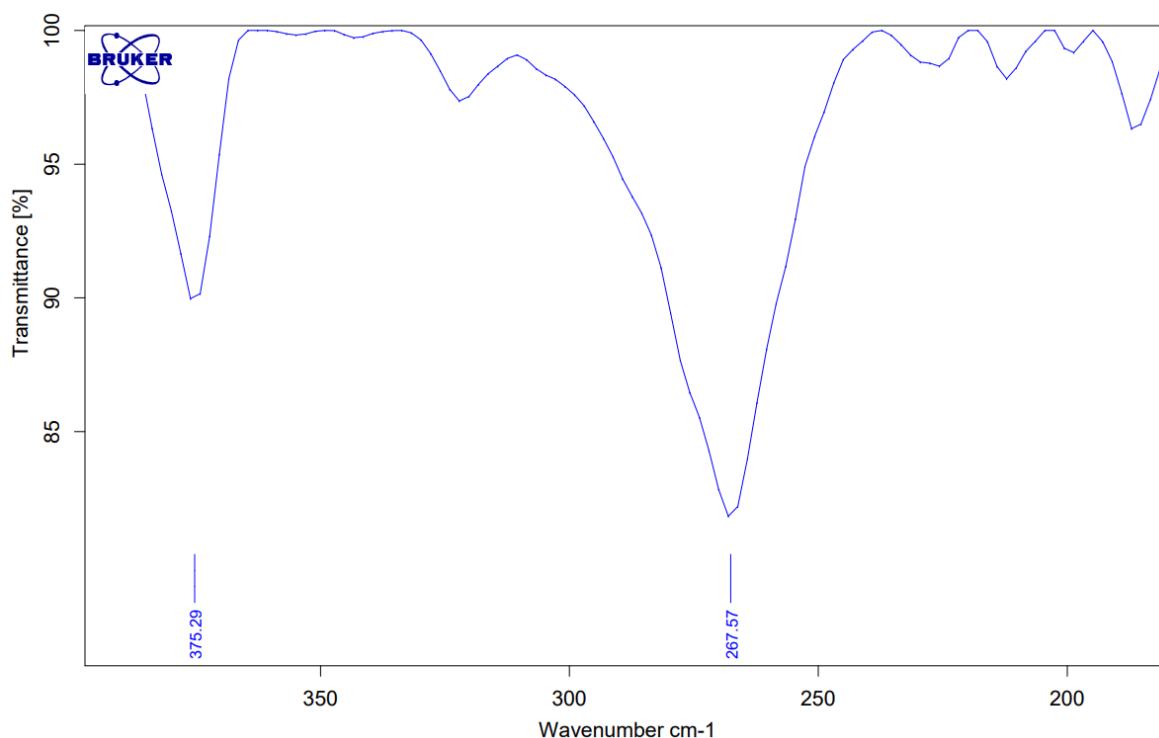


Figure 44: FAR spectrum of PGCuBM6L

FAR (Csl pellet) (cm^{-1}): 375.29 s, 267.57 s [$\nu(\text{Cu}-\text{Cl})$].

Similar peaks were confirmed to agree with reported literature [39] being one validation that the expected complex **1** structure was obtained. For both samples we can observe that after 15 min the complex is formed, regardless of the number of spheres used and the rpm. This shows that the solid reactants can react quickly and form the desired complex.

From the samples presented of Table 3, it can be highlighted that the best conditions to prepare the C-scorpionate copper(II) complex $[\text{CuCl}_2(\text{Tpm})]$ (**1**) are: time of reaction 15 min, using 5 spheres and 250 rpm, since PGCuBM6 was the sample that get the best yield (82.6%). It was followed by PGCuBM4 (15 min, 3 spheres, 500 rpm and yield of 82.3%). As expected, the worst yield was obtained for PGCuM7 (mortar sample). Comparing with the method reported in literature [39] where the yield of 83% of complex **1** was obtained, mechanochemistry method showed great performance and quick obtention of the same complex with practically same yield.

Elementary analysis of PGCuBM4L sample was obtained through the IST analysis laboratory. When comparing the result obtained by the analysis with the predicted values, presented in Table 15, it is observed that the two coincide, within an acceptable error, being one more validation of the reaction result.

Table 15: Comparison between theoretical values and those obtained in elementary analysis.

	%C	%H	%N
Theoretical	34.44	2.89	24.10
Exp1	32.59	2.68	22.34
Exp2	32.61	2.76	22.36
Exp Average	32.60	2.72	22.35
Error	1.30	0.12	1.24

3.2 Nickel C-scorpionate complex $[\text{NiCl}(\text{Tpm})]\text{Cl}$ (2)

3.2.1 Characterization

MIR ($4000\text{--}400\text{ cm}^{-1}$) and FAR-IR ($400\text{--}100\text{ cm}^{-1}$) were recorded on a Vertex 70 (Bruker) instrument in KBr pellets for IR and CsI for the FAR analysis.

Like with copper samples, two samples above all were selected for proper MIR and FAR regions (Figure 45, Figure 46, Figure 47, and Figure 48): PGNiBM4 and PGNiBM6' because their representative time, number of spheres and rpm.

PGNiBM4 was 15 min inside PM100 Planetary Ball Mill, with 4 spheres and 500 rpm:

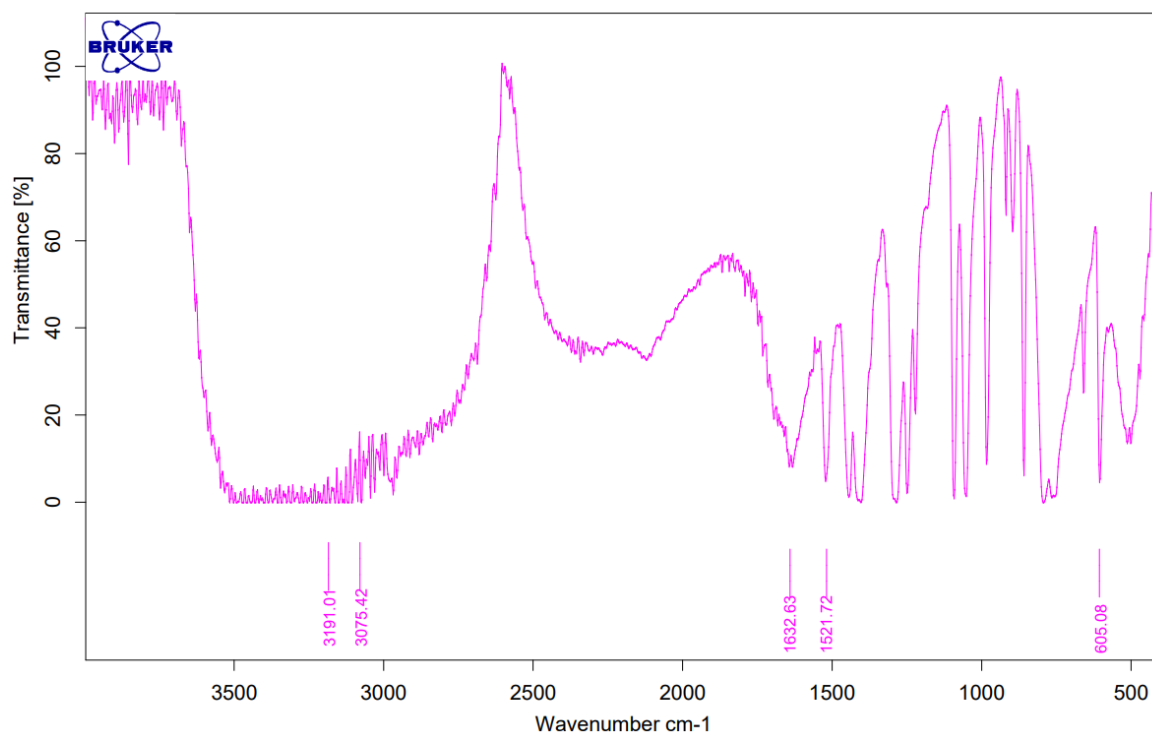


Figure 45: PGNiBM4 MIR spectrum.

IR (cm^{-1}): 3191.01 sh, 3075.42 m [$\nu(\text{C-H})$], 1632.63 br, 1521.72 m [$\nu(\text{O-H})$], 605.08 s [$\nu(\text{Ni-Cl})$].

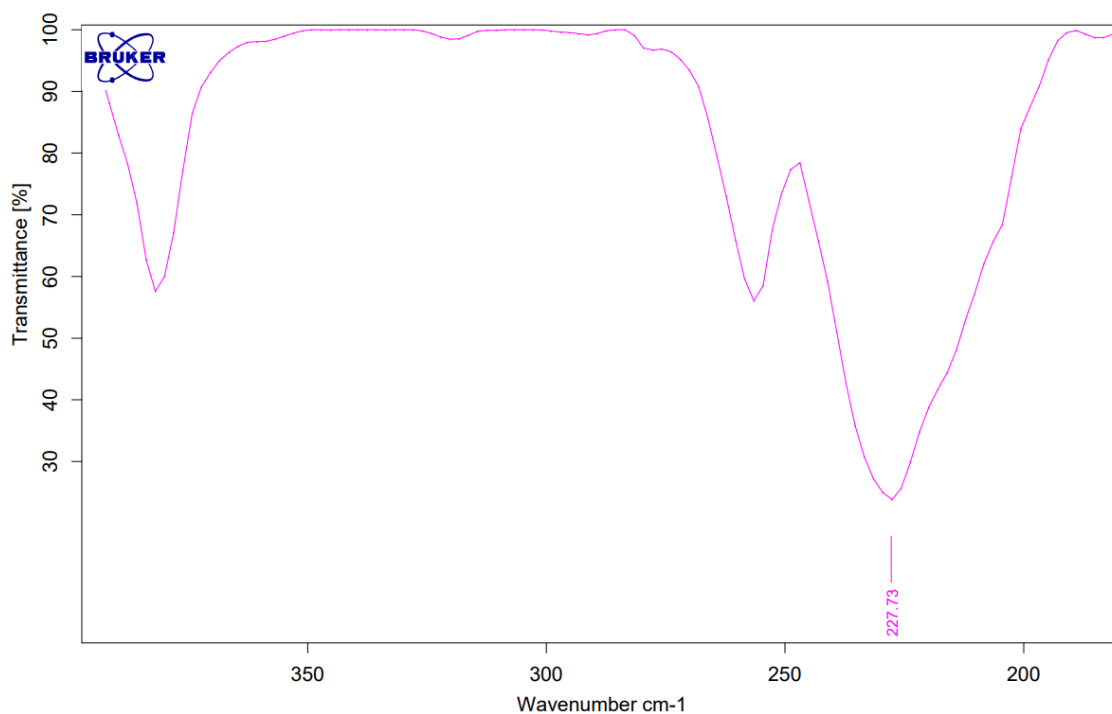


Figure 46: PGNiBM4 FAR spectrum.

FAR (CsI pellet) (cm^{-1}): 227.73 s [$\nu(\text{Ni-Cl})$].

In the case of PGNiBM6', it was also 15 minutes inside the ball mill, but with 5 spheres and 250 rpm.

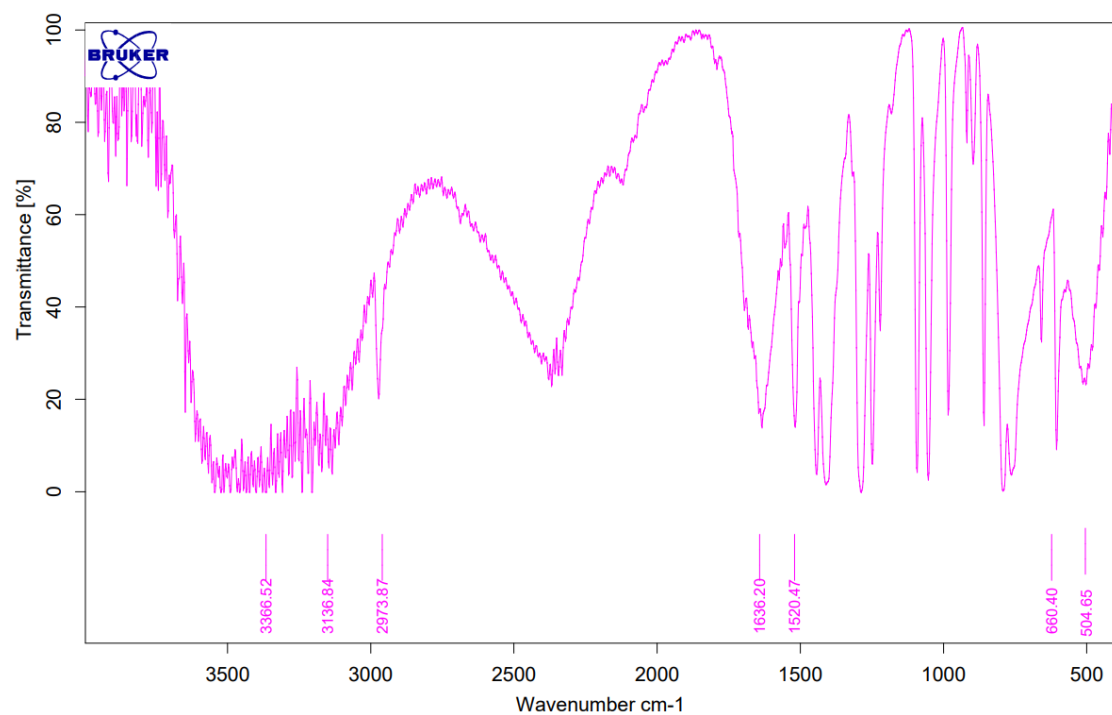


Figure 47: PGNiBM6' MIR spectrum.

IR (cm^{-1}): 3366.52 sh, 3136.84 sh, 2973.87 m [$\nu(\text{C-H})$], 1632.20 br, 1520.47 m [$\nu(\text{O-H})$], 660.40 s, 504.65 s [$\nu(\text{Ni-Cl})$].

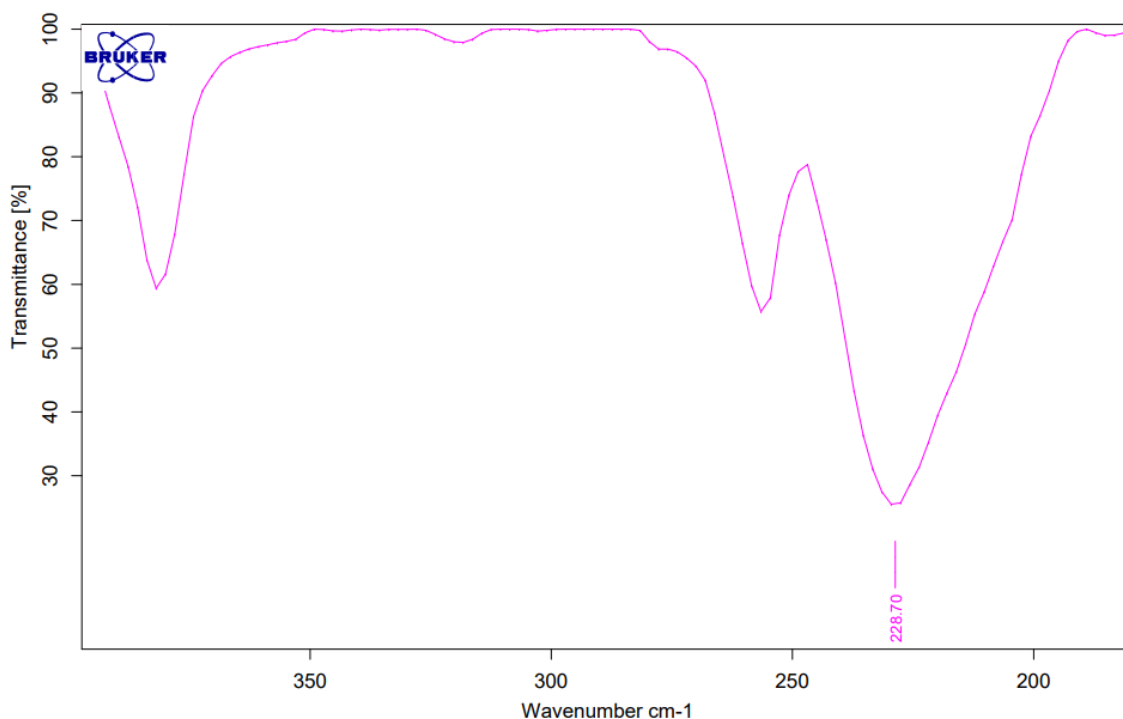


Figure 48: PGNiBM6' FAR spectrum.

FAR (CsI pellet) (cm^{-1}): 227.73 s [$\nu(\text{Ni-Cl})$].

Similar peaks were confirmed to agree with reported literature [41] being one validation that the expected complex **2** structure was obtained. For both samples we can observe that after 15 min the complex is formed, regardless of the number of spheres used and the rpm. This shows that the solid reactants can react quickly and form the desired complex.

For the C-scorpionate Ni(II) complex, it can be highlighted from the samples of Table 4 that the best conditions to prepare the C-scorpionate nickel(II) complex $[\text{NiCl}(\text{Tpm})]\text{Cl}$ (**2**) are: reaction time 15 min, using 3 spheres and 500 rpm (yield of 55.9%), which led to almost the same value as the obtained with 15 min. reaction time, 5 spheres and 250 rpm (54.6%). Again, as expected, the worst yield was obtained for PGNiM7 (mortar sample). Worst yield result was obtained compared with the 86% of yield reported on literature [41], the reason was probably the fact that the Nickel chloride was hexahydrate, and was difficult to remove the product from reactor and spheres of the ball mill machine.

Elementary analysis of PGNiBM4 sample was obtained through the IST analysis laboratory. When comparing the result obtained by the analysis with the predicted values, presented in Table 16, it is observed that there is some error, being one more validation of the reaction result. This could be due to the experimental procedure, probably the washing step and the removal of Tpm.

Table 16: Comparison between theoretical values and those obtained in elementary analysis.

	%C	%H	%N
Theoretical	34.93	2.93	24.44
Exp1	30.22	3.80	20.91
Exp2	30.18	3.80	20.92
Exp Average	30.20	3.80	20.92
Error	3.35	0.61	2.49

3.3 Cobalt C-scorpionate complex [CoCl₂(H₂O)(Tpm)] (3)

3.3.1 Characterization

MIR (4000–400 cm⁻¹) and FAR-IR (400–100 cm⁻¹) were recorded on a Vertex 70 (Bruker) instrument in KBr pellets for IR and CsI for the FAR analysis.

Like with the previous metal C-scorpionate synthesis experiences, two samples above all were selected for proper MIR and FAR regions (Figure 49, Figure 50, Figure 51, and Figure 52): PGC_oBM4 and PGC_oBM6 because their representative time, number of spheres and rpm.

PGC_oBM4 was 15 min inside PM100 Planetary Ball Mill, with 4 spheres and 500 rpm:

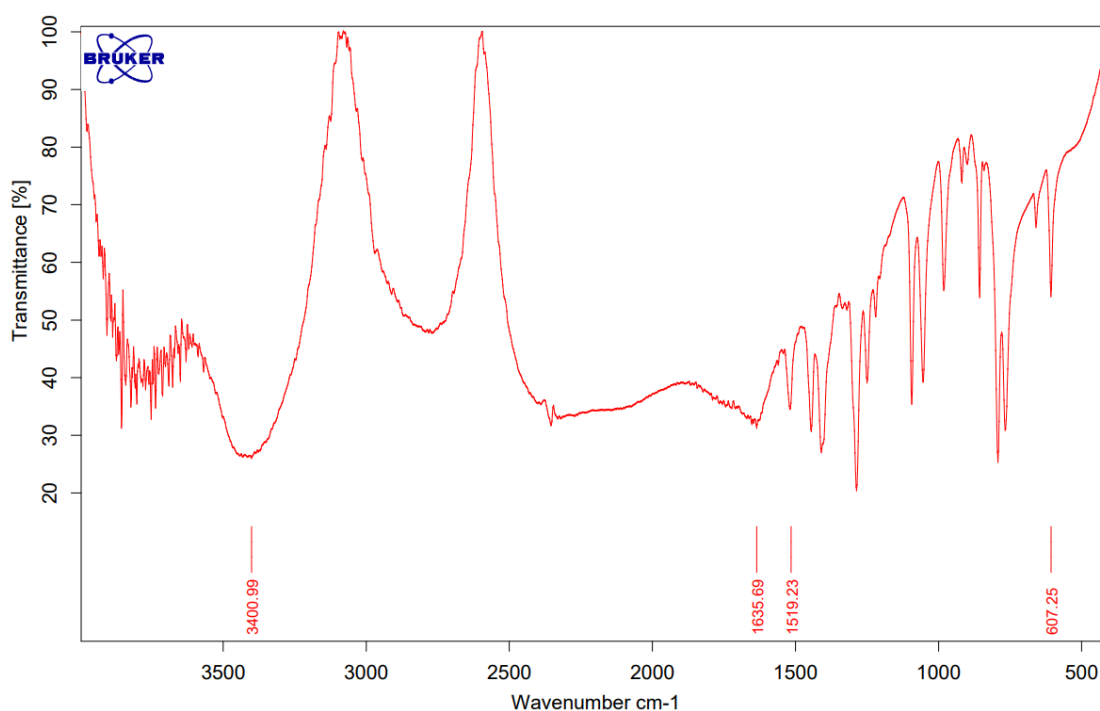


Figure 49: PGC_oBM4 MIR spectrum.

IR (cm⁻¹): 3401.00 br[ν(C-H)], 1635.69 br, 1519.23 m [ν(O-H)], 607.25 s [ν(Co-Cl)].

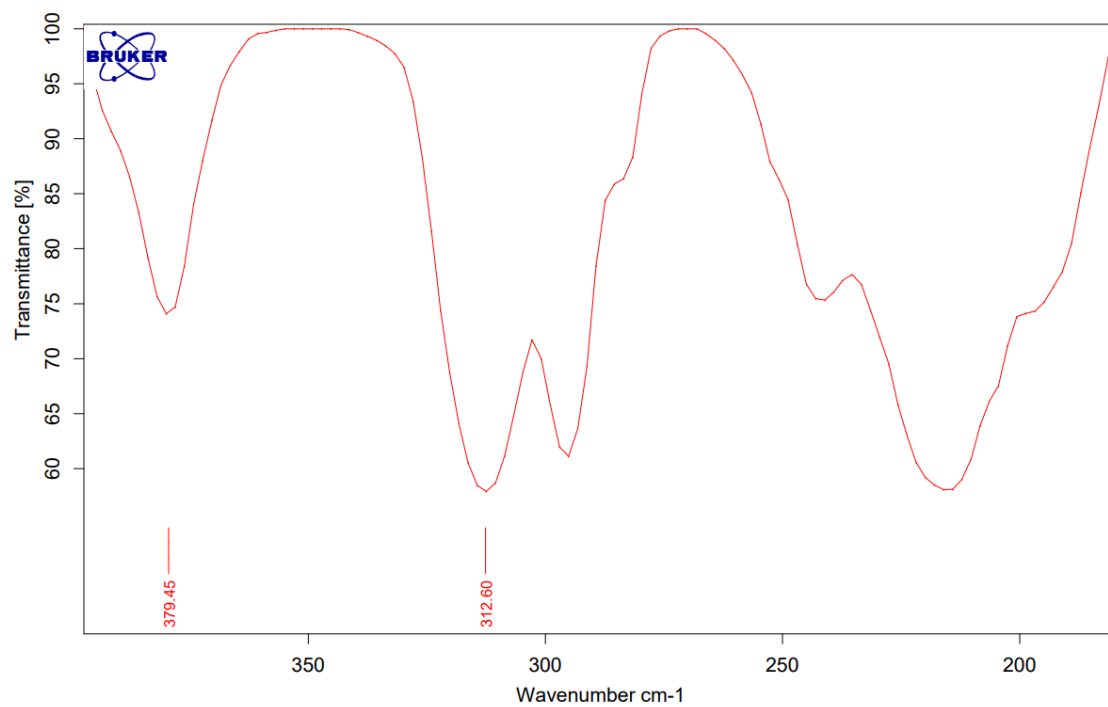


Figure 50: PGC0BM4 FAR spectrum.

FAR (CsI pellet) (cm^{-1}): 379.456 s, 312.60 s [$\nu(\text{Co-Cl})$].

In the case of PGC0BM6, it was also 15 minutes inside the ball mill, but with 5 spheres and 250 rpm:

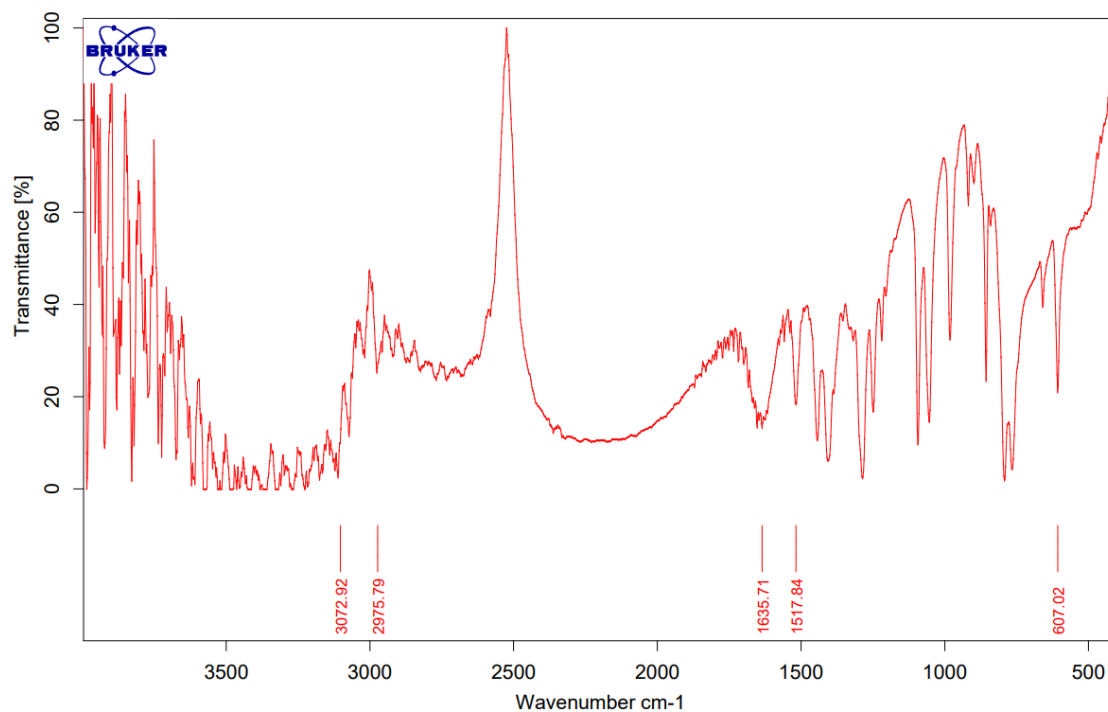


Figure 51: PGC0BM6 MIR spectrum.

IR (cm^{-1}): 3072.92 br, 2975.79 m [$\nu(\text{C-H})$], 1635.71 br, 1517.84 m [$\nu(\text{O-H})$], 607.02 s [$\nu(\text{Co-Cl})$].

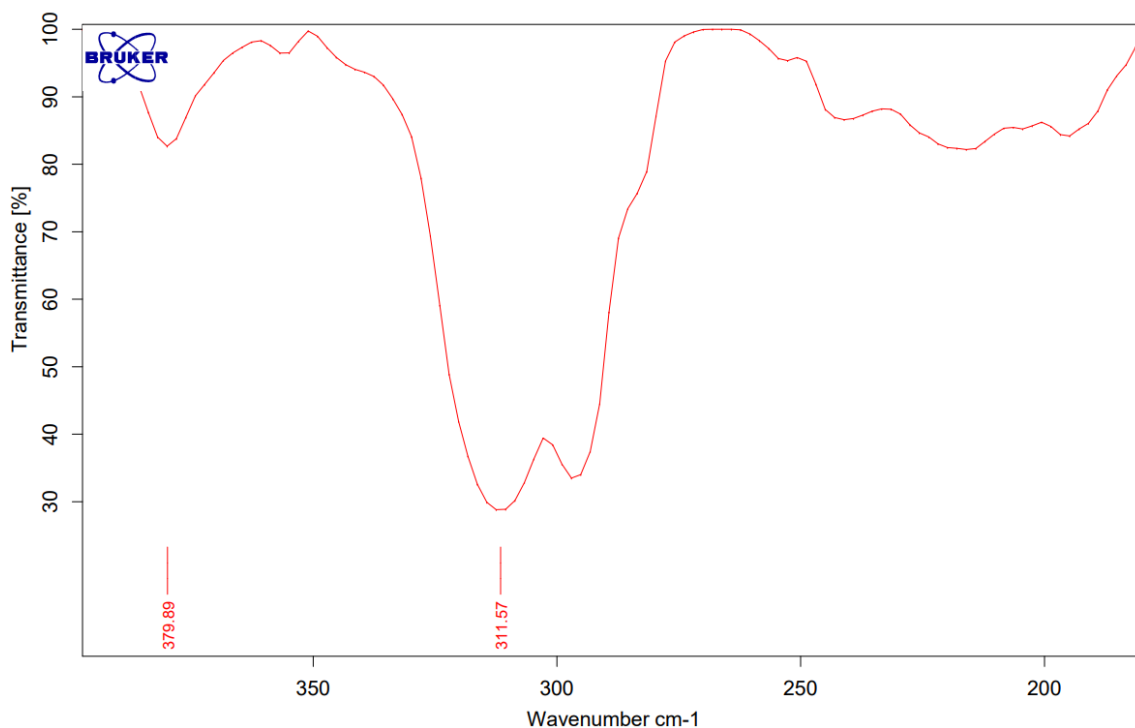


Figure 52: PGCobM6 FAR spectrum.

FAR (CsI pellet) (cm^{-1}): 379.89 s, 311,57 s [$\nu(\text{Co-Cl})$].

As complex **3** was tried to synthesized for first time, Tpm peaks were confirmed as reported in literature [77] , and the rest of peaks for Co, were confirmed comparing the difference of the bands due to the formation of N-Co bonds, reported on [42] For both samples we can observe that after 15 min the complex is formed, regardless of the number of spheres used and the rpm. This shows that the solid reactants can react quickly and form the desired complex.

For the different complex **3** samples presented in Table 5, it can be highlighted that PGCobM4 was the sample that get the best yield (69.5%, being time of reaction 15 min, using 3 spheres and 500 rpm) followed by, PGCobM2' (66.9%, 10 min, 3 spheres, 250 rpm washed with diethyl ether) and PGCobM2 (65.3%, 10 min, 3 spheres and 250 rpm). The worst yield was obtained for PGCobM7 (mortar sample).

As mentioned above, there's no literature to compare the synthesis yield for complex **3**, but another Co C-scorpionate complexes were reported [42] with yields under 60%, being the obtained yields for ball milling method higher than these ones.

Elementary analysis of PGC_oBM₄ sample was obtained through the IST analysis laboratory. When comparing the result obtained by the analysis with the predicted values, presented in Table 17, it is observed that the two coincide, in some elements with a better error than others, being one more validation of the reaction result. The error is probably due the washing procedure at the end of the synthesis.

Table 17: Comparison between theoretical values and those obtained in elementary analysis.

	%C	%H	%N
Theoretical	33.17	3.34	23.21
Exp1	28.15	3.44	19.16
Exp2	28.36	3.37	19.99
Exp Average	28.26	3.41	19.58
Error	3.48	0.05	2.57

3.4 Gold C-scorpionate complex $[\text{AuCl}_2(\text{Tpm})]\text{Cl}$ (**4**)

3.4.1 Characterization

MIR ($4000\text{--}400\text{ cm}^{-1}$) and FAR-IR ($400\text{--}100\text{ cm}^{-1}$) were recorded on a Vertex 70 (Bruker) instrument in KBr pellets for IR and CsI for the FAR analysis.

To compare traditional and ball milling synthesis, two samples above all were selected (Figure 53, Figure 54, Figure 55, and Figure 56): BMAu3L and one sample made by traditional method [44].

As explained in the previous experimental procedure chapter, BMAu3L was synthesised using PM100 Planetary Ball Mill during 15 min, 500 rpm and 3 spheres. After the experience was cleaned with methanol.

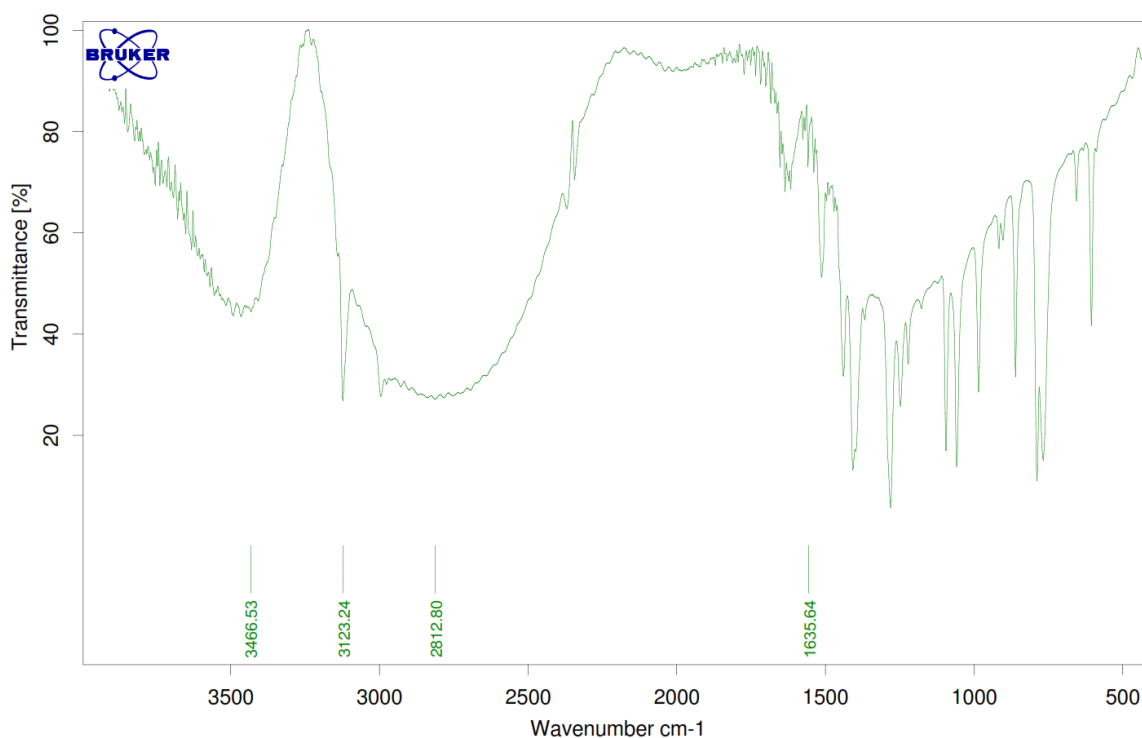


Figure 53: BMAu3L MIR spectrum.

IR (cm^{-1}): 3466.53 br, 3123.24 sh, 2812.80 m [v(C-H)], 1635.64 br [v(O-H)],

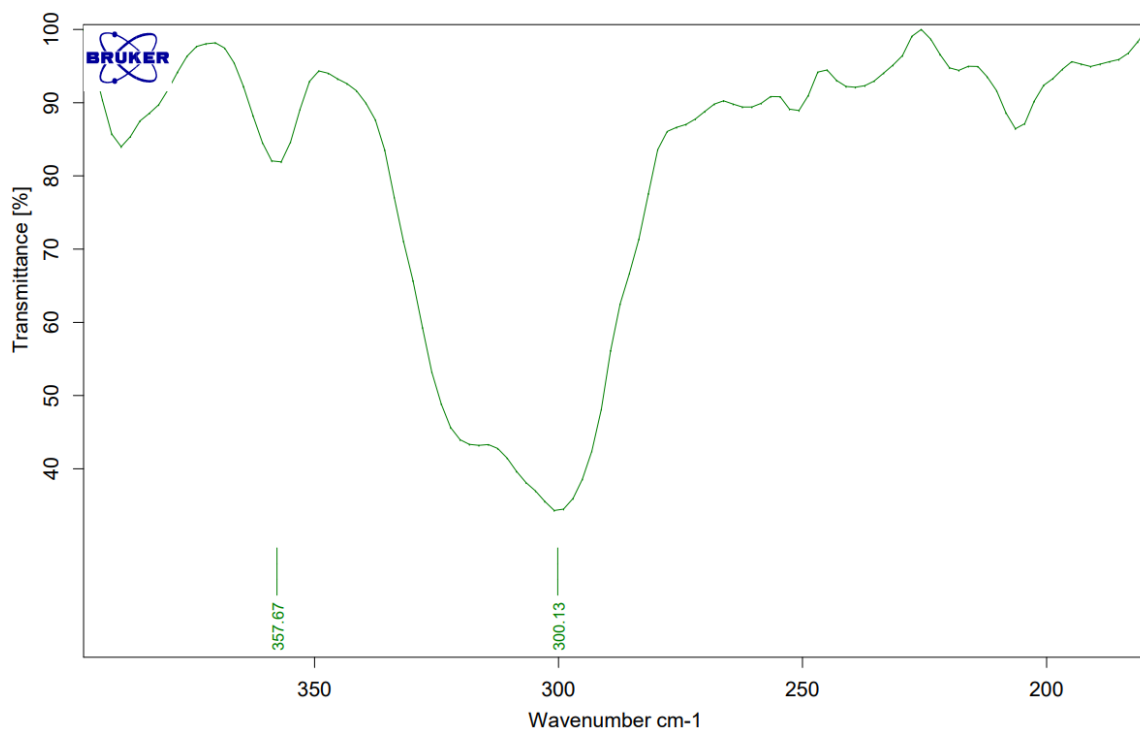


Figure 54: BMAu3L FAR spectrum.

FAR (CsI pellet) (cm^{-1}): 357.67 s [$\nu(\text{Au-Cl})$] asymmetric, 300.13 s [$\nu(\text{Au-Cl})$] symmetric.

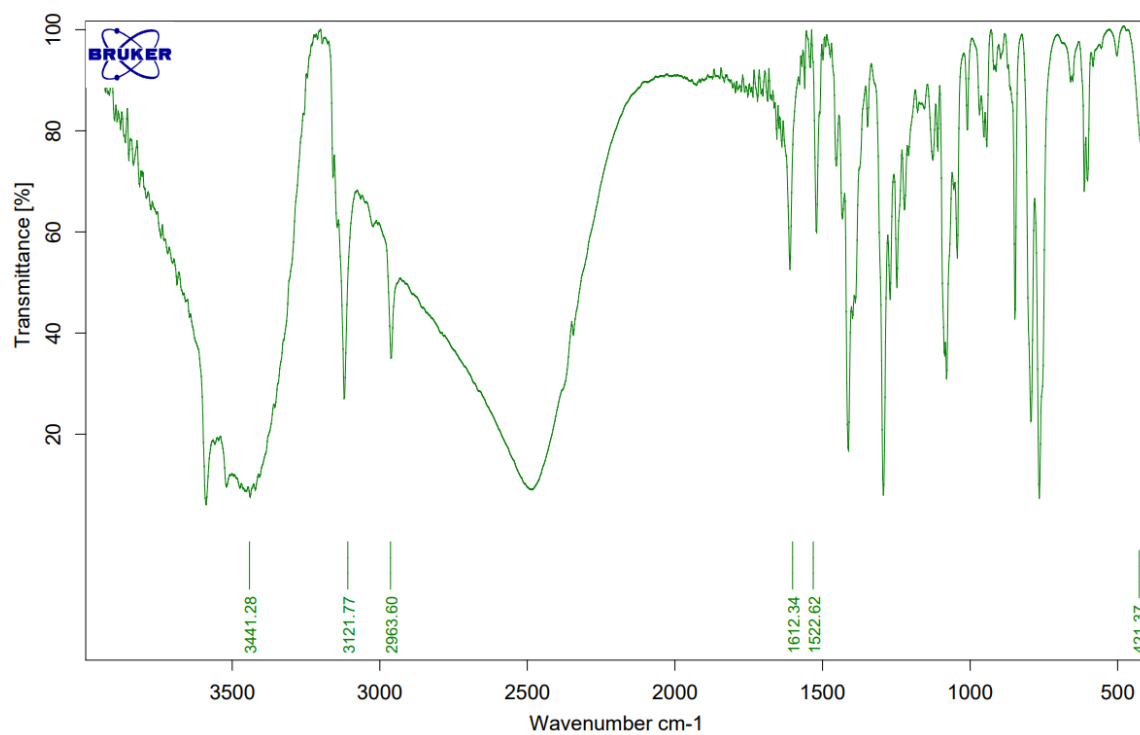


Figure 55: $[\text{AuCl}_2(\text{Tpm})]\text{Cl}$ synthesised by traditional method MIR spectrum.

IR (cm^{-1}): 3441.28 br, 3121.77 sh, 2963.60 m [$\nu(\text{C-H})$], 1612.34 br, 1522.62 m [$\nu(\text{O-H})$], 421.37 s [$\nu(\text{Au-Cl})$]

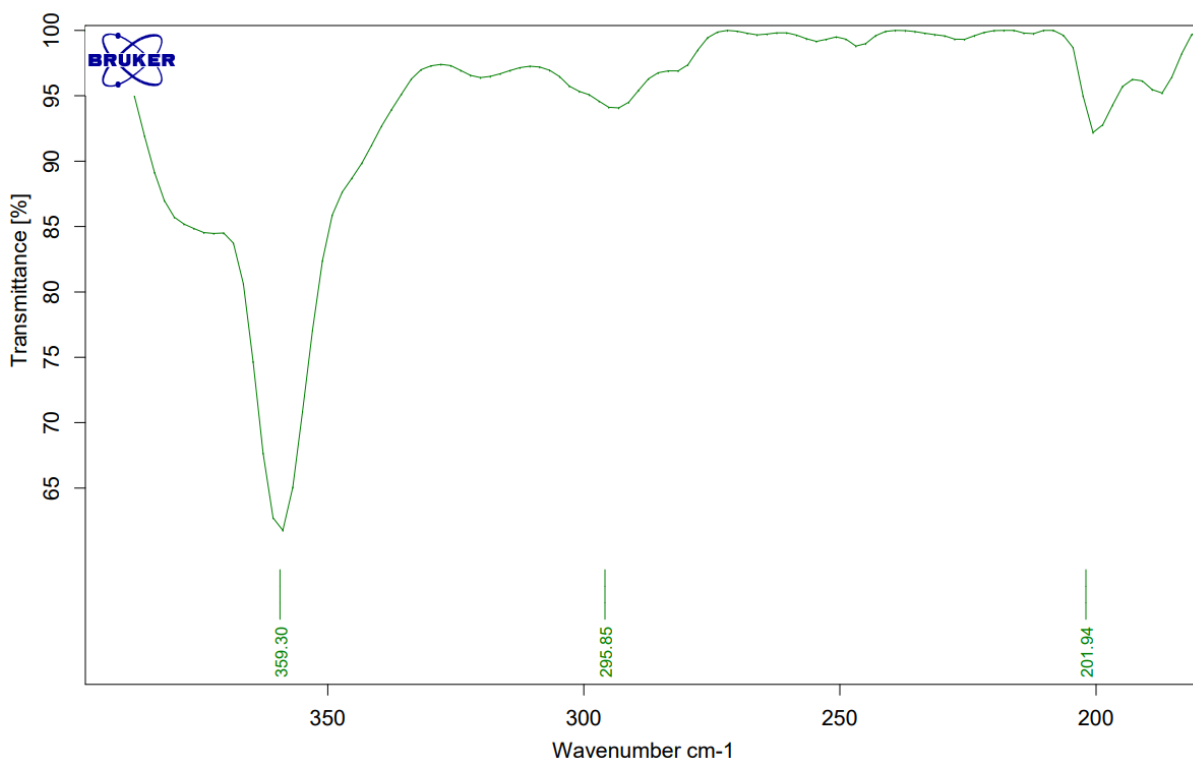


Figure 56: [AuCl₂(Tpm)]Cl synthesised by traditional method FAR spectrum.

FAR (Csl pellet) (cm⁻¹): 359.30 s, 201.94 s [ν (Au-Cl)] asymmetric, 295.85 s [ν (Au-Cl)] symmetric.

Similar peaks were confirmed to agree with reported literature [44] being one validation that the expected complex **4** structure was obtained. For BMAu3L sample it can be observed that after 15 min the complex is formed. This shows that the solid reactants can react quickly and form the desired complex like it happens with traditional method synthesis.

From the samples presented on Table 7, it can be highlighted that the best conditions to prepare the C-scorpionate gold(III) complex [AuCl₂(Tpm)]Cl (**4**) are: reaction time of 15 min, 3 spheres and 500 rpm, since PGAuBM4 was the sample that get the best yield (59.9%). It was followed by PGAuBM6 (yield of 52.1%, 15 min, 5 spheres, 250 rpm). As expected, the worst yield was obtained for PGAuM7 (mortar sample).

Similar yields were obtained with the samples BMAu1, BMAu2 and BMAu3L, with the same synthetic conditions of PGAuBM6.

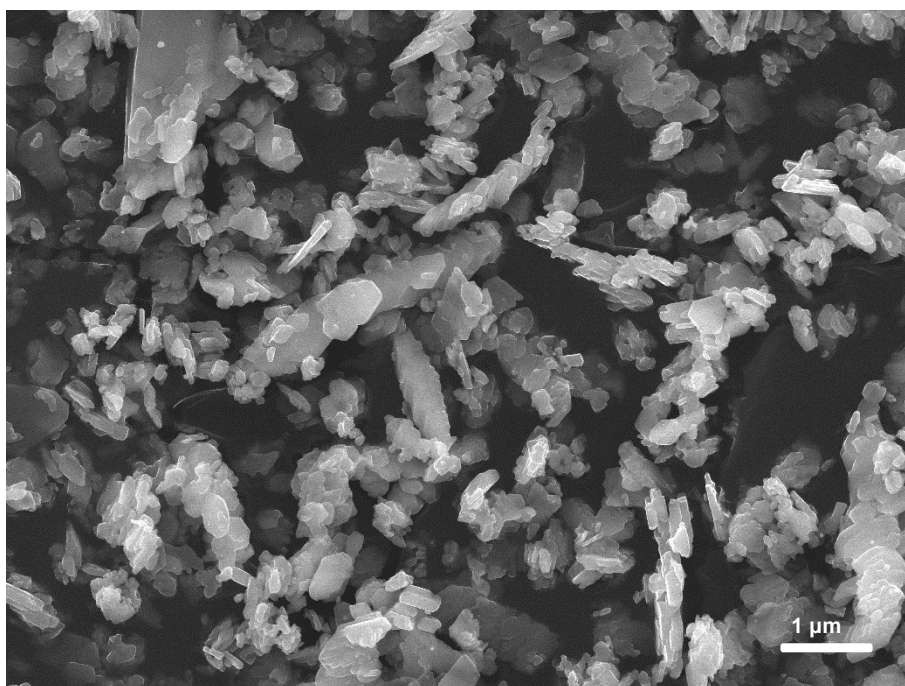
The synthesis yield reported for the traditional method was of 72% [44], being better than the ones obtained for ball milling samples. This could be, again, due to the difficulties removing the product from the spheres and jar, being the gold chloride hydrated.

Elementary analysis of BMAu3L sample was obtained through the IST analysis laboratory. When comparing the result obtained by the analysis with the predicted values, presented in Table 18, it is observed that the two coincide, although with a higher error, being one more validation of the reaction result. The error is probably due the washing procedure at the end of the synthesis and most likely related with Tpm.

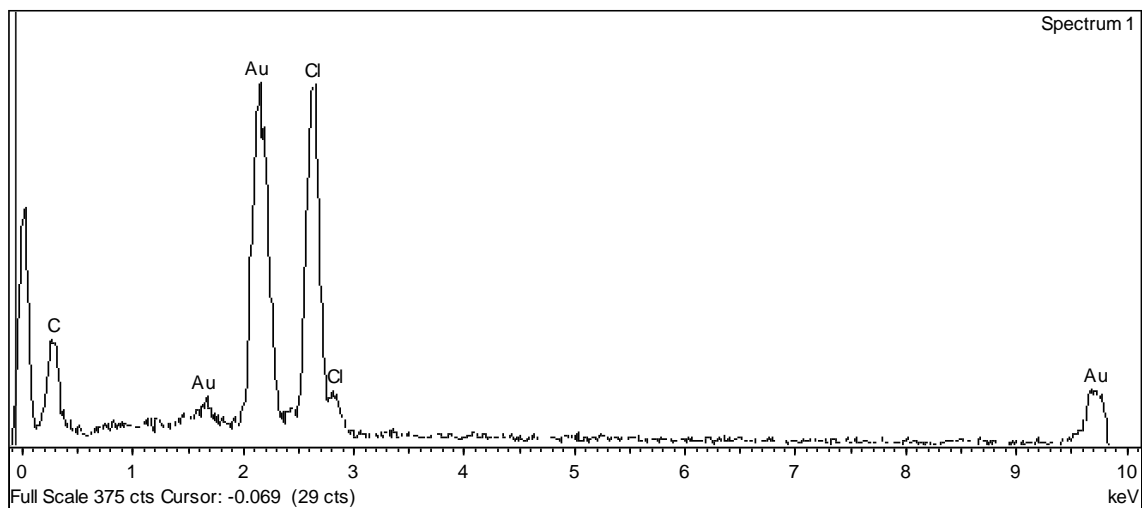
Table 18: Comparison between theoretical values and those obtained in elementary analysis.

	%C	%H	%N
Theoretical	23.21	1.95	16.24
Exp1	18.46	2.00	12.36
Exp2	18.29	2.00	12.19
Exp Average	18.38	2.00	12.28
Error	3.42	0.04	2.80

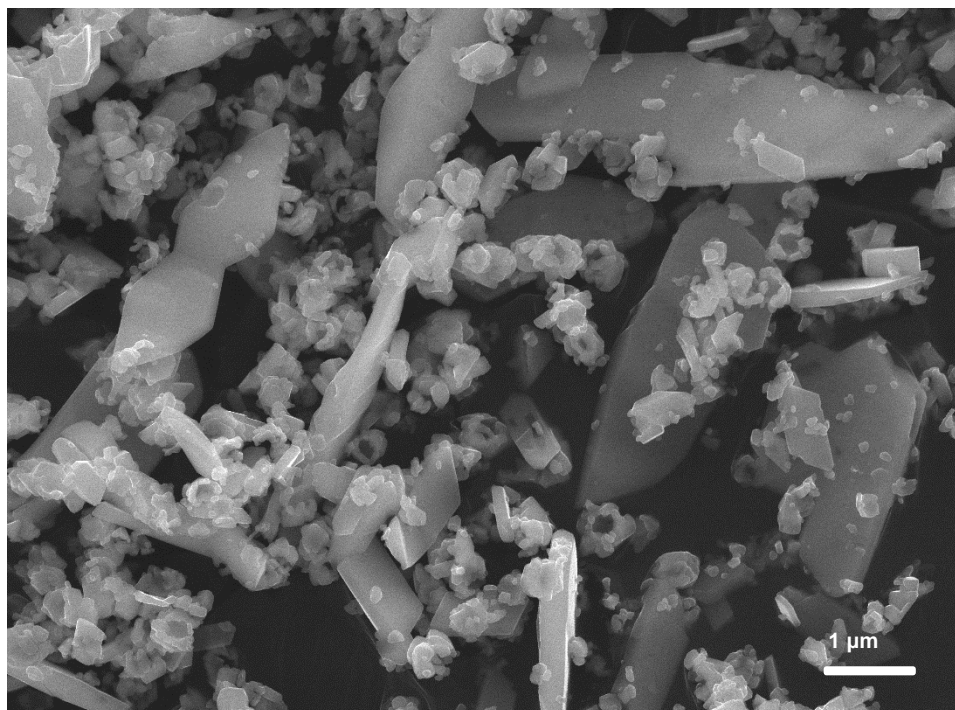
SEM and EDS were performed to observe the morphology of the surface of the complex, and its elements at the surface for the catalysts made by different techniques. Both SEM and EDS were performed by MicroLab-Electron Microscopy Laboratory of IST.



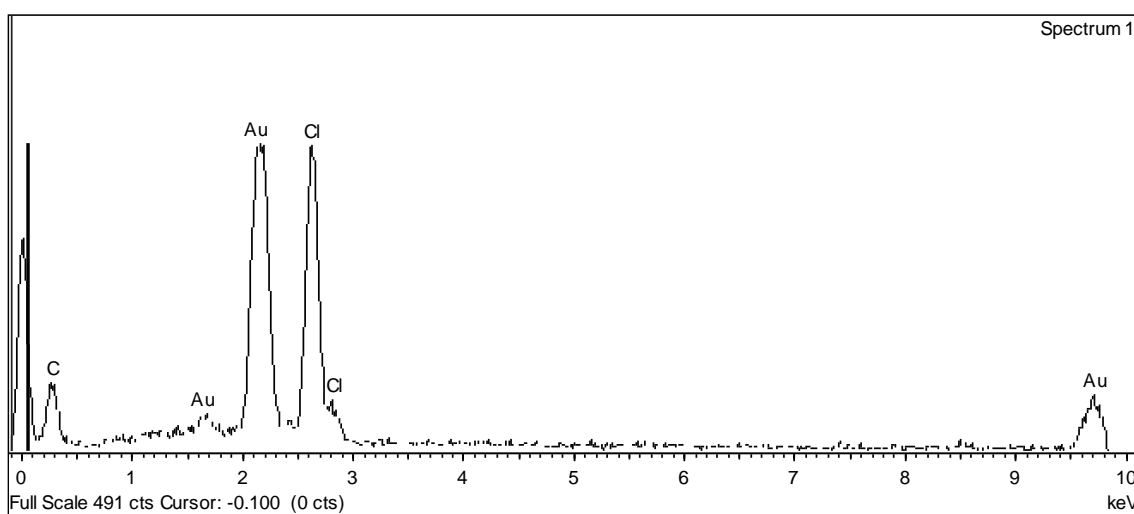
a)



b)



c)



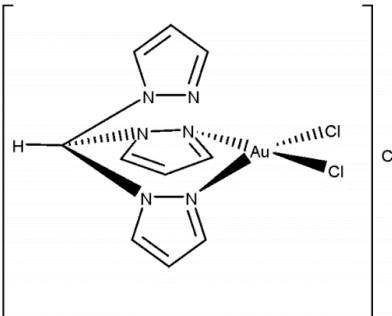
d)

Figure 57: SEM and EDS for the gold(III) complex. a) and b) represent ball milling and c) and d) traditional method reported in [44].

As it can be observed in Figure 57, the ball milled sample shows smaller pieces and more scattered. Although both samples show the same type of surface, in the case of the ball milled the have smaller size. It is the first time that the comparison of surfaces is performed for the gold(III) complex, and it is expected to have a different performance when used as catalysts, since it is at the surface that the catalytic mechanism occurs. In terms of EDS, they are quite similar, and it is further confirmation that the samples are the same complex.

XPS analysis was performed in the C-scorpionate gold(III) complex $[\text{AuCl}_2(\text{Tpm})]\text{Cl}$ (**4**) used for performing the catalytic studies that will be described in topics 3.5, 3.6 and 3.7. As presented in Table 19, the XPS global quantification shows accordance with the reported structure **4** and with the oxidation state of the gold (Au^{3+}). The analysis was kindly performed by Dr. Ana Ferraria, from IBB.

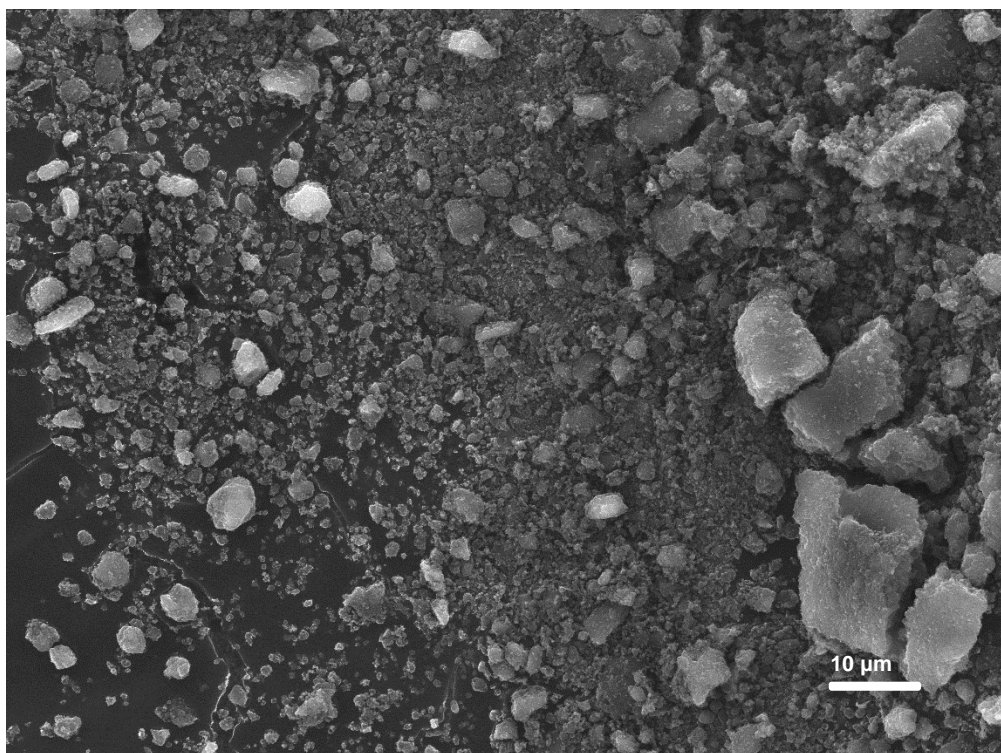
Table 19: XPS global quantification of gold(III) C-scorpionate complex $[\text{AuCl}_2(\text{Tpm})]\text{Cl}$ (**4**)

$[\text{AuCl}_2(\text{Tpm})]\text{Cl}$		
At. Conc. (%)		
Au	5.00	
Cl	11.90	
C	59.30	
O	7.00	
N	16.80	

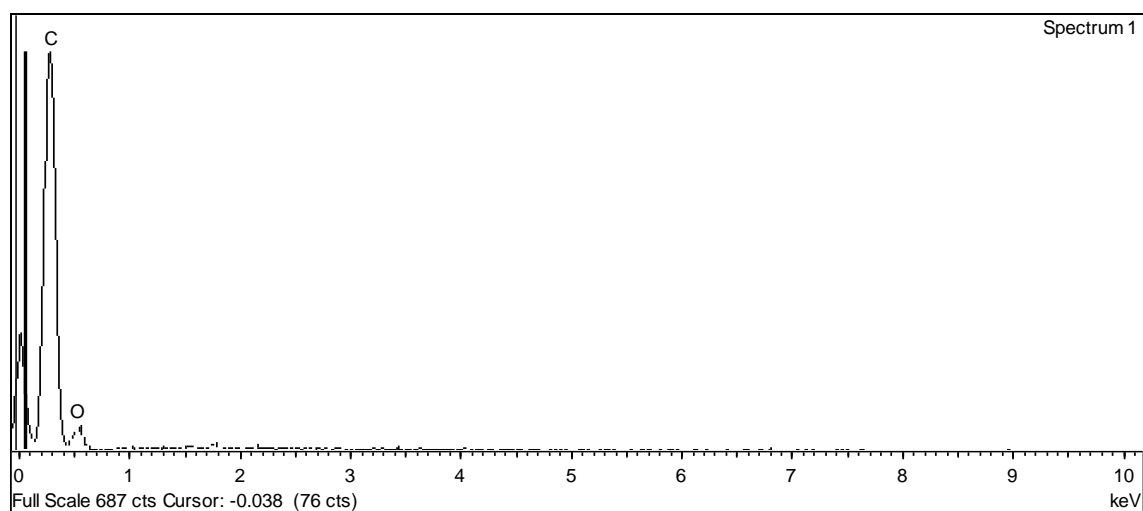
Gold(III) C-scorpionate complex **4** was the one used to perform the oxidation reactions due to its exceptional selectivity towards oxidation [44], but anyone of the complexes **1**, **2** and **3** could have been tried as low-cost catalysts. Complexes **1** and **2** were reported [40, 41] as promising green catalysts, being complex **2** a promising one to replace Pd in several reactions. Complex **3** was for first time synthesized and its use would have been interesting, but limited time during the realization of this preliminary work forced the decision of support only complex **4** to open a research gate in the future of the rest of the complex synthesized.

3.4.2 WI graphene supported gold(III) C-scorpionate complex $[\text{AuCl}_2(\text{Tpm})]\text{Cl}$ (4)

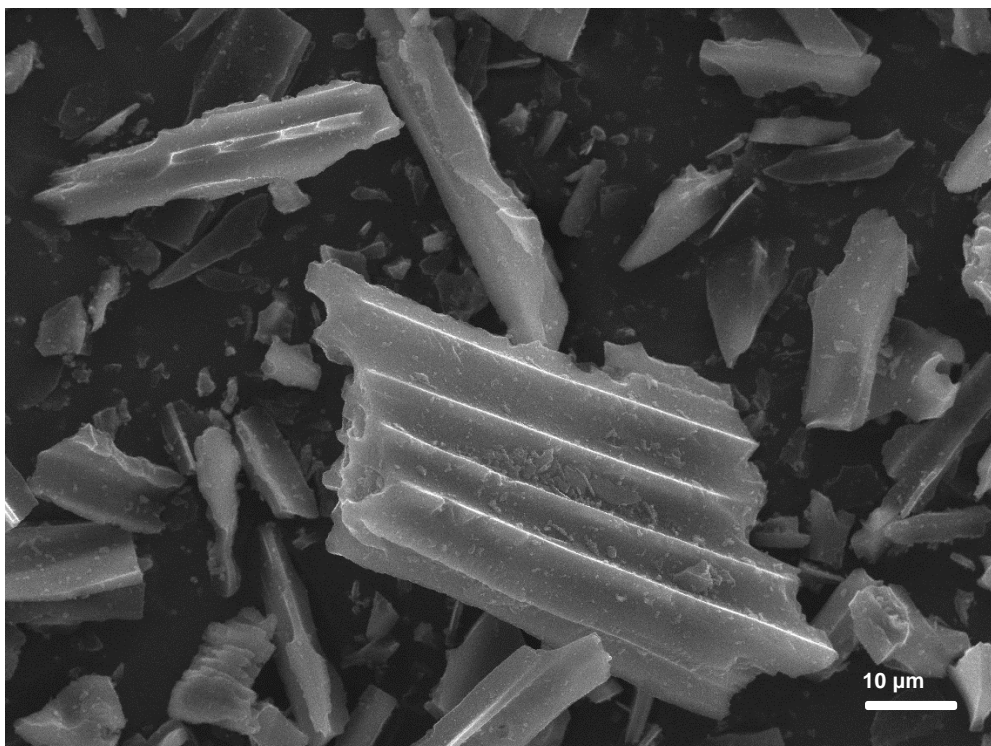
For the characterization of the different supported WI gold C-scorpionate catalysts, SEM/EDS was used. First, the 2 supports were characterized (Figure 58). The gold(III) complex used was the one synthesized by ball milling in the case of graphene and the one synthesized by reported in literature [44] method for ultra-pure graphene.



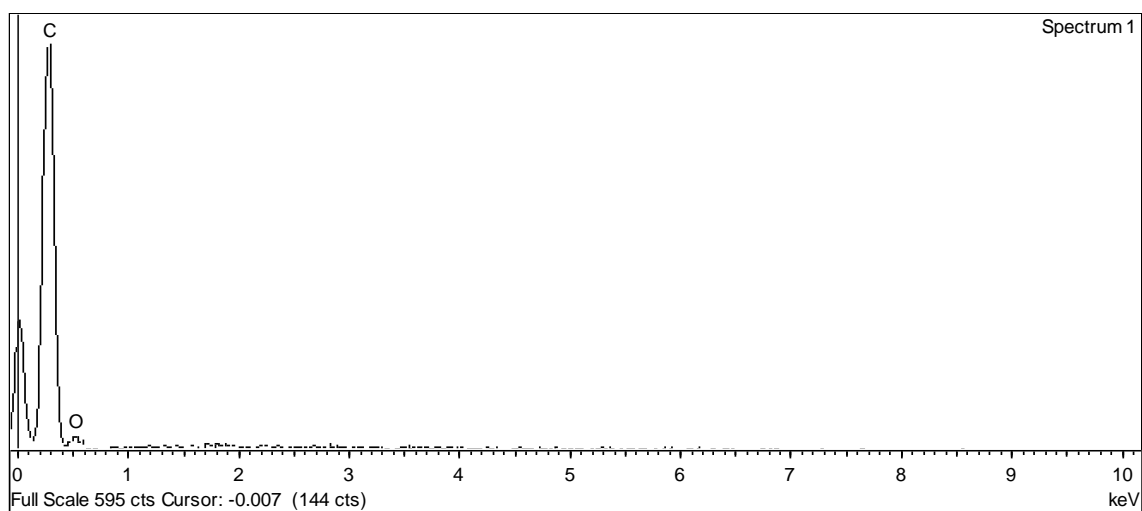
a)



b)



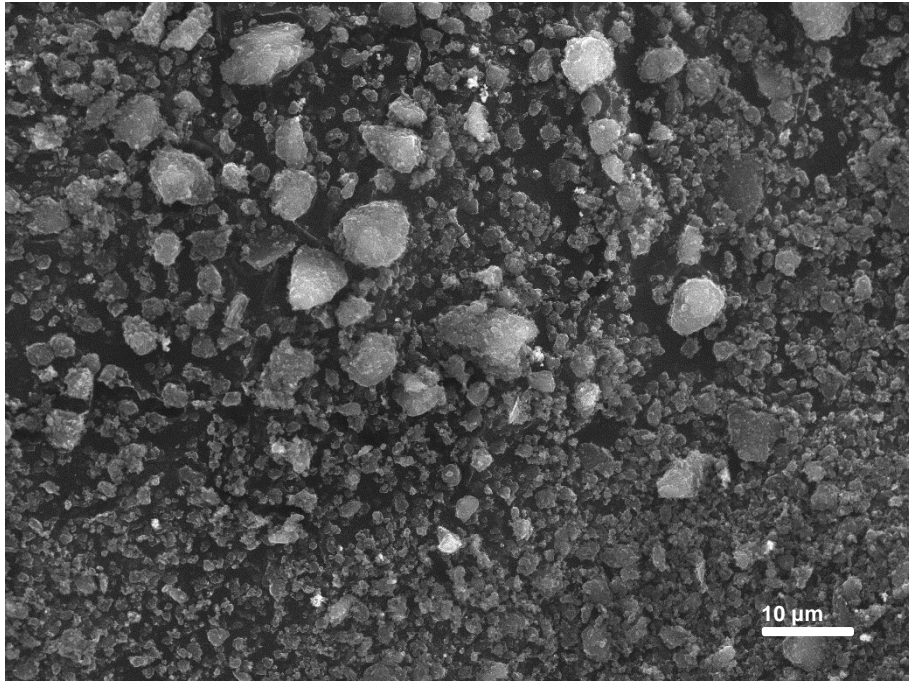
c)



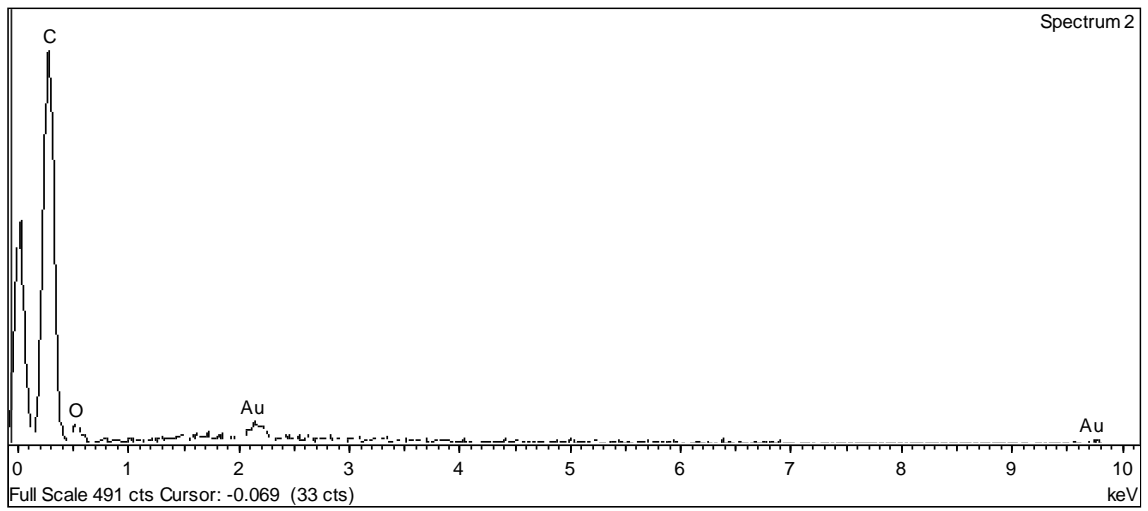
d)

Figure 58: SEM and EDS of the carbon supports a) and b) are graphene and c) and d) are ultra-pure graphene.

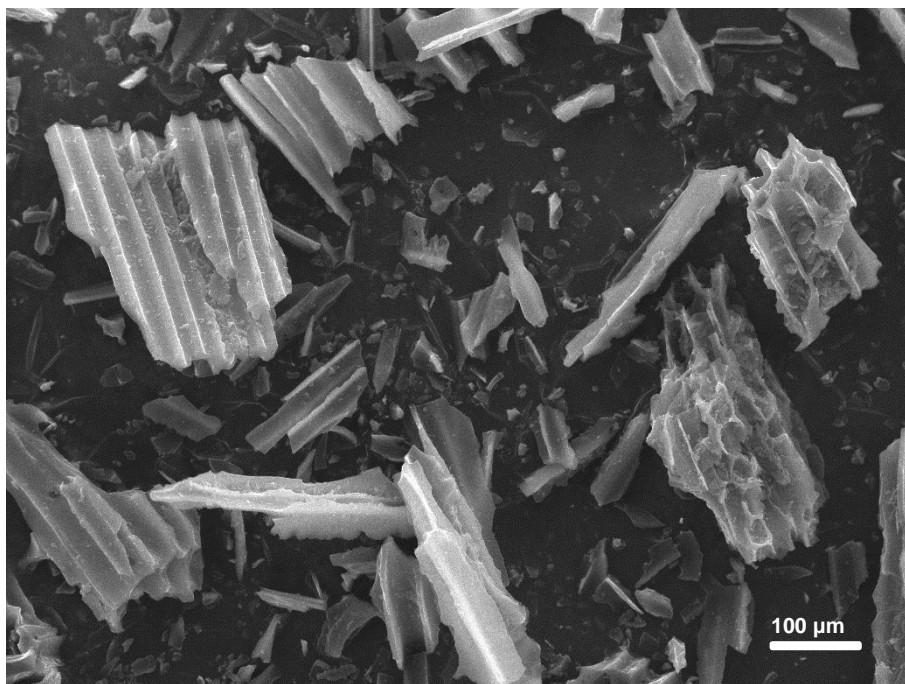
It can be observed that the type of area changes dramatically when comparing the graphene with the ultra-pure graphene, being the ultra-pure graphene structure very well defined and bigger. EDS shows, as expected, the same elements as both are graphenes. This will surely affect their ability as supports for the gold complex and their catalytic activity.



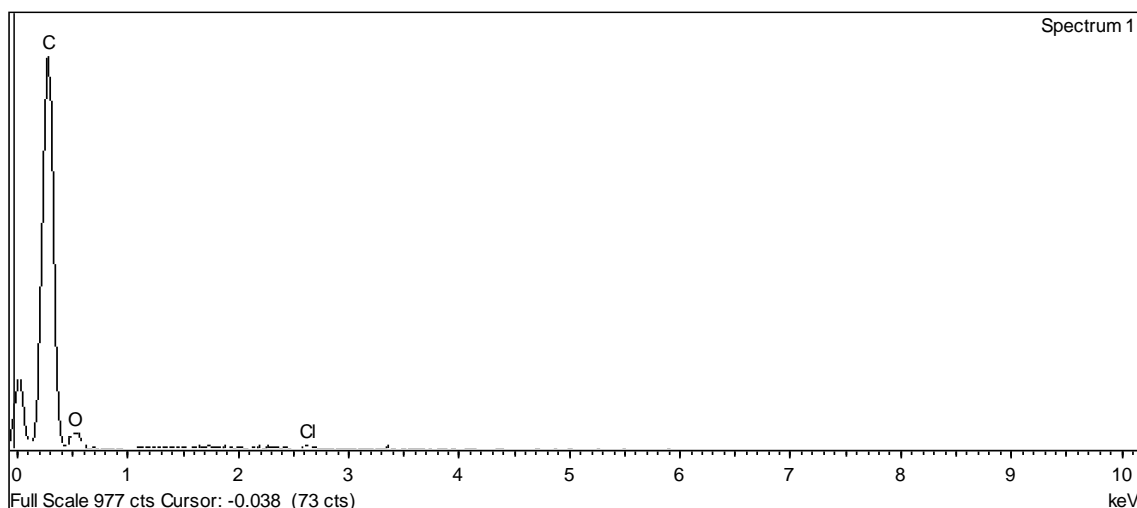
a)



b)



c)

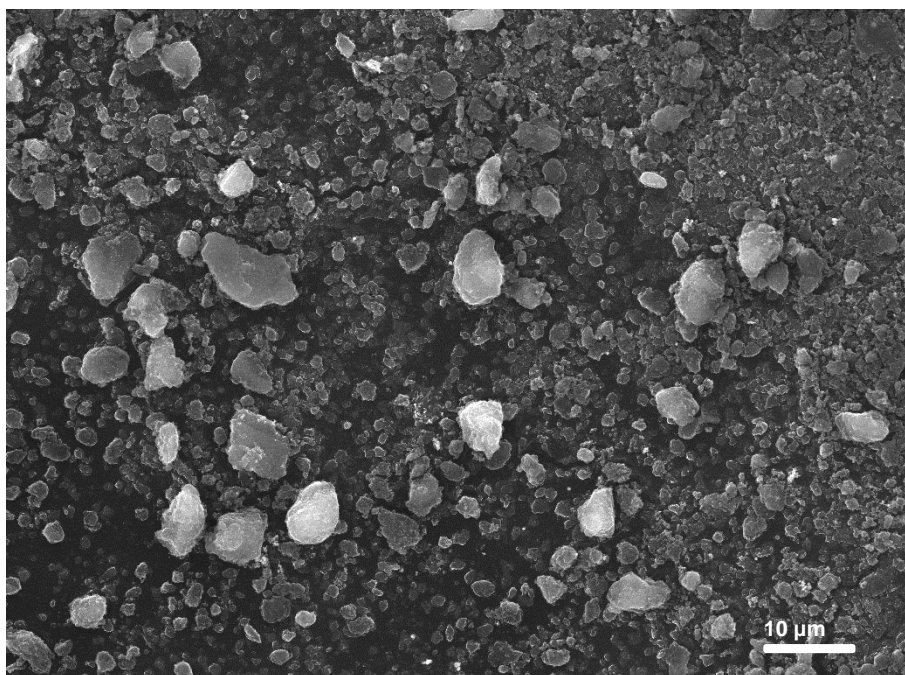


d)

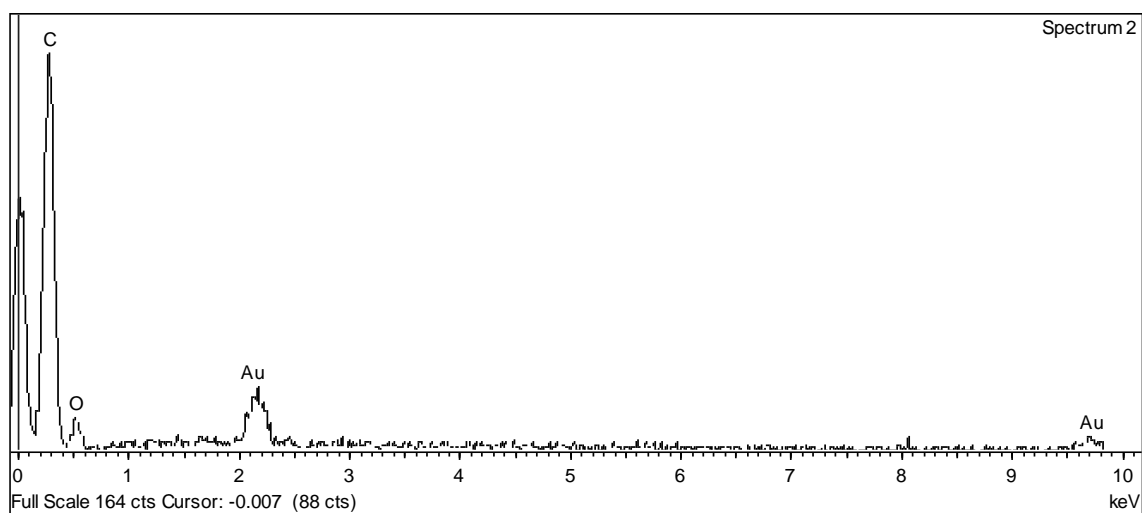
Figure 59: SEM and EDS of the gold complex made by the wet impregnation method with carbon supports. a) and b) are graphene and c) and d) are ultra-pure graphene.

As showed in Figure 59, the structure of the supports is not affected, it is clear that ultra-graphene sample structure remains being well defined. Looking at the EDS, the intake of gold seems to be better at the surface, for the graphene sample, considering that 2 %wt was tried to support. This method did not work good for the ultra-pure graphene sample as no intake of gold is observed on its EDS spectrum.

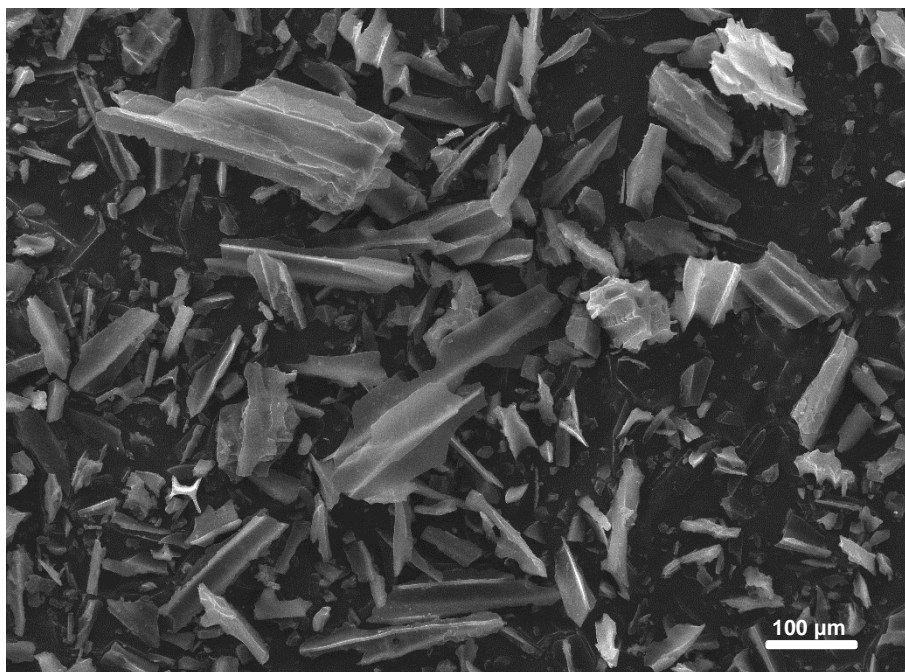
3.4.3 MW supported gold(III) C-scorpionate complex $[AuCl_2(Tpm)]Cl$ (4)



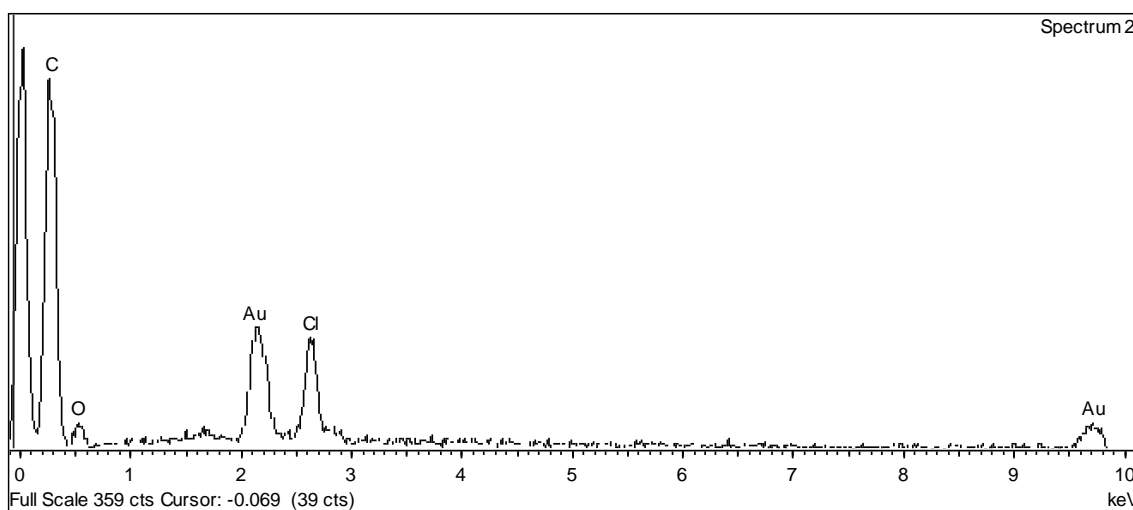
a)



b)



c)

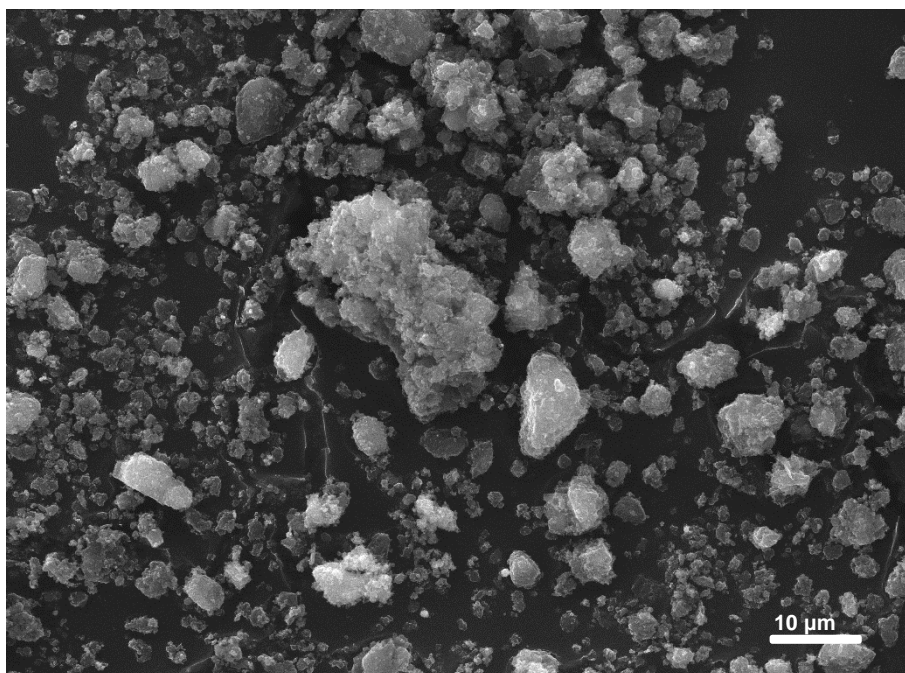


d)

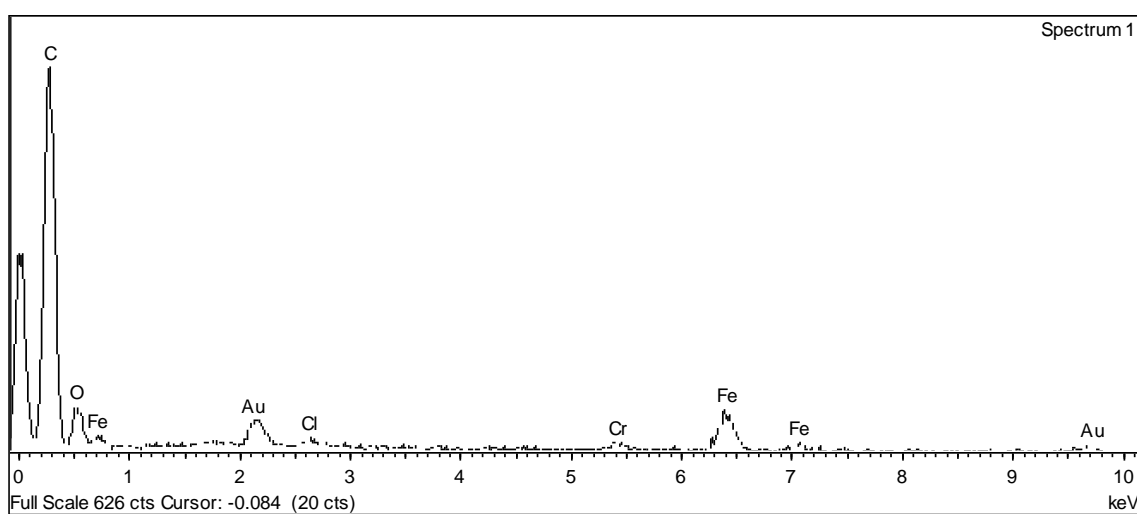
Figure 60: SEM and EDS of the gold complex made by the MW method with carbon supports. a) and b) are graphene and c) and d) are ultra-pure graphene.

Figure 60 shows that this method worked much better to produce the supported catalysts, since a better intake of gold for both samples was obtained comparing with WI method specially in ultra-pure graphene. It's important to highlight that the intake of gold was better also without losing the structure of the supports.

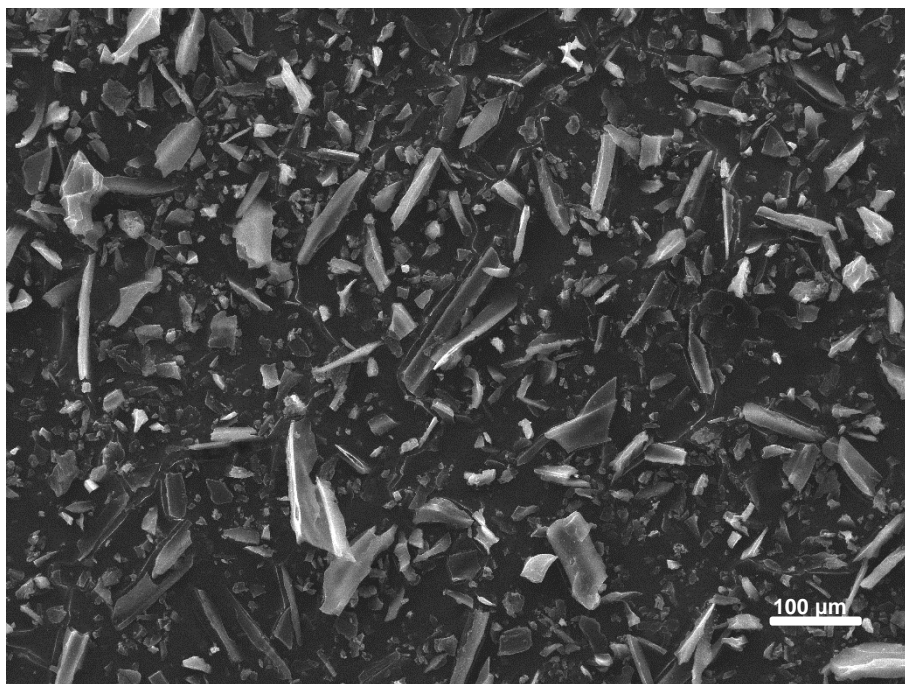
3.4.4 LAG supported C-scorpionate gold(III) complex $[\text{AuCl}_2(\text{Tpm})]\text{Cl}$ (4)



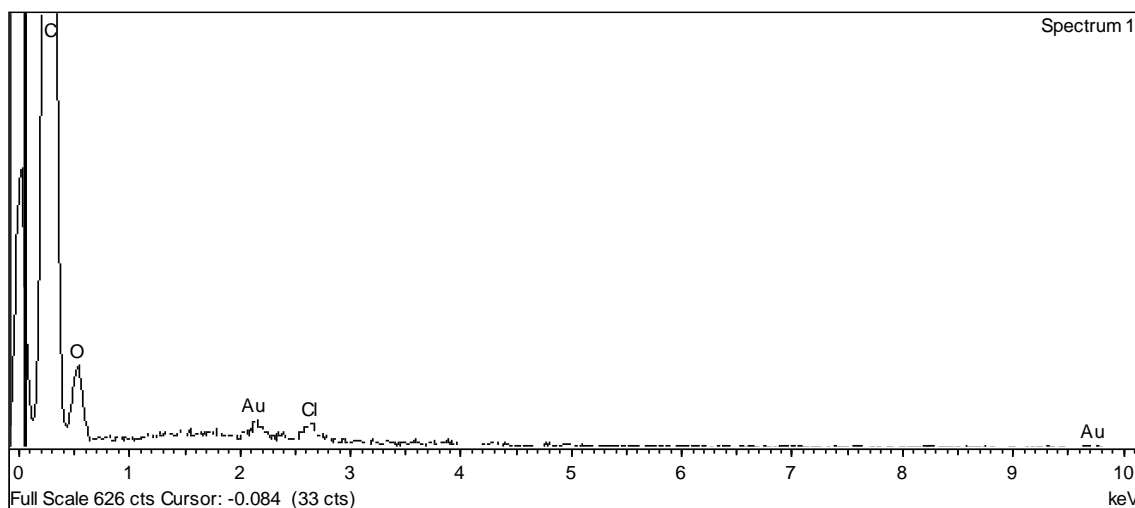
a)



b)



c)



d)

Figure 61: SEM and EDS of the gold complex made by the LAG method with carbon supports. a) and b) are graphene and c) and d) are ultra-pure graphene.

As it can be observed in Figure 61, this technique crushes the support and the gold complex in smaller size particles, in the case of the sample with graphene, the intake of gold seems to be better but there is also a contamination with iron and chromium. This contamination is probably due to the spheres and the reactor that are from stainless steel and most likely the spheres were becoming deformed. A validation of this hypothesis was obtained when the spheres were observed and looked clearly deformed (Figure 62).



Figure 62: The deformed spheres

3.5 Glycerol microwave-assisted oxidation

The reaction that occurs for the glycerol microwave-assisted oxidation is presented in Figure 63:

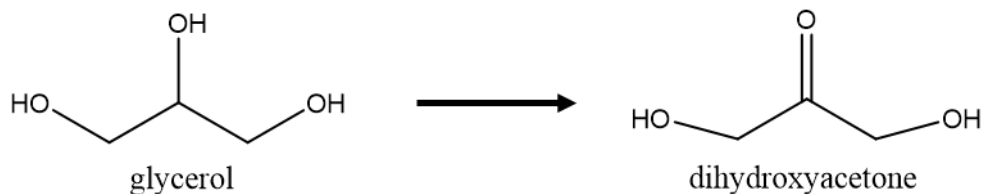


Figure 63: Oxidation of glycerol to dihydroxyacetone.

Before presenting the different data of each reaction tested, for homogeneous conditions of microwave-assisted oxidation of glycerol several catalysts have been used:

- BMAu2 → Gold(III) C-scorpionate made by BM
- [AuCl₂(Tpm)]Cl → Gold(III) C-scorpionate made by traditional method reported in ref. [44]
- HAuCl₄·xH₂O → Gold(III) chloride hydrate used as precursor for producing the gold(III) complexes.
- No use of catalyst is indicated with an "-".

The code of the samples of glycerol microwave-assisted oxidation starts always with "PGAu" and then the number of the experience that goes from 1 to 30.

As indicated in Chapter 2, ¹H NMR characterization was performed for glycerol and furfural derivatives on Bruker Advance 300 MHz at room temperature and using deuterated acetone as solvent. This characterization method was used to identify the compounds obtained in each oxidation test.

The different conversion of the targeted products presented on Table 20, Table 21, Table 22, and Table 23, were obtained as detailed in referenced literature [85] after ¹H NMR spectrum analysis.

Table 20: Glycerol oxidation using homogeneous conditions.

Code	T(°C)	Catalyst	Catalyst (mmol)	m _{catalyst} (mg)	DHA yield(%)	Conversion(%)	TON	TOF(h ⁻¹)
PGAu1	50	BMAu2	0.010	5	2.00	2.30	10.31	5.15
PGAu2	50	BMAu3	0.019	10	8.00	8.40	20.73	10.36
PGAu3	80	BMAu4	0.010	5	10.01	10.30	51.60	25.80
PGAu4	50	HAuCl ₄ ·xH ₂ O	0.015	5	2.37	2.50	8.06	4.03
PGAu5	50	[AuCl ₂ (Tpm)]Cl	0.010	5	25.00	25.80	128.87	64.43
PGAu6	50	[AuCl ₂ (Tpm)]Cl	0.019	10	73.44	74.10	190.26	95.13
PGAu7	80	[AuCl ₂ (Tpm)]Cl	0.010	5	0.96	1.30	4.95	2.47
PGAu8	50	HAuCl ₄ ·xH ₂ O	0.015	5	0.20	0.50	0.68	0.34
PGAu9	50	HAuCl ₄ ·xH ₂ O	0.029	10	0.16	0.30	0.27	0.14
PGAu10	80	HAuCl ₄ ·xH ₂ O	0.015	5	0.08	1.10	0.27	0.14
PGAu14	50	-	-	-	1.16	1.20	0.00	0.00

Reaction conditions: 5mmol of substrate; 10mmol of TBHP (70%); 650 rpm; 25W; 2h reaction time; Yield (%) = (moles of product / 100 moles of substrate). TON = Moles of product / mole of catalyst. TOF = TON / time in hours

For heterogeneous conditions, the different experiences were catalysed by:

- Graphene
- Ultra-pure graphene
- PGAuGLAG → Gold(III) C-scorpionate made by BM supported on graphene by LAG
- PGAuGMW → Gold(III) C-scorpionate made by BM supported on graphene by MW
- PGAuGWI → Gold(III) C-scorpionate made by BM supported on graphene by WI
- PGAuGLAG_up → Gold(III) C-scorpionate made by traditional method reported in ref. [44] supported on ultra-pure graphene by LAG
- PGAuGMW_up → Gold(III) C-scorpionate made by traditional method reported in ref. [44] supported on ultra-pure graphene by MW
- PGAuGWI_up → Gold(III) C-scorpionate made by traditional method reported in ref. [44] supported on ultra-pure graphene by WI.

Table 21: Catalytic data for glycerol oxidation using heterogeneous conditions.

Code	T(°C)	Catalyst	Catalyst (mmol)	m _{catalyst} (mg)	DHA yield(%)	Conversion(%)	TON	TOF(h ⁻¹)
PGAu11	50	PGAuGLAG	0.817	10	12.55	13.00	0.77	0.38
PGAu12	50	PGAuGMW	0.817	10	76.50	77.00	4.68	2.34
PGAu13	50	PGAuGWI	0.817	10	44.50	45.50	2.72	1.36
PGAu15	50	graphene	0.833	10	1.40	1.60	0.08	0.04
PGAu16	50	ultrapure graph.	0.833	10	1.80	1.90	0.11	0.05
PGAu17	80	PGAuGLAG	0.817	10	76.00	76.10	4.65	2.33
PGAu18	80	PGAuGMW	0.817	10	46.90	47.90	2.87	1.44
PGAu19	80	PGAuGWI	0.817	10	75.40	76.40	4.61	2.31
PGAu20	50	PGAuGLAG_up	0.752	10	85.70	86.20	5.70	2.85
PGAu21	50	PGAuGMW_up	0.752	10	82.60	82.70	5.49	2.75
PGAu22	50	PGAuGWI_up	0.752	10	8.60	9.50	0.57	0.29
PGAu23	80	PGAuGLAG_up	0.752	10	65.30	65.70	4.34	2.17
PGAu24	80	PGAuGMW_up	0.752	10	81.60	81.80	5.43	2.71
PGAu25	80	PGAuGWI_up	0.752	10	75.50	75.90	5.02	2.51
PGAu26	50	PGAuGLAG	0.409	5	11.20	11.30	1.37	0.69
PGAu27	50	PGAuGLAG_up	0.376	5	56.00	56.20	7.45	3.72
PGAu28	50	ultrapure graph.	0.417	5	37.70	37.90	4.52	2.26
PGAu29	50	PGAuGWI_up	0.376	5	54.90	55.80	7.30	3.65
PGAu30	80	PGAuGWI_up	0.376	5	52.30	53.10	6.96	3.48

Reaction conditions: 5mmol of substrate; 10mmol of TBHP (70%); 650 rpm; 25W; 2h reaction time; Yield (%) = (moles of product / 100 moles of substrate). TON = Moles of product / mole of catalyst. TOF = TON / time in hours.

As it can be observed from Table 20 and Table 21, PGAu20 sample was the best in terms of DHA yield (85.7%) followed by PGAu21 (82.7%), being the LAG and MW supported complex **4** on ultra-pure graphene the catalysts used, obtaining much more yield than traditional WI ones.

Comparing with reported literature [5], yields of 80 and 89% were obtained for the obtention of glycerate using gold nanoparticles on graphene, being the values obtained for DHA obtention successful. It is important to highlight the selectivity for DHA of complex **4**, as no other possible products were observed in the different ¹H NMR spectra.

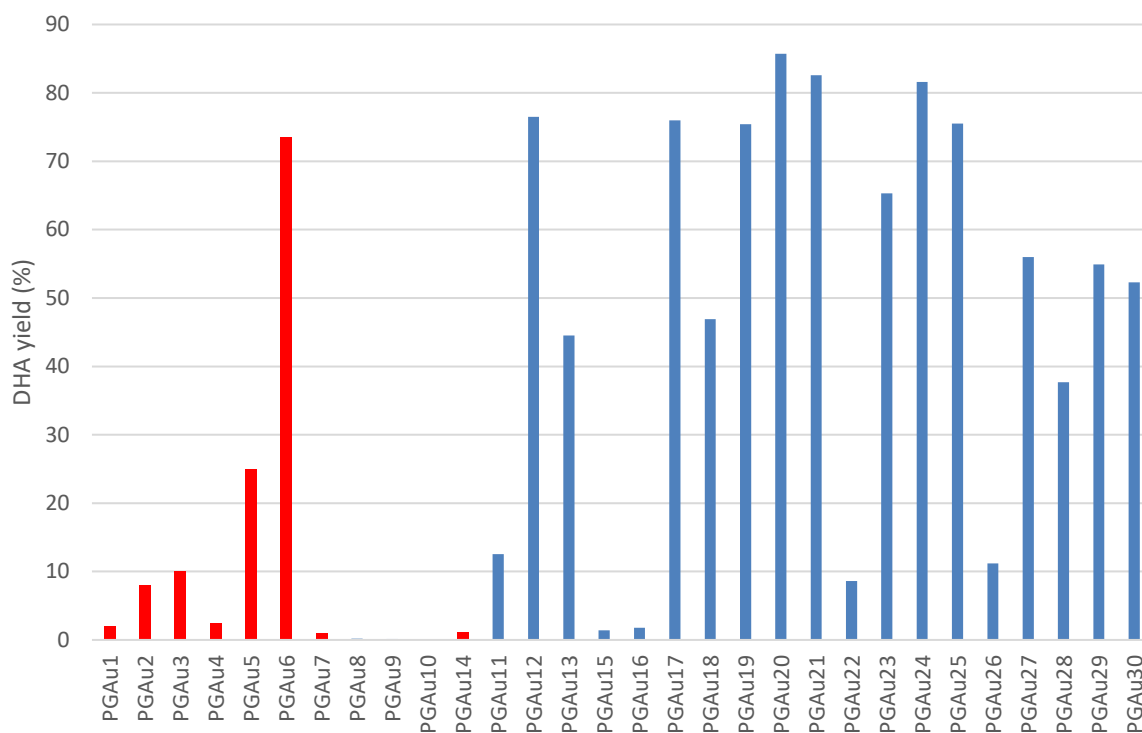


Figure 64: DHA yield for the different homogeneous (red) and heterogeneous (blue) conditions for the glycerol oxidation.

Observing the yields comparison from Figure 64, heterogenized catalysts clearly show an improvement in catalytic behaviour. The best-performing sample was complex 4 under homogeneous conditions.

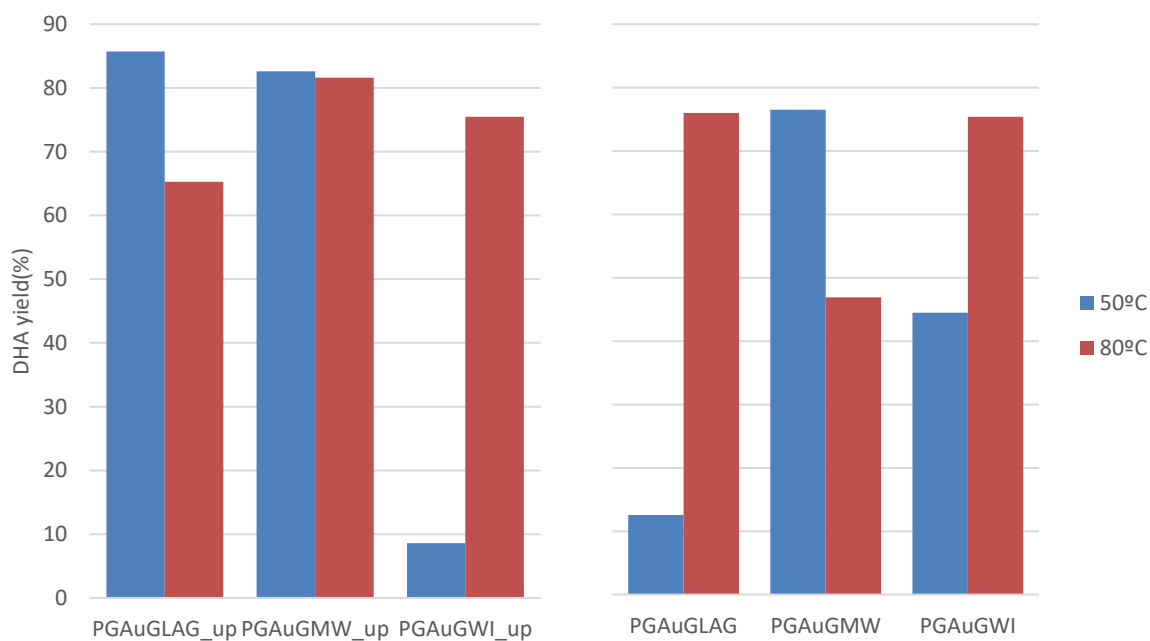


Figure 65: The influence of temperature (80°C and 50°C) and support being ultra-pure graphene (left) and graphene (right) on DHA yield.

As it can be observed in Figure 65, performing glycerol oxidation at 80 °C always affords DHA yields >40%. The use of ultra-pure graphene allows in general, higher yields when compared to those obtained for graphene ones.

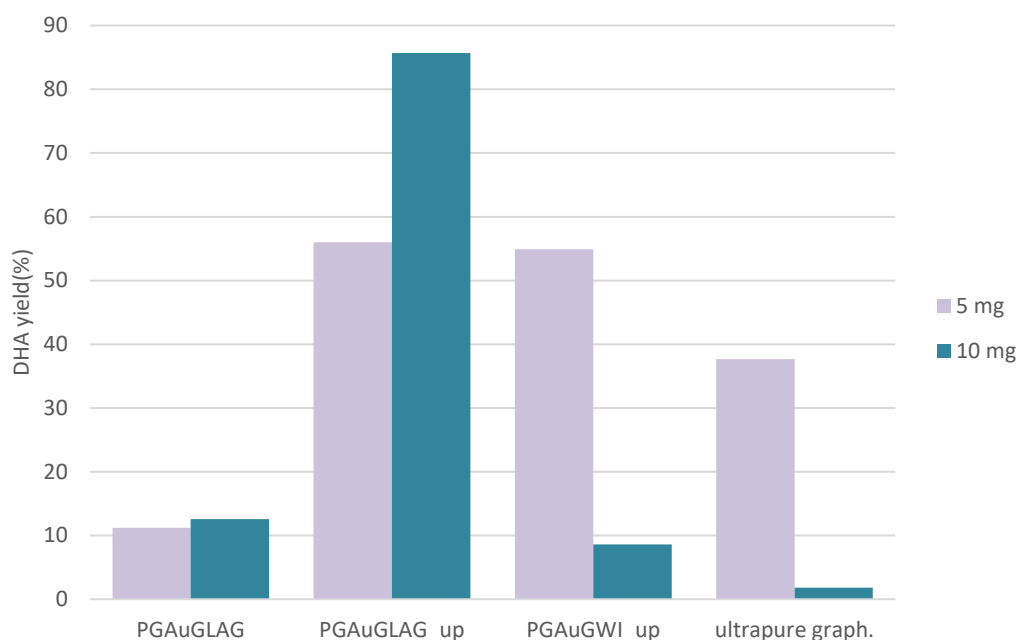


Figure 66: Influence of catalyst amount in DHA yields, under the same reaction conditions.

No influence of the quantity of catalyst can be determined observing Figure 66, as in some cases 10 mg shows better yields, but in other cases 5 mg.

Recovery of the catalyst used in PGLAu20 was performed and the reaction was repeated at same conditions, obtaining a DHA yield of 53.7% as it can be observed in Figure 67.

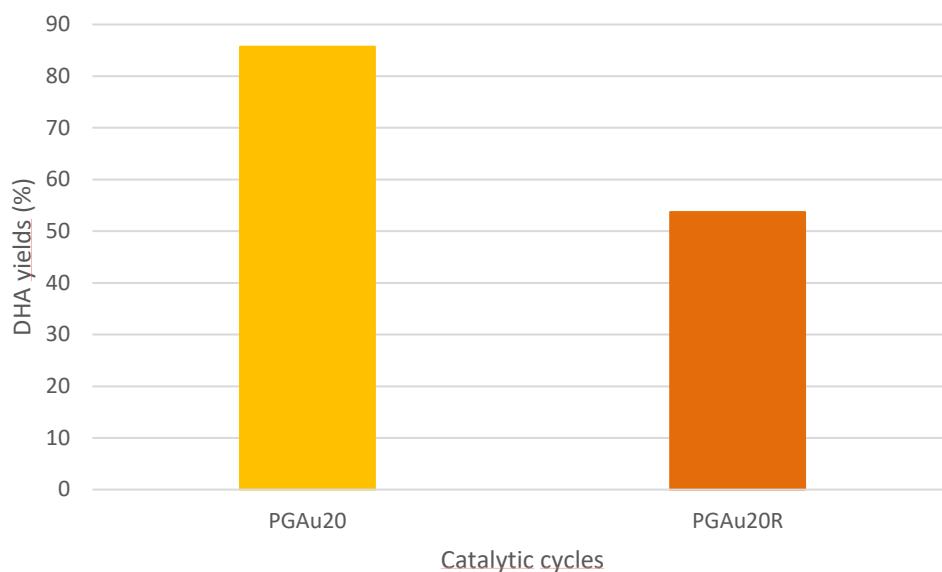


Figure 67: DHA yield for original vs. recovered catalyst.

3.6 HMF microwave-assisted oxidation

The reaction that occurs is presented in Figure 68.

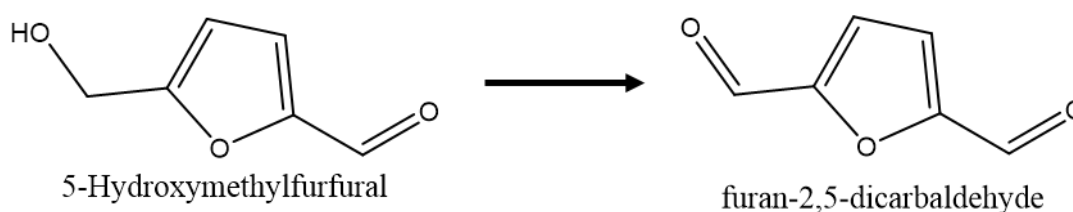


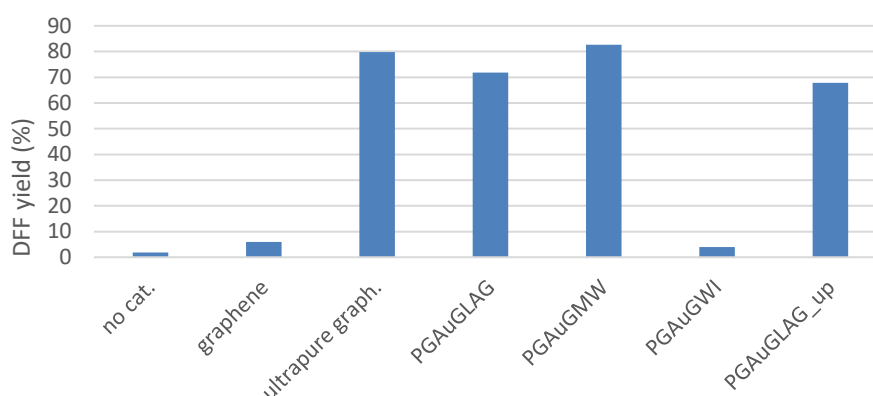
Figure 68: 5-Hydroxymethylfurfural oxidation to furan-2,5-dicarbaldehyde.

Only one homogeneous condition was performed (no catalyst) and the rest of the experiences were made using graphenes and supported gold complexes on graphene as in glycerol oxidation experiences. Different HMF oxidation conditions and samples are presented in Table 22:

Table 22: HMF MW-assisted oxidation conditions and results.

Code	T(°C)	Catalyst	Catalyst (mmol)	m _{catalyst} (mg)	DFF yield (%)	Conversion (%)	TON	TOF(h ⁻¹)
PGff1	50	-	-	-	1.90	2.00	0.00	0.00
PGff2	50	graphene	0.417	5	5.92	6.30	0.71	0.36
PGff3	50	ultrapure graph.	0.417	5	79.78	80.00	9.57	4.79
PGff4	50	PGAuGLAG	0.408	5	71.87	72.40	8.80	4.40
PGff5	50	PGAuGMW	0.408	5	82.68	83.20	10.12	5.06
PGff6	50	PGAuGWI	0.408	5	4.02	4.90	0.49	0.25
PGff7	50	PGAuGLAG_up	0.376	5	67.81	67.90	9.02	4.51

Reaction conditions: 5mmol of substrate; 10mmol of TBHP (70%, aq. solution); 650 rpm; 25W; 2h reaction time Yield (%) = (moles of product / 100 moles of substrate). TON = Moles of product / mole of catalyst. TOF = TON / time in hours.

**Figure 69:** Graphic showing different catalysts used in HMF oxidation and its DFF yields.

As it can be observed in Table 22 and Figure 69, best DFF yield was obtained for PGff5 sample (83.2%) being MW the method used for supporting complex **4** made by mechanochemistry on graphene. Comparing with the literature [64], better yields were obtained for FDCA, with higher temperature and reaction time, but is important to highlight that the selectivity to DFF was high as no other possible products were observed in the ¹H NMR spectra.

Different conditions and more samples were thought to be performed, but due to limited time and problems with the supply of the reagent, this could not be done.

Recycling of PGff5 was performed, leading to a DFF yield of 10.4% as it can be observed in Figure 70. Characterization of the recovered catalyst is thus, of great importance, to observe if the intake the gold was lost, or the structure of the supported catalyst poisoned.

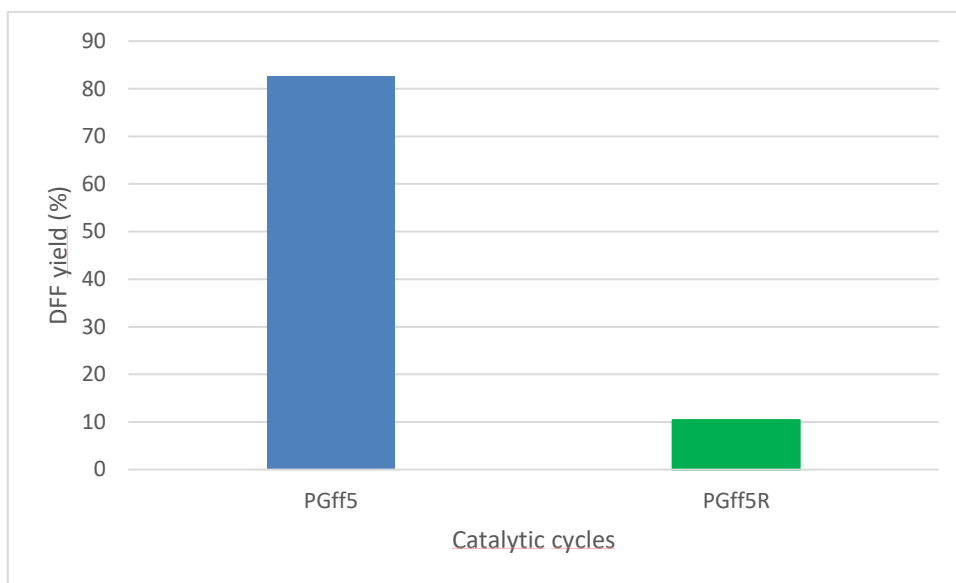


Figure 70: DFF yield for original vs. recovered catalyst.

3.7 HFCA microwave-assisted oxidation

The reaction that occurs for HFCA MW-assisted oxidation is presented in Figure 71:

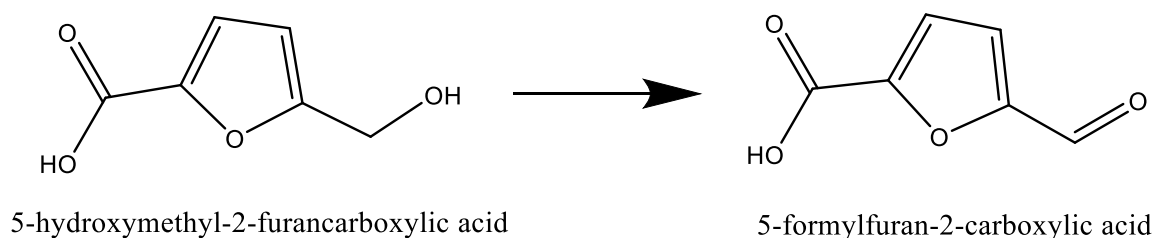


Figure 71: 5-hydroxymethyl-2-furancarboxylic acid oxidation to 5-formylfuran-2-carboxylic acid.

Table 23: HFCA MW-assisted oxidation conditions and results.

Code	T(°C)	Catalyst	Catalyst (mmol)	m_{catalyst} (mg)	FFCA yield (%)	Conversion (%)	TON	TOF(h^{-1})
PGff8	50	-	-	-	0.00	0.00	0.00	0.00
PGff9	50	PGAuGLAG_up	0.752	10	12.00	12.40	0.08	0.04
PGff10	50	PGAuGMW_up	0.752	10	11.80	12.30	0.08	0.04
PGff11	50	PGAuGWI_up	0.752	10	14.80	14.90	0.10	0.05
PGff12	50	Ultra-pure graphene	0.833	10	1.20	2.00	0.01	0.00
PGff13	50	BMAu2	0.019	10	0.00	0.30	0.00	0.00
PGff14	50	BMAu2	0.019	10	0.00	0.50	0.00	0.00
PGff15	50	HAuCl ₄ ·xH ₂ O	0.029	10	0.00	0.40	0.00	0.00
PGff16	80	PGAuGLAG_up	0.752	10	29.10	29.90	0.19	0.10

Reaction conditions: 0,5mmol of substrate; 1mmol of TBHP (70%, aq. Solution)); 650 rpm; 25W; 2h reaction time; Yield (%) = (moles of product / 100 moles of substrate). TON = Moles of product / mole of catalyst. TOF = TON / time in hours.

As it can be observed in Table 23, the heterogenized catalysts show an improvement in catalytic behaviour as all homogeneous reactions showed no catalytic activity. On the other hand, switching the temperature from 50°C to 80°C, in the case of PGAuGLAG_up improves the FFCA yield from 12 to 29.1% (PGff9 and PGff16).

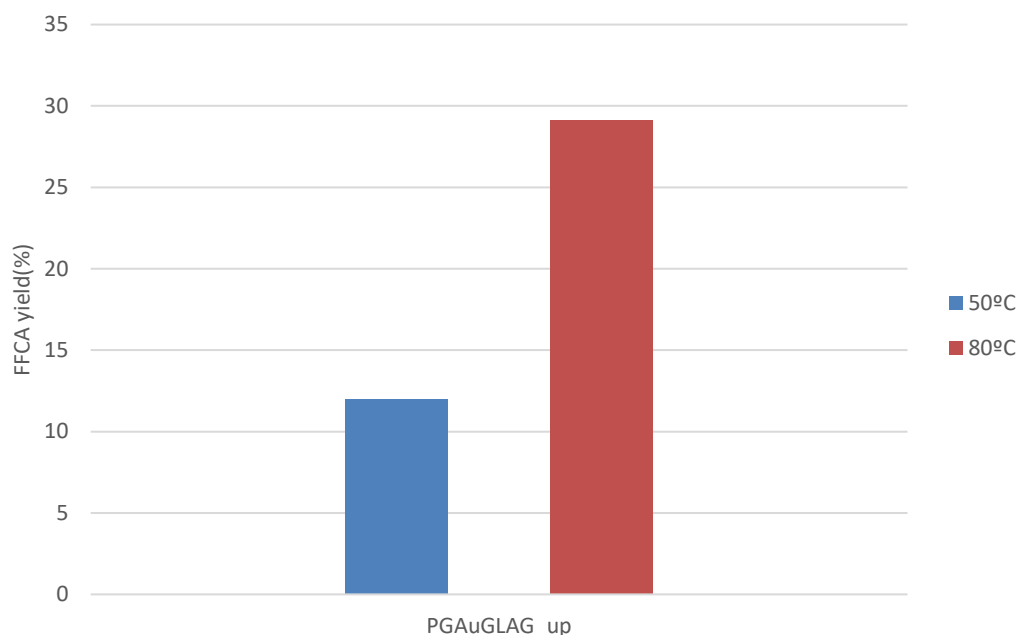


Figure 72: Influence of temperature on HFCA oxidation.

As observed in Figure 72, in this case, with 80 °C the FFCA yield obtained is more than 2 times higher than with 50 °C, showing better performance at higher temperatures. More samples should be performed and compared at same conditions but different temperatures in order to get better analysis of temperature influence.

Again, the recover of the best sample was mad, and the same reaction performed, showing this time no conversion an no products. As with HMF oxidation, characterization of the recovered catalyst is thus, of great importance, to observe if the intake the gold was lost, or the structure of the supported catalyst poisoned.

4 Conclusions and future work

The main objectives of this work were the synthesis of a gold(III) complex using a C-scorpionate as ligand by a sustainable technique, the ball milling mechanochemistry, its heterogenization in graphene and its use in industrial oxidation reactions as a heterogeneous catalyst. The evaluation of its activity was performed for the glycerol and furfural derivatives oxidation.

The synthetic results show that the complexation of Tpm with the gold(III) precursor is quickly and possible to achieve without solvent, when using ball milling. Its structure obtained was confirmed by several techniques and showed that the gold metallic centre is coordinated with two pyrazolyl rings and that the spectroscopic characteristics are in agreement with the referenced in the literature.

Different methods for support complex **4** were performed, trying to avoid the use of solvents if a possible scale-up of the process is made, appearing as an alternative to traditional WI methods. MW and LAG support methods showed better intake of gold when characterized and better oxidation results.

The glycerol and furfural derivatives oxidation was successful, using homogeneous and heterogeneous catalysis and the best results were obtained for the later.

In the case of glycerol oxidation, appropriated values of DHA yield were obtained, comparing with literature, highlight the selectivity for DHA of complex **4**, as no other possible products were observed in the different ¹H NMR spectra.

Furfural derivatives oxidation showed better results for HMF than for HFCA, being probably due the fact that HMF is more reactive due to the absence of an acid group in its structure.

As an area still little explored, the use of gold(III) complexes can be a focus of investigation as they have an excellent selectivity to reactions. Some possible suggestions are described below:

- Further analysis of the glycerol and furfural products to ensure a better insight into the reaction path of both catalysts, thus improving conditions.
- Investigation of reaction mechanisms for all oxidations studied
- Testing of different compounds that are essential to produce commodities

It is also important to highlight that if available time and circumstances were better, more samples of supported complex **4** on graphene would have been made, and the use of the complexes **1**, **2**, and **3** for perform the oxidations tried, as all three complexes are promising low-cost catalysts for the future. A better and more thorough characterization and recovery of catalysts would have been done, as is of great importance for the study of the heterogeneous catalysis.

Annex 1

^1H NMR spectra

In this annex, different representative ^1H NMR spectra are presented from the 3 different microwave-assisted oxidation samples.

A.1 Glycerol oxidation

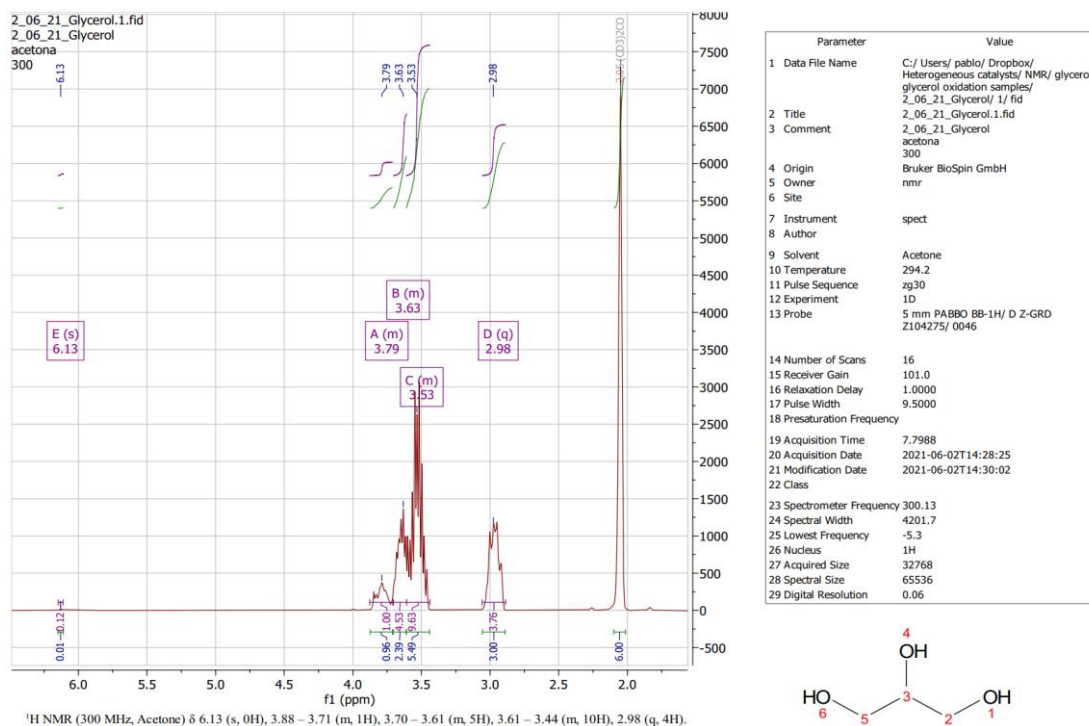


Figure A. 1: glycerol.

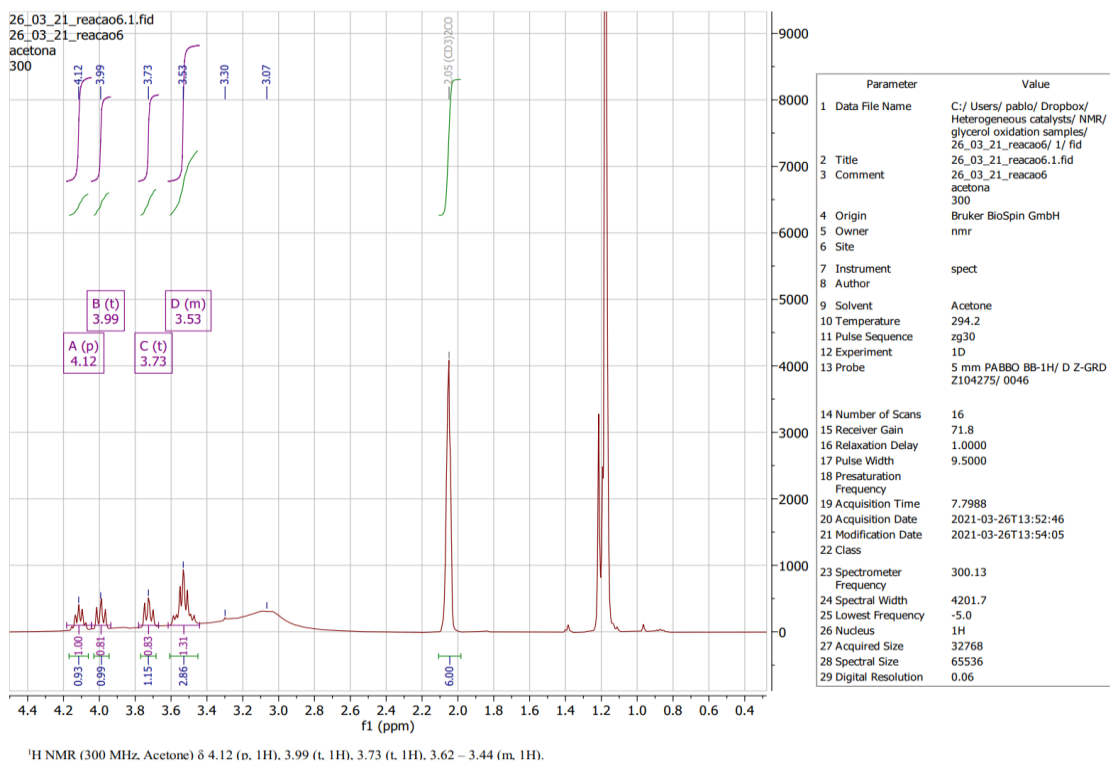
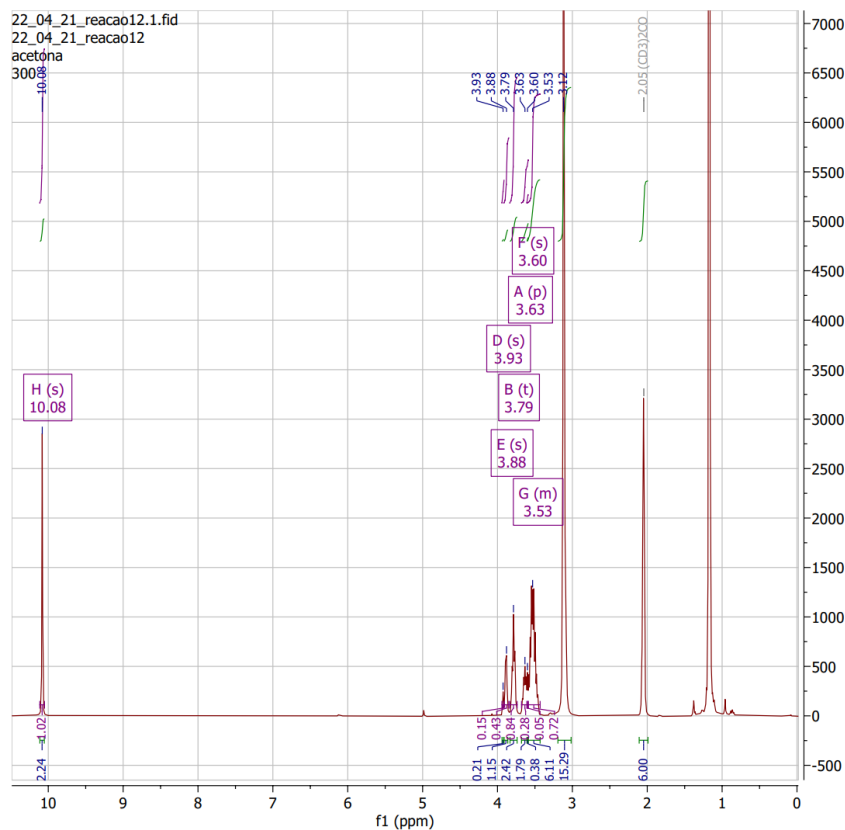


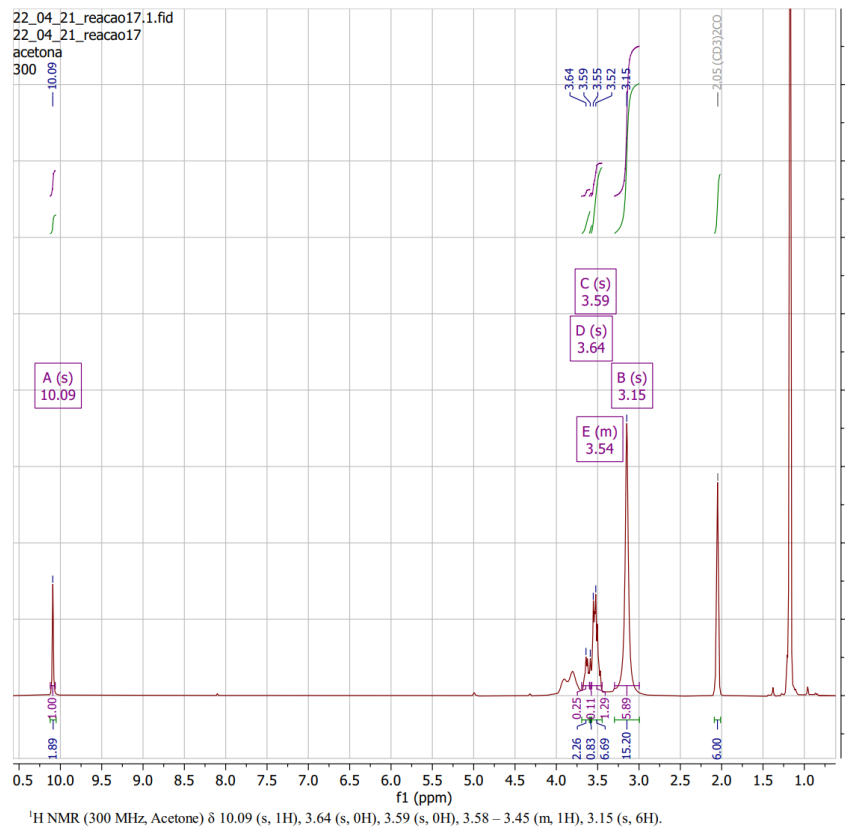
Figure A. 2: PGau6 with 73.44% DHA yield.



¹H NMR (300 MHz, Acetone) δ 3.79 (t, 1H), 3.60 (s, 0H), 3.60 – 3.43 (m, 1H), 10.08 (s, 1H), 3.93 (s, 0H), 3.88 (s, 0H), 3.63 (p, 0H).

Parameter	Value
1 Data File Name	C:/ Users/ pablo/ Dropbox/ Heterogeneous catalysts/ NMR/ glycerol oxidation samples/ 22_04_21_reacao12/ 1/ fid
2 Title	22_04_21_reacao12.1.fid
3 Comment	22_04_21_reacao12 acetona 300
4 Origin	Bruker BioSpin GmbH
5 Owner	nmr
6 Site	
7 Instrument	spect
8 Author	
9 Solvent	Acetone
10 Temperature	294.4
11 Pulse Sequence	zg30
12 Experiment	1D
13 Probe	5 mm PABBO BB-1H/ D Z-GRD Z104275/ 0046
14 Number of Scans	16
15 Receiver Gain	57.0
16 Relaxation Delay	1.0000
17 Pulse Width	9.5000
18 Presaturation	Frequency
19 Acquisition Time	7.7988
20 Acquisition Date	2021-04-22T17:04:24
21 Modification Date	2021-04-22T17:06:00
22 Class	
23 Spectrometer	300.13
24 Spectral Width	4201.7
25 Lowest Frequency	-5.6
26 Nucleus	1H
27 Acquired Size	32768
28 Spectral Size	65536
29 Digital Resolution	0.06

Figure A. 3: PG Au12 with 76.5% DHA yield.



¹H NMR (300 MHz, Acetone) δ 10.09 (s, 1H), 3.64 (s, 0H), 3.59 (s, 0H), 3.58 – 3.45 (m, 1H), 3.15 (s, 6H).

Parameter	Value
1 Data File Name	C:/ Users/ pablo/ Dropbox/ Heterogeneous catalysts/ NMR/ glycerol oxidation samples/ 22_04_21_reacao17/ 1/ fid
2 Title	22_04_21_reacao17.1.fid
3 Comment	22_04_21_reacao17 acetona 300
4 Origin	Bruker BioSpin GmbH
5 Owner	nmr
6 Site	
7 Instrument	spect
8 Author	
9 Solvent	Acetone
10 Temperature	294.4
11 Pulse Sequence	zg30
12 Experiment	1D
13 Probe	5 mm PABBO BB-1H/ D Z-GRD Z104275/ 0046
14 Number of Scans	14
15 Receiver Gain	57.0
16 Relaxation Delay	1.0000
17 Pulse Width	9.5000
18 Presaturation	Frequency
19 Acquisition Time	7.7988
20 Acquisition Date	2021-04-22T17:10:03
21 Modification Date	2021-04-22T17:11:40
22 Class	
23 Spectrometer	300.13
24 Spectral Width	4201.7
25 Lowest Frequency	-5.3
26 Nucleus	1H
27 Acquired Size	32768
28 Spectral Size	65536
29 Digital Resolution	0.06

Figure A. 4: PG Au17 with 76% DHA yield.

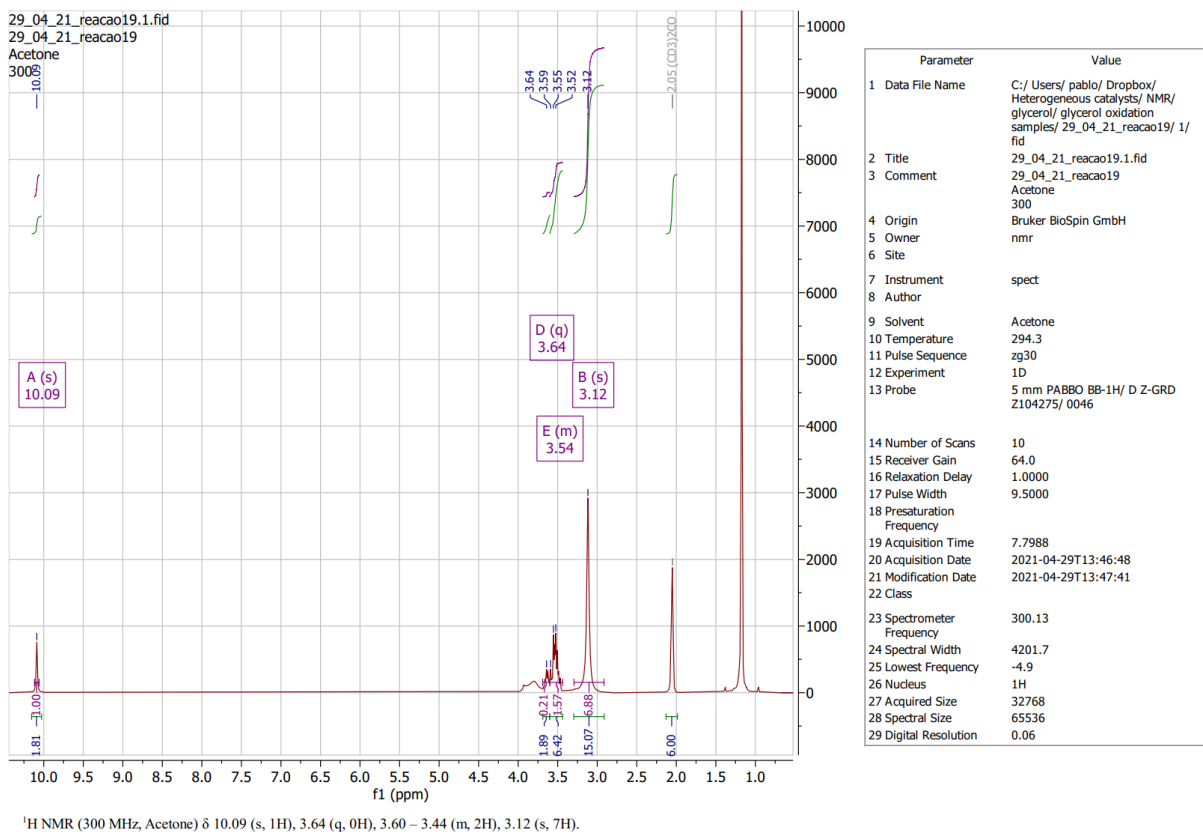


Figure A. 5: PGau19 with 75.4% DHA yield.

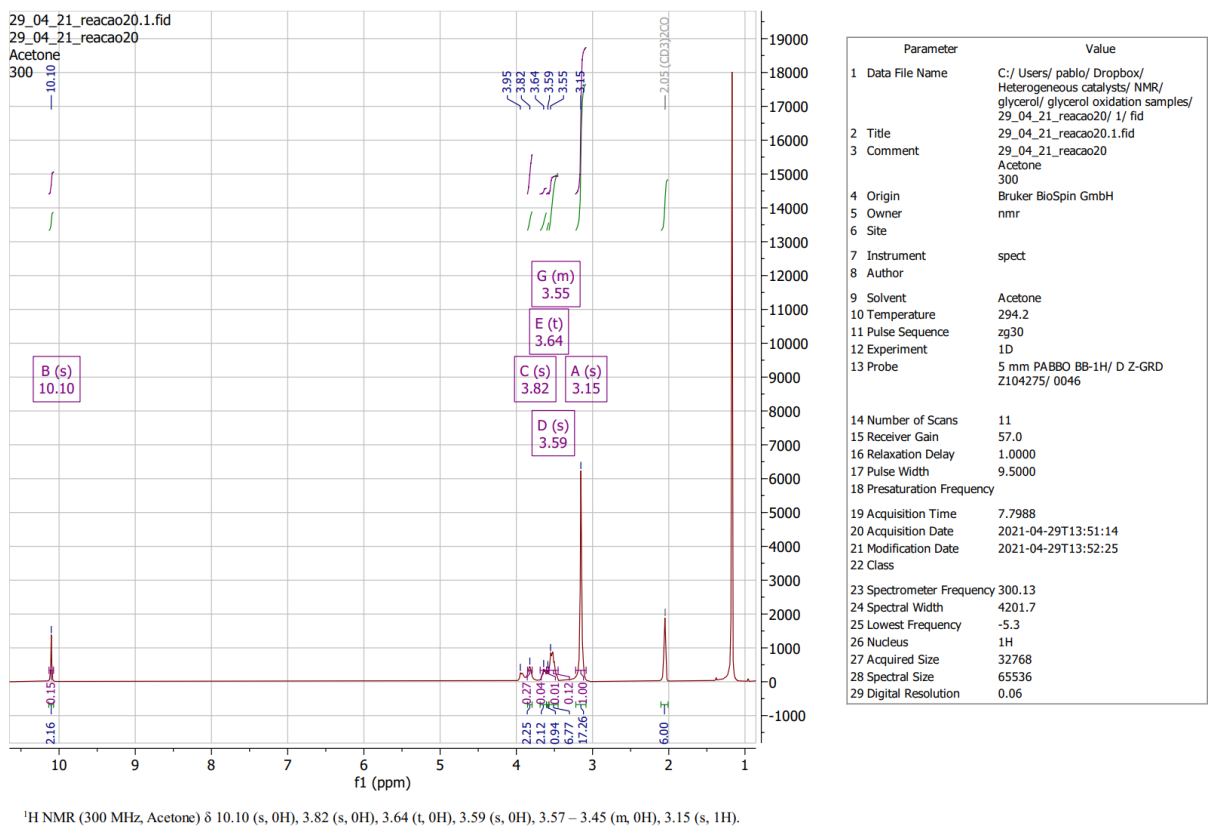


Figure A. 6: PGau20 with 85.7% DHA yield.

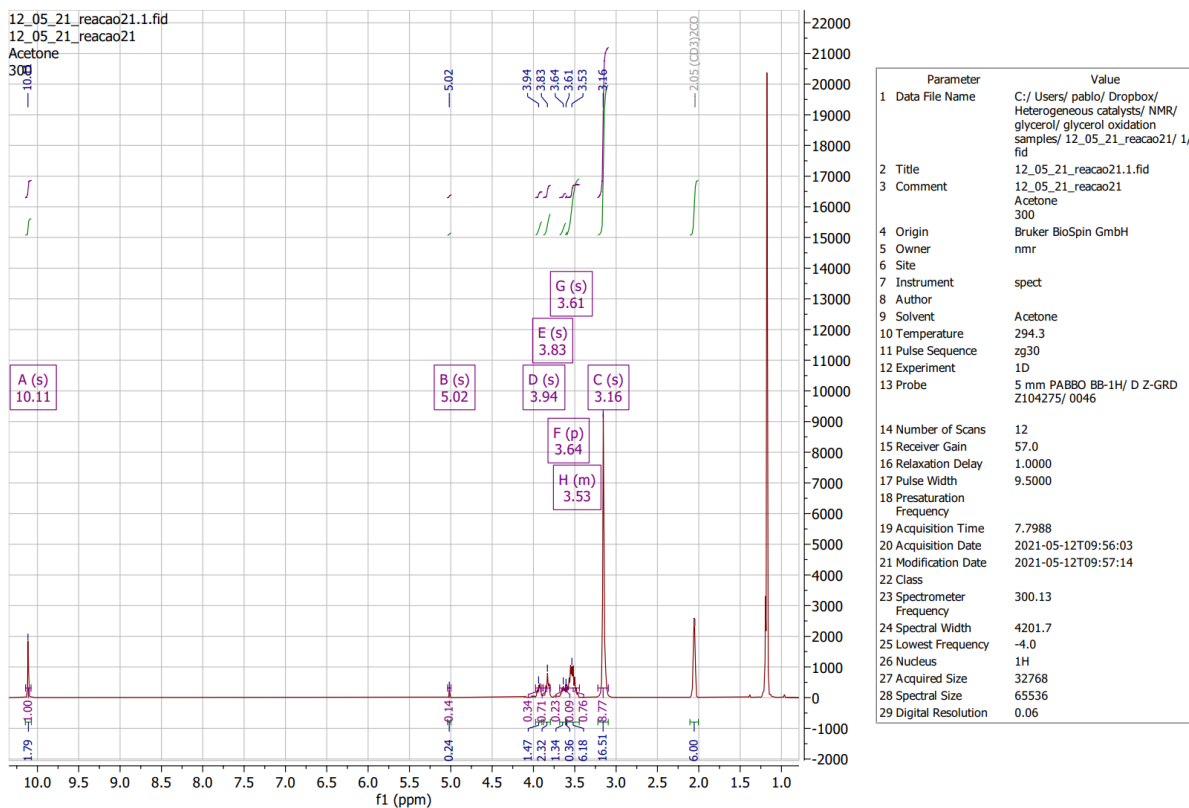


Figure A. 7: PG Au21 with 82.6% DHA yield.

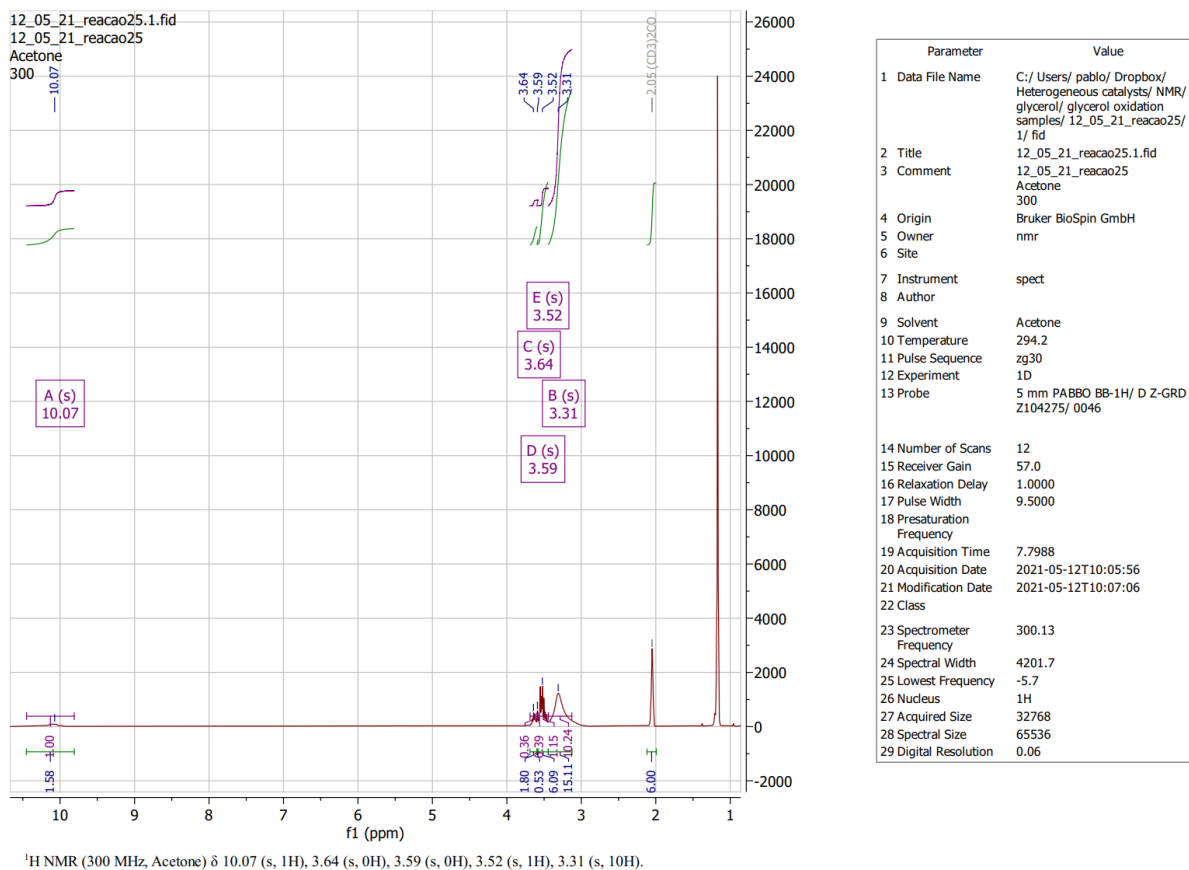


Figure A. 8: PG Au25 with 75.5% DHA yield.

A.2 HMF oxidation

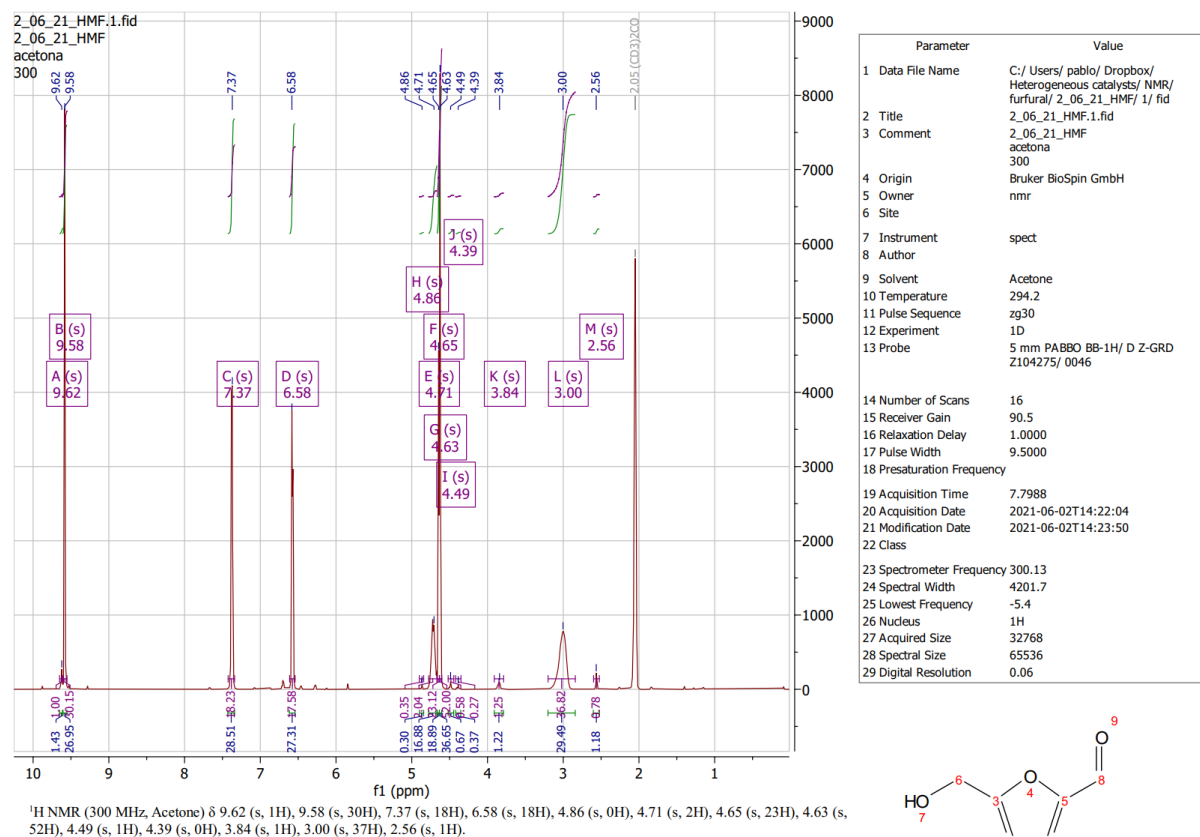


Figure A. 9: HMF.

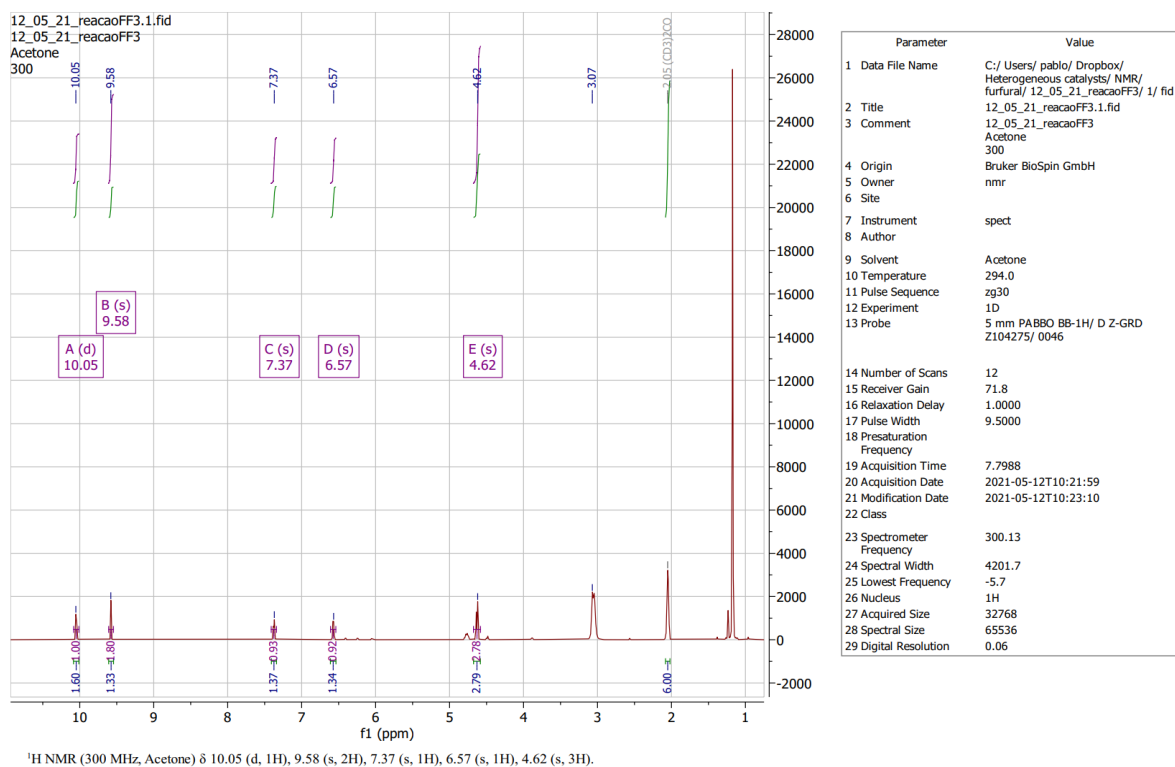


Figure A. 10: PGff3 with 79.78% DFF yield.

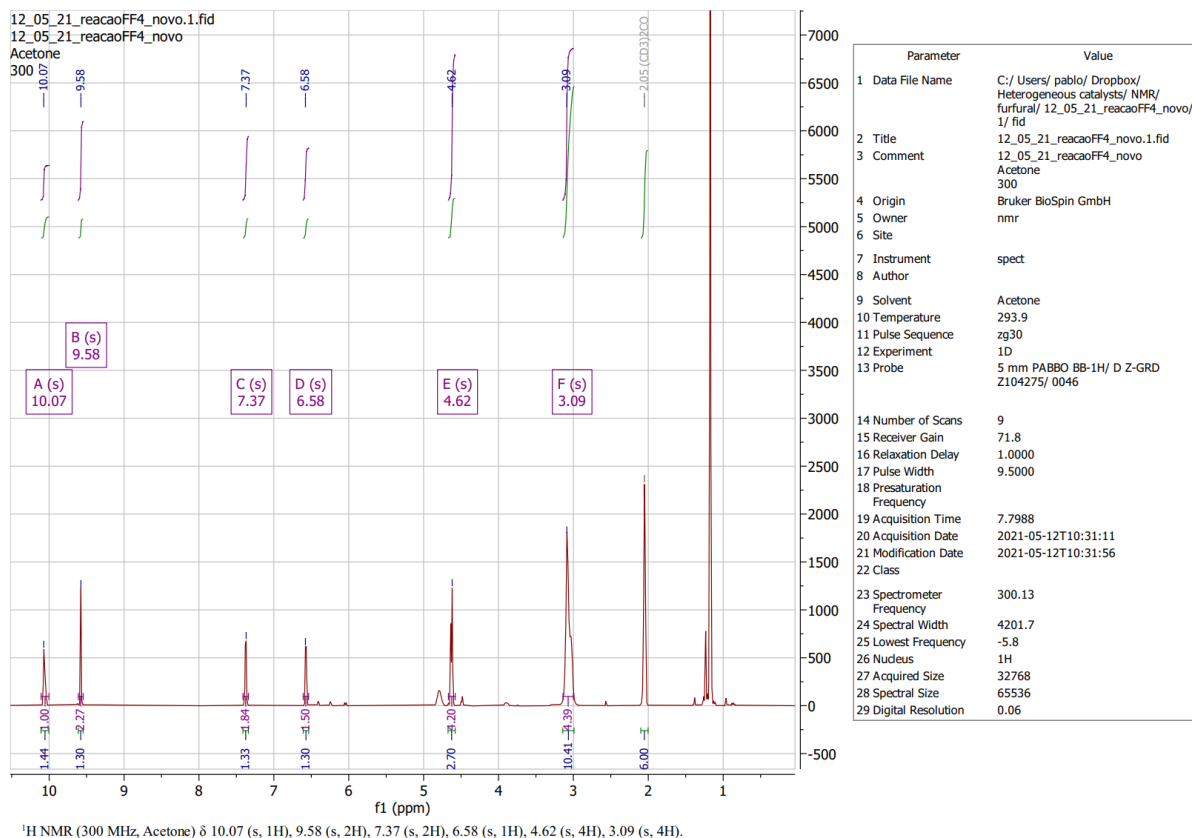


Figure A. 11: PGff4 with 71.87% DFF yield.

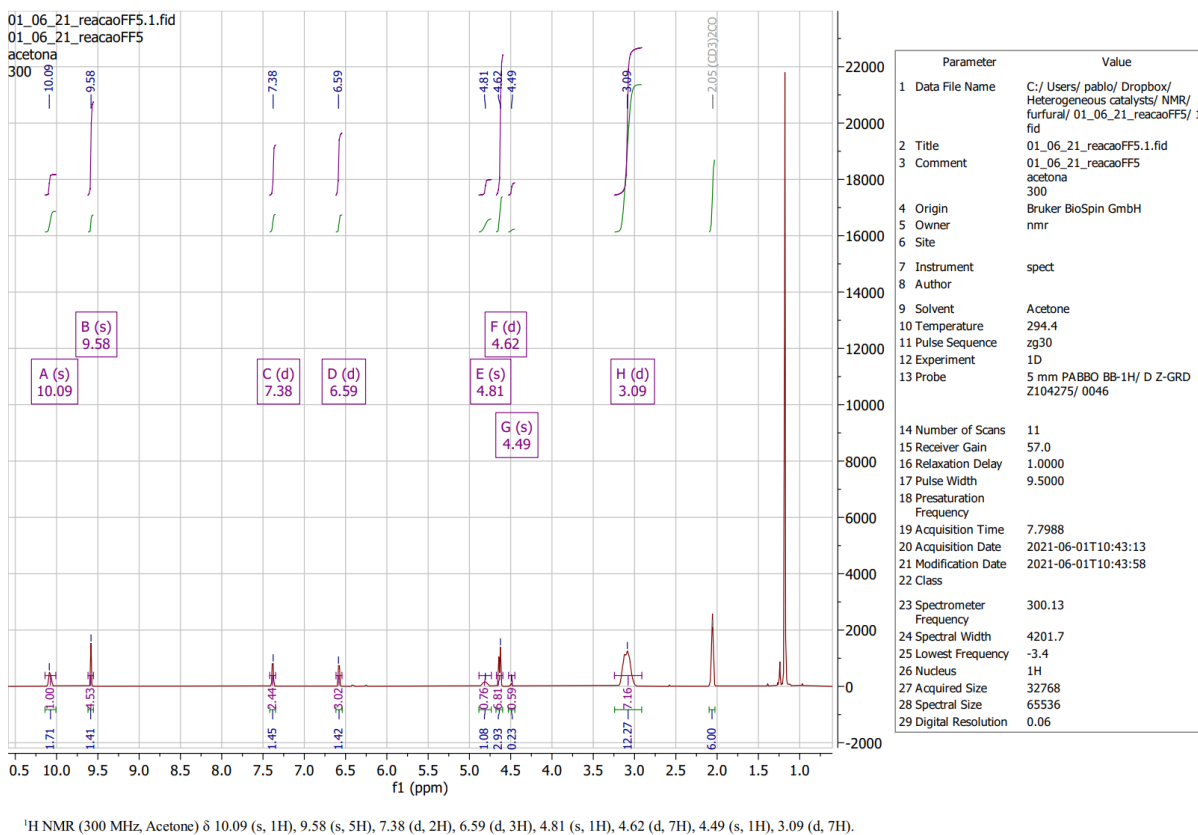


Figure A. 12: PGff5 with 82.68% DFF yield.

A.3 HFCA oxidation

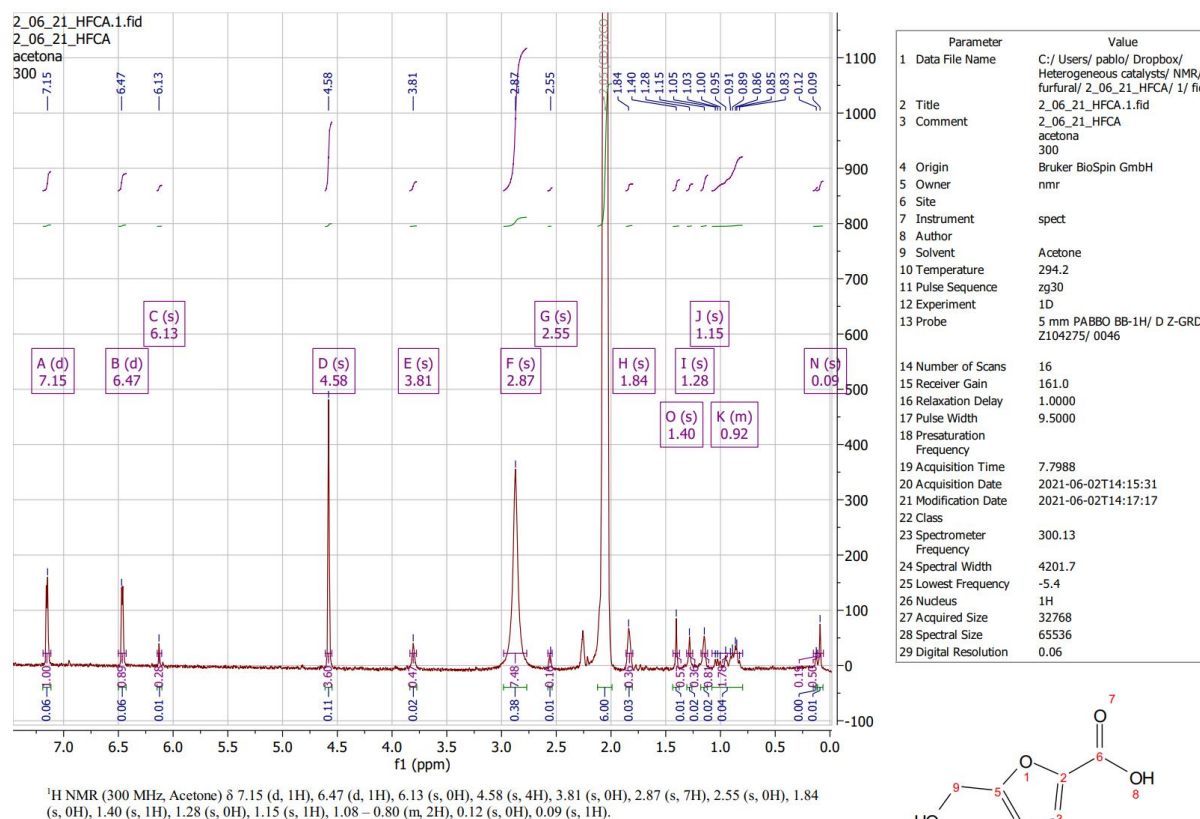


Figure A. 13: HFCA.

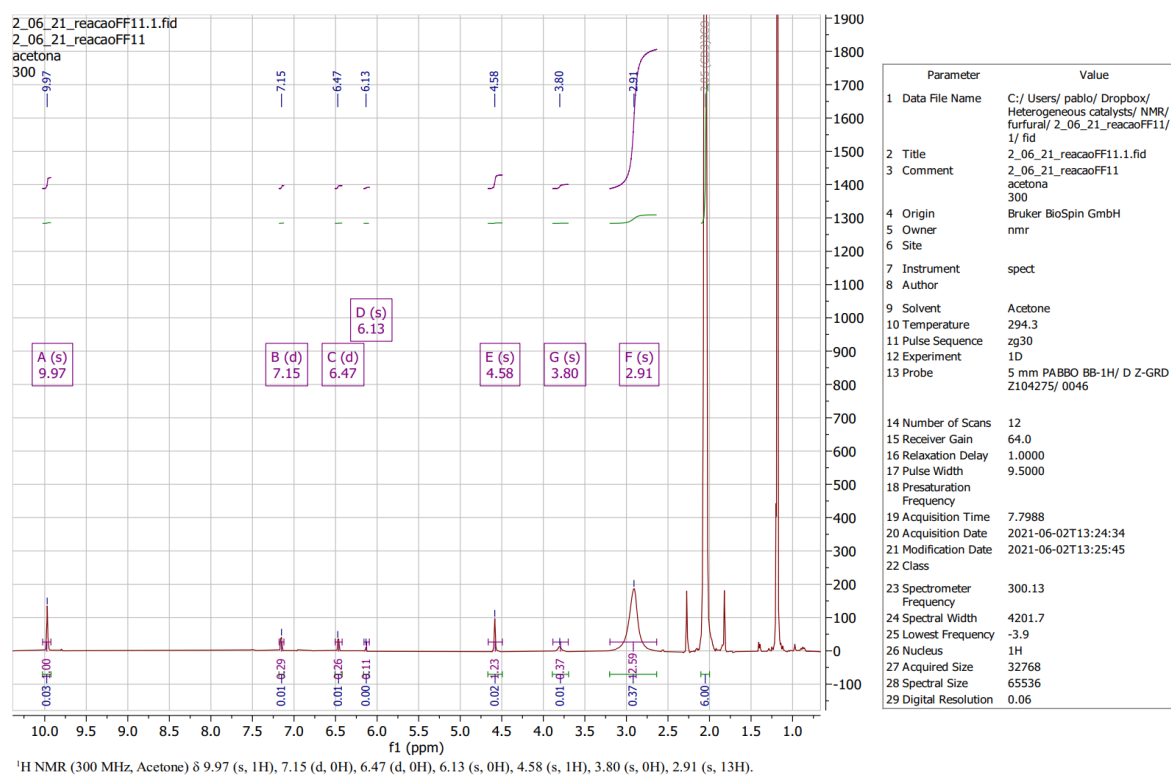


Figure A. 14: PGff11 with a yield of 14.8% in FFCA.

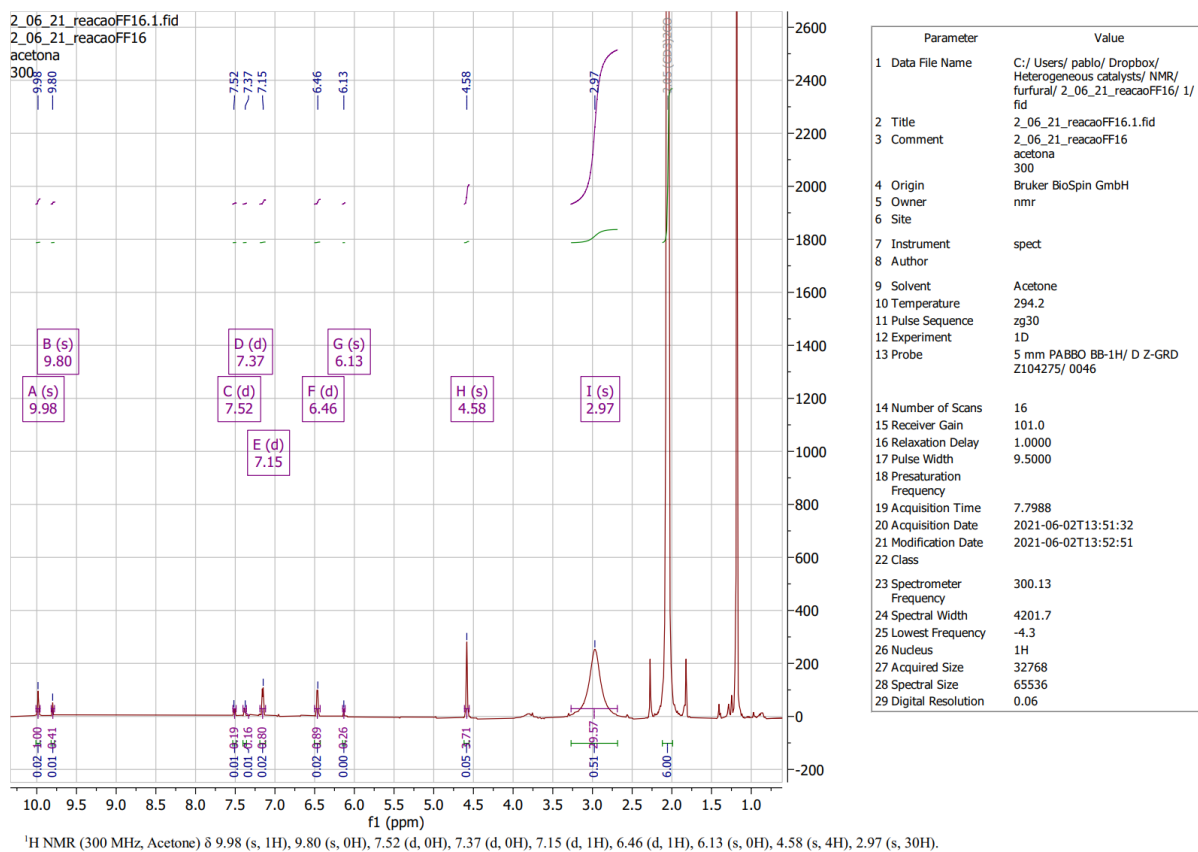


Figure A. 15: PGff16 with FFCA yield of 29.1%.

References

- [1] U.S Census, "U.S. and World Population Clock," [Online]. Available: <https://www.census.gov/popclock/>. [Accessed 27 04 2021].
- [2] Eurostat, "Waste statistics- Statistics Explained," [Online]. Available: https://ec.europa.eu/eurostat/statistics-explained/index.php?title=Waste_statistics#Total_waste_generation. [Accessed 2021 04 27].
- [3] A. Ribeiro, L. Martins and A. Pombeiro, "Carbon dioxide-to-methanol single-pot conversion using a C-scorpionate iron(II) catalyst," *Green Chem.*, 2017.
- [4] C. Okkerse and H. v. Bekkum, "From fossil to green," *Green Chemistry*, vol. 1, pp. 107-114, 1999.
- [5] A. Villa, N. Dimitratos, C. E. Chan-Thaw, C. Hammond and L. Prati, "Glycerol Oxidation Using Gold-Containing Catalysts," *Accounts of chemical research*, 2015.
- [6] J. J. Bozell and G. R. Petersen, "Technology development for the production of biobased products from biorefinery carbohydrates," *Green Chem.*, vol. 12, no. 4, pp. 539-554, 2010.
- [7] W. Abdussalam-Mohammed and A. O. Amna Qasem Ali, "Green Chemistry: Principles, Applications, and Disadvantages," pp. 408-423, January 2020.
- [8] P. T. Anastas and J. C. Warner, *Green chemistry: Theory and practice.*, Oxford, pp. 301-312, 1998.
- [9] "The Twelve Principles of Green Chemistry: What it is, & Why it Matters," [Online]. Available: <https://www.compoundchem.com/2015/09/24/green-chemistry/>. [Accessed 05 05 2021].
- [10] ACS, "12 Principles of Green Chemistry," 05 05 2021. [Online]. Available: <https://www.acs.org/content/acs/en/greenchemistry/principles/12-principles-of-green-chemistry.html>.
- [11] A. a. Pino, *Química verde: Enfoque sistemático*, Ediciones UNL, pp. 49-72, 2020.

- [12] C. Jiménez-González, C. Ponder, Q. Broxterman and J. Manley, "Using the Right Green Yardstick: Why Process Mass Intensity Is Used in the Pharmaceutical Industry To Drive More Sustainable Processes," *Organic Process Research & Development*, 2011.
- [13] "Biodisolventes para industria agroquímica," comindex, 2019. [Online]. Available: <https://www.comindex.es/novedades/biodisolventes-para-industria-agroquimica>. [Accessed 05 05 2021].
- [14] A. D. McNaught and A. W. Blackwell, "IUPAC. Compendium of Chemical Terminology," in "*the Gold Book*", Oxford, 1997.
- [15] P. Ying, J. Yu and Weike Sub, "Liquid-Assisted Grinding Mechanochemistry in the Synthesis of Pharmaceuticals," *Advanced Synthesis and Catalysis*, 2021.
- [16] F. Shen, X. Xiong, J. Fu, J. Yang, M. Qiu, X. Qi and D. C. Tsang, "Recent advances in mechanochemical production of chemicals and carbon materials from sustainable biomass resources," *Renewable and Sustainable Energy Reviews*, vol. 130, 2020.
- [17] C. Xu, S. De, A. M. Balu, M. Ojeda and R. Luque, "Mechanochemical synthesis of advanced nanomaterials for catalytic applications," *Chem. Commun*, vol. 51, pp. 6698-6713, 2015.
- [18] T. Ji, R. Tu, L. Mu, X. Lu and J. Zhu, "Enhancing Energy Efficiency in Saccharide–HMF Conversion with Core/shell Structured Microwave Responsive Catalysts," *ACS Sustainable Chemistry & Engineering*, vol. 5, no. 5, pp. 4352-4358, 2017.
- [19] C. O. Kappe, "Controlled Microwave Heating in Modern Organic Synthesis," *German Chemical Society*, 2004.
- [20] J. Wang, L. M. D. R. S. Martins and A. P. C. Ribeiro, "Supported C-Scorpionate Vanadium(IV) Complexes as Reusable Catalysts for Xylene Oxidation," *Chem. Asian J.*, 2017.
- [21] L. M. D. R. S. Martins, A. P. C. Ribeiro, S. A. C. Carabineiro, J. L. Figueiredo and A. J. L. Pombeiro, "Highly efficient and reusable CNT supported iron(ii) catalyst for microwave assisted alcohol oxidation," *Dalton Trans.*, vol. 45, no. 16, pp. 6816-6819, 2016.
- [22] S. Hazra, L. M. Martins, M. F. C. G. d. Silva y A. J. Pombeiro, «Sulfonated Schiff base dimeric and polymeric copper(II) complexes: Temperature dependent synthesis, crystal structure and catalytic alcohol oxidation studies,» *Inorganica Chimica Acta*, vol. 455, pp. 549-556, 2017.
- [23] L. M. D. R. S. Martins, "Alkane Oxidation with C-Scorpionate Metal Complexes," in *Alkane Functionalization*, John Wiley & Sons Ltd, 2018, pp. 113-123.

- [24] L. M. D. R. S. Martins, "C-Homoscorpionate Oxidation Catalysts—Electrochemical and Catalytic Activity," *Catalysts*, vol. 7, 2017.
- [25] L. M. D. R. S. Martins and A. J. L. Pombeiro, "Water-Soluble C-Scorpionate Complexes – Catalytic and Biological Applications," *Eur. J. Inorg. Chem.*, pp. 2236-2252, 2016.
- [26] W. Hückel and H. B. Chneider, "N-Tripyrazolyl-methan," *Berichte der deutschen chemischen Gesellschaft (A and B Series)*, vol. 70, no. 9, pp. 2024-2026, 1937.
- [27] S. Trofimenko, "Boron-pyrazole chemistry," *Journal of the American Chemical Society*, pp. 1842-1844, 1966.
- [28] J. P. Jesson, «Isotropic Nuclear Resonance Shifts in Some Trigonal Co(II) and Ni(II) Chelate Systems,» *The Journal of Chemical Physics*, vol. 47, nº 2, pp. 582-591, 1967.
- [29] J. Elguero, S. Juliá, J. M. d. Mazo and L. Avila, "IMPROVED SYNTHESIS OF POLYAZOLYLMETHANES UNDER SOLID-LIQUID PHASE-TRANSFER CATALYSIS," *Organic Preparations and Procedures International*, vol. 16, pp. 299-307, 1984.
- [30] E. C. B. Alegria, L. M. D. R. S. Martins, M. Haukko and A. J. L. Pombeiro, "Rhenium complexes of tris(pyrazolyl)methanes and sulfonate derivative," *Dalton Trans.*, pp. 4954-4961, 2006.
- [31] C. Titze, J. Hermann and H. Vahrenkamp, "Highly Substituted Tris(pyrazolyl)methane Ligands and Some Zinc Complexes Thereof," *Chemische Berichte*, vol. 128, 1995.
- [32] T. F. Silva, K. Luzyanin, M. Kirillova, M. F. G. da Silva, L. M. Martins and A. J. Pombeiro, "Novel Scorpionate and Pyrazole Dioxovanadium Complexes, Catalysts for Carboxylation and Peroxidative Oxidation of Alkanes," *Advanced Synthesis & Catalysis*, vol. 352, no. 1, pp. 171-187, 2010.
- [33] M. Mendes, A. P. C. Ribeiro, E. C. Alegria, L. M. Martins and A. J. Pombeiro, "Liquid phase oxidation of xylenes catalyzed by the tripodal C-scorpionate iron(II) complex [FeCl₂{κ³-HC(pz)₃}]," *Polyhedron*, vol. 125, pp. 151-155, 2017.
- [34] L. M. Martins and A. J. Pombeiro, "C-scorpionate rhenium complexes and their application as catalysts in Baeyer-Villiger oxidation of ketones," *Inorganica Chimica Acta*, vol. 455, pp. 390-397, 2017.
- [35] M. Adediran Mesubi and F. Okwudilichukwu Anumba, "Coordination chemistry of poly(1-pyrazolyl)alkanes, part IV. Copper(II) complexes of bis- and tris-(1-pyrazolyl)methane," *Transition Metal Chemistry*, 1985.

- [36] A. M. Santos, F. E. Kuhn, K. Bruus-Jensen, C. C. R. I. Lucas and E. Herdtweck, "Molybdenum(VI) cis-dioxo complexes bearing (poly)pyrazolyl-methane and -borate ligands:," *J. Chem. Soc., Dalton Trans.*, pp. 1332-1337, 2001.
- [37] D. L. Reger, E. A. Foley and M. D. Smith, "Structural Impact of Multitopic Third-Generation Bis(1-pyrazolyl)methane Ligands: Double, Mononuclear Metallacyclic Silver(I) Complexes," *Inorganic Chemistry*, vol. 49, pp. 234-242, 2010.
- [38] M. Yamaguchi, M. Tomizawa, K. Takagaki, M. Shimo, D. Masui and T. Yamagishi, "Photooxidation of alkane under visible light irradiation catalyzed by ruthenium complexes," *Catalysis Today*, vol. 117, pp. 206-209, 2006.
- [39] T. A. Duarte, A. P. Carvalho and L. M. Martins, "Styrene oxidation catalyzed by copper(II) C-scorpionates in homogenous medium and immobilized on sucrose derived hydrochars," *Catalysis Today*, vol. 357, pp. 56-63, 2020.
- [40] T. F. Silva, E. C. Alegria, L. M. Martins and A. J. Pombeiro, "Half-Sandwich Scorpionate Vanadium, Iron and Copper Complexes: Synthesis and Application in the Catalytic Peroxidative Oxidation of Cyclohexane under Mild Conditions," *Advanced Synthesis & Catalysis*, vol. 350, no. 5, pp. 706-716, 2008.
- [41] I. A. Matias, A. P. Ribeiro and L. M. Martins, "New C-scorpionate nickel(II) catalyst for Heck C-C coupling under unconventional conditions," *Journal of Organometallic Chemistry*, vol. 896, pp. 32-37, 2019.
- [42] T. F. S. Silva, L. M. D. R. S. Martins, M. F. C. Guedes da Silva, A. R. Fernandes, A. Silva, P. M. Borralho, S. Santos, C. M. P. Rodrigues and A. J. L. Pombeiro, "Cobalt complexes bearing scorpionate ligands: synthesis, characterization, cytotoxicity and DNA cleavage," *Dalton Trans.*, vol. 41, no. 41, pp. 12888-12897, 2012.
- [43] A. J. Canty, N. J. Minchin, P. C. Healy and A. H. White, "Co-ordination chemistry of dimethylgold(III). Synthesis, spectroscopic and structural studies of complexes with neutral aromatic nitrogen-donor ligands," *Journal of the Chemical Society, Dalton Transactions*, pp. 1795-1802, 1982.
- [44] M. P. d. Almeida, L. M. D. R. S. Martins, S. A. C. Carabineiro, T. Lauterbach, F. Rominger, A. J. L. P. A. S. K. Hashmi and J. L. Figueiredo, "Homogeneous and heterogenised new gold C-scorpionate complexes as catalysts for cyclohexane oxidation," *Catal. Sci. Technol.*, pp. 3056-3069, 2013.

- [45] A. Corma and H. Garcia, "Supported gold nanoparticles as catalysts for organic reactions," *Chem. Soc. Rev.*, vol. 37, pp. 2096-2126, 2008.
- [46] S. M. Thomas, «The Advantages of Exploring the Interface Between Heterogeneous and Homogeneous Catalysis,» *ChemCatChem*, vol. 2, nº 2, pp. 127-132, 2010.
- [47] L. Martins, A. Martins, E. Alegria, A. Carvalho and A. Pombeiro, "Efficient cyclohexane oxidation with hydrogen peroxide catalysed by a C-scorpionate iron(II) complex immobilized on desilicated MOR zeolite," *Applied Catalysis*, Vols. 464-465, pp. 43-50, 2013.
- [48] S. Carabineiro, L. Martins, M. Avalos-Borja, J. Buijnsters, A. Pombeiro and J. Figueiredo, "Gold nanoparticles supported on carbon materials for cyclohexane oxidation with hydrogen peroxide," *Applied Catalysis*, vol. 467, pp. 279-290, 2013.
- [49] W. H. Bragg and W. L. Bragg, "The reflection of X-rays by crystals," *Proceedings of the Royal Society of London*, vol. 88, no. 605, pp. 428-438, 1913.
- [50] K. S. Novoselov, A. K. Geim, S. V. Morozov, D. Jiang, Y. Zhang and S. Dubonos, "Electric Field Effect in Atomically Thin Carbon," *Science*, vol. 306, no. 5696, pp. 666-669, 2004.
- [51] Quizlet. [Online]. Available: <https://quizlet.com/455943233/igcse-giant-covalent-structures-flash-cards/>. [Accessed 06 05 2021].
- [52] F. Libisch, «Wiley Analytical science,» [Online]. Available: <https://analyticalscience.wiley.com/do/10.1002/gitlab.15487/full/>. [Last access: 2021 05 06].
- [53] A. Peigney, C. Laurent, E. Flahaut, R. R. Bacsá y A. Rousset, «Specific surface area of carbon nanotubes and bundles of carbon nanotubes,» *Carbon*, vol. 39, nº 4, pp. 507-514, 2001.
- [54] S. Park and R. S. Ruoff, "Chemical methods for the production of graphenes," *Nat Nano*, vol. 4, no. 4, p. 217, 2009.
- [55] I. Esteve Adell, H. García Gómez and A. M. Primo Arnau, *Grafenos como carbocatalizadores y soporte de nanopartículas metálicas orientadas*, Valencia: Universitat Politècnica de València, 2018.
- [56] J. C. Jiménez-García, J. A. Olmos-Asar, E. E. Franceschini and M. M. Mariscal, "Electrochemical area of graphene-supported metal nanoparticles from an atomistic approach," *Journal of Applied Electrochemistry*, 2020.
- [57] C. Liang, Z. Li and S. Dai, "Mesoporous Carbon Materials: Synthesis and Modification,"

- [58] I. Janowska, M.-S. Moldovan, O. Ersen, H. Bulou, K. Chizari and M. J. Ledoux, "High temperature stability of platinum nanoparticles on few-layer graphene investigated by In Situ high resolution transmission electron microscopy.," *Nano Research*, 2011.
- [59] S. Sarkar, M. L. Moser, X. Tian, X. Zhang, Y. F. Al-Hadeethi and R. C. Haddon, "Metals on Graphene and Carbon Nanotube Surfaces: From Mobile Atoms to Atomtronics to Bulk Metals to Clusters and Catalysts," *Chemistry of Materials*, 2014.
- [60] R. Wang, Z. Wu, C. Chen, Z. Qin, H. Zhu, G. Wang, H. Wang, C. Wu, W. Dong and W. Fan, "Graphene-supported Au-Pd bimetallic nanoparticles with excellent catalytic performance in selective oxidation of methanol to methyl formate," *Chemical Communications*, 2013.
- [61] E. Henrich, N. Dahmen, E. Dinjus and J. Sauer, "The Role of Biomass in a Future World without Fossil Fuels," *Chemie Ingenieur Technik*, vol. 87, no. 12, pp. 1667-1685, 2015.
- [62] A. F. Cristino, I. A. S. Matias, D. E. N. Bastos, R. Galhano dos Santos, A. P. C. Ribeiro and L. M. D. R. S. Martins, "Glycerol Role in Nano Oxides Synthesis and Catalysis," *Catalysts*, no. 12, 2020.
- [63] W. W. Chong, "ResearchGate," [Online].
Available: https://www.researchgate.net/figure/Transesterification-process-for-biodiesel-production_fig4_300425785. [Accessed 2021 05 19].
- [64] M. Sajid, X. Zhao and D. Liu, "Production of 2{,}5-furandicarboxylic acid (FDCA) from 5-hydroxymethylfurfural (HMF): recent progress focusing on the chemical-catalytic routes," *Green Chem.*, vol. 20, no. 24, pp. 5427-5453, 2018.
- [65] J. N. Chheda, Y. Roma´n-Leshkov and J. A. Dumesic, "Production of 5-hydroxymethylfurfural and furfural by dehydration of biomass-derived mono- and poly-saccharides," *Royal Society of Chemistry*, 2007.
- [66] M. Bartoli, L. Rosi and M. Frediani, "Introductory Chapter: A Brief Insight about Glycerol, Glycerine Production and Transformation—An Innovative Platform for Sustainable Biorefinery and Energy," *IntechOpen*, 2019.
- [67] T. Dang-Bao, C. Pradel, I. Favier and M. Gómez, "Making Copper(0) Nanoparticles in Glycerol: A Straightforward Synthesis for a Multipurpose Catalyst," *Advanced Synthesis & Catalysis*, vol. 359, no. 16, pp. 2832-2846, 2017.

- [68] S. E. Davis, M. S. Ide and R. J. Davis, "Selective oxidation of alcohols and aldehydes over supported metal nanoparticles," *green Chem.*, vol. 15, no. 1, pp. 17-45, 2013.
- [69] B. Katryniok, H. Kimura, E. a. G. J.-S. Skrzyńska, P. Fongarland, M. Capron, R. Ducoulombier, N. Mimura, S. Paul and F. Dumeignil, "Selective catalytic oxidation of glycerol: perspectives for high value chemicals," *Green Chem.*, vol. 13, no. 8, pp. 1960-1979, 2011.
- [70] Z. Zhang and K. Deng, "Recent Advances in the Catalytic Synthesis of 2,5-Furandicarboxylic Acid and Its Derivatives," *ACS Catalysis*, vol. 5, no. 11, pp. 6529-6544, 2015.
- [71] J. Niemanstverdriet, "Introduction," in *Spectroscopy in Catalysis*, John Wiley & Sons, Ltd, 2007, pp. 1-10.
- [72] J. Libuda and H.-J. Freund, "Molecular beam experiments on model catalysts," *Surface Science Reports*, vol. 57, no. 7, pp. 157-298, 2005.
- [73] Ulvac-Phi, "X-Ray Photoelectron Spectroscopy (XPS)," [Online]. Available: [https://www.phi.com/surface-analysis-techniques/xps-esca.html#:~:text=X%2Dray%20Photoelectron%20Spectroscopy%20\(XPS\)%20also%20known%20as%20Electron,surface%20of%20the%20material%20being](https://www.phi.com/surface-analysis-techniques/xps-esca.html#:~:text=X%2Dray%20Photoelectron%20Spectroscopy%20(XPS)%20also%20known%20as%20Electron,surface%20of%20the%20material%20being). [Accessed 20 05 2021].
- [74] P. Raja y A. Barron, «Introduction to Elemental Analysis,» 21 March 2021. [En línea]. Available: <https://chem.libretexts.org/@go/page/55810>. [Accessed: 25 June 2021].
- [75] K. R. Jennings, "Spectrometric identification of organic compounds," *Organic Mass Spectrometry*, 1991.
- [76] R. Laboratories, "SEM/EDS Analysis," [Online]. Available: [https://rtlab.com/techniques/sem-eds-analysis/#:~:text=Scanning%20electron%20microscopy%20\(SEM\)%20and,solder%20joint%20analysis%20and%20more..](https://rtlab.com/techniques/sem-eds-analysis/#:~:text=Scanning%20electron%20microscopy%20(SEM)%20and,solder%20joint%20analysis%20and%20more..) [Accessed 2021 05 20].
- [77] D. L. Reger, T. Grattan, K. J. Brown, C. A. Little, J. J. Lamba, A. L. Rheingold and R. D. Sommer, "Syntheses of tris(pyrazolyl)methane ligands and {[tris(pyrazolyl)methane]Mn(CO)₃}SO₃CF₃ complexes: comparison of ligand donor properties," *Journal of Organometallic Chemistry*, vol. 607, no. 1, pp. 120-128, 2000.
- [78] Retsch, "Planetary Ball Mill PM100- RETSCH," [Online]. Available: https://www.retsch.com/products/milling/ball-mills/planetary-ball-mill-pm-100/function-features/?gclid=CjwKCAjwqcKFBhAhEiwAfEr7zR7F3cXs-acfBjsGE7zBuMwETlwQSm8T5SODVnaqCQ9kNP5-8UMpJR0C0D0QAvD_BwE. [Accessed

26 05 2021].

- [79] A. Paar, "Microwave reactor: Monowave Anton Paar," [Online]. Available: <https://www.anton-paar.com/in-en/products/details/microwave-synthesis-monowave-400200/>. [Accessed 27 05 2021].
- [80] Retsch, "Emax- High Energy Ball Mill," [Online]. Available: <https://www.retsch.com/products/milling/ball-mills/emax/function-features/>. [Accessed 28 05 2021].
- [81] S. Aldrich, "Glycerol | 56-81-5| Sigma Aldrich," [Online]. Available: https://www.sigmaaldrich.com/catalog/product/mm/104093?lang=pt®ion=PT&gclid=CjwKCAjwqcKFBhAhEiwAfEr7zav2KNtSp9T3lyGvxmURTIEVWe7elfD_qQ3qzxlKnqDC31flQpaVMxoc_hUQAvD_BwE. [Accessed 28 05 2021].
- [82] S. Aldrich, "ter-Butyl hydroperoxide solution | Sigma-Aldrich," [Online]. Available: https://www.sigmaaldrich.com/catalog/substance/tertbutylhydroperoxidesolution90127591211?lang=pt®ion=PT&gclid=CjwKCAjwqcKFBhAhEiwAfEr7zQ_xu1mkj-_nsB9GcNzxnlgTTtoEQQZK_xtPoMXs6qAfVpR2onpYZHxocUMUQAvD_BwE. [Accessed 28 05 2021].
- [83] T. Chemicals, "5-Hydroxymethyl-2-furaldehyde 67-47-0 | TCI AMERICA," [Online]. Available: <https://www.tcichemicals.com/US/en/p/H0269>. [Accessed 28 05 2021].
- [84] T. Chemicals, «5-(Hydroxymethyl)furan-2-carboxylic Acid 6338-41-6 | TCI AMERICA,» [En línea]. Available: <https://www.tcichemicals.com/AR/en/p/H1750>. [Último acceso: 28 05 2021].
- [85] G. Shul'pin, Y. N. Kozlov, L. Shul'pina, T. Strelkova y D. Mandelli, «Oxidation of Reactive Alcohols with Hydrogen Peroxide Catalyzed by Manganese Complexes.,» *Catalysis Letters*, vol. 138, pp. 193-204, 2010.